

DEVELOPMENT AND VALIDATION OF AN INNOVATIVE HINGED SYSTEM FOR THE CONVERSION OF WAVE ENERGY IN COASTAL STRUCTURES

GIOVANNI ALBARELLO MARTINS

DISSERTATION SUBMITTED FOR THE DEGREE IN:

MASTER'S IN ENVIRONMENTAL ENGINEERING

AT THE FACULTY OF ENGINEERING OF THE UNIVERSITY OF PORTO

PRESIDENT OF THE JURY: ADRIÁN MANUEL TAVARES DA SILVA

SUPERVISOR: PROFESSOR DR. PAULO JORGE ROSA SANTOS

CO-SUPERVISOR: DR. GIANMARIA GIANNINI

2023, OCTOBER

MASTER'S IN ENVIRONMENTAL ENGINEERING 2022/2023

DEPARTMENT OF CIVIL ENGINEERING

Tel. +351-22-508 1901

Fax +351-22-508 1446

✉ mea@fe.up.pt

Edited by

FACULTY OF ENGINEERING OF THE UNIVERSITY OF PORTO

Rua Dr. Roberto Frias

4200-465 PORTO

Portugal

Tel. +351-22-508 1400

Fax +351-22-508 1440

✉ feup@fe.up.pt

🌐 <http://www.fe.up.pt>

Partial reproductions of this document will be authorized under the condition that the Author is mentioned, and reference is made to Master's in Environmental Engineering - 2022/2023 - Department of Civil Engineering, Faculty of Engineering of the University of Porto, Porto, Portugal, 2023.

The opinions and information included in this document represent only the respective Author's point of view, and the Publisher cannot accept any legal or other responsibility concerning errors or omissions that may exist.

This document was produced from an electronic version provided by the respective Author. The decimal separator used in this text is the comma (","), in accordance with the international system of units. For the thousands the dot (".") is used.

To everyone who ever taught me something

"The more I learn, the less I know"

Socrates

ACKNOWLEDGMENTS

Firstly, I would like to express my gratitude to Professor Paulo Rosa Santos not only for the support and guidance provided throughout the development of this thesis but also for never undervaluing my work and always motivating me to go beyond what was required, encouraging me to be increasingly curious and to seek only for satisfactory answers.

I would also like to super thank my co-supervisor: Dr. Gianmaria Giannini. Thank you so much for your special and careful guidance throughout the last few months, for all the hints and tips that you gave me, for all the after-work hours you spent with me in the laboratory working on the experimental model, for all the infinite concerns about work safety and for the amazing little desk you built within your desk allowing me to work. You have undoubtedly had a huge impact on the quality of this work.

Additionally, I would like to thank everyone who ever taught me something or helped from the FEUP community during my time as a student. I think that everyone played a fundamental role in my development not only as an engineer but also as a person. An even more special thanks to the professors who never discouraged me from going beyond what was supposed to and duly appreciated my effort as a student.

I couldn't also not thank my colleagues from A400, especially Mafalda Correia and Gonçalo Ramalho who always understood the challenges of conciliating a full-time job with thesis development and never blocked me from leaving earlier or for being on remote work when I needed to. Thank you Gonçalo, for being a humane and understanding boss, for carefully listening to my concerns and advising me in the best way possible. And thanks Mafalda, for all the hours spent teaching me things, for reviewing my documents and emails, and for sometimes even covering me from work in order to work on my thesis.

I also want to give a large acknowledgment to all my friends, mainly the ones from Porto, for being my second family for all those years, when our real families were far away. Thanks for the incredible moments together, for the craziest European trips, for the best party nights ever, for the best dinners, for the infinite laughs together, for the longest bike rides, for all Christmas together, and mainly for the company. I will always remember those good memories from university.

To my amazing family—Mom, Dad, and Luly—I want to express my heartfelt thanks for always being there for me from the very beginning. You've believed in me, encouraged me, and supported me wholeheartedly in chasing my dreams. I honestly couldn't have come this far without your love and support. You inspire me every day, and I'm so grateful to have you by my side whenever I need you. Thank you for everything!

And to Amanda, who throughout all these months never tired of listening to my explanations about topics she had no idea about, advising me always in the best possible way, and wishing me the best and greatest success. You surely have a great impact on the quality of this work.

This research was also partially funded by the Ports Towards Energy Self-Sufficiency (PORTOS) project, co-financed by the Interreg Atlantic Area Programme through the European Regional Development Fund, grant number EAPA-784/2018, and by the project WEC4Ports – A hybrid Wave Energy Converter for Ports (OCEANERA-NET COFUND) funded under the frame of FCT. Now, let's move on to what really matters!

ABSTRACT

The growing necessity of exploring new energy sources in order to contribute to decarbonization goals and to keep energy supply for a world growing population make it crucial to investigate for different sources of renewables that are reliable, affordable and abundant. With wave energy things are no different, however, it is still not an affordable option of energy. Therefore, strong research and development should be done in order to make this abundant and consistent energy source a feasible option. This dissertation aims to contribute to renewables development, specifically with useful insights about the potential of conversion of wave energy in breakwaters using hinged system devices.

The technology studied in this dissertation is of the point absorber type and consists of a floating body (in this study a half sphere) fixed to a breakwater by means of a hinged arm. The rising and falling movement promoted by the incoming waves causes the floater to move up and down. This movement is then used to generate clean energy through a power take-off system.

The study focused on modeling and subsequent validation of the hinged device in the north breakwaters of Porto de Leixões and the Douro River, through a numerical and experimental model. This study is part of the PORTOS and WEC4Ports projects, which aim to contribute to the energy self-sufficiency of European ports, which are usually large energy consumers. For this, several simulations were carried out with ANSYS® AQWA software initially. Later, based on the outcomes of that numerical study, an experimental model was built on a geometrical scale of 1:14 and then tested in the wave-current flume of the Hydraulics Laboratory of the Hydraulics, Water Resources and Environment Division of FEUP.

The numerical study allowed to estimate annual energy productions on the order of 190MWh/year and 135MWh/year for sloped (rubble-mound) and for vertical breakwaters, respectively. Thus, the developed technology has potential to contribute significantly to the energy self-sufficiency of ports and decarbonization goals. Finally, the experimental model allowed validating the results obtained numerically through a relative error of less than 21%.

KEYWORDS

Wave Energy, Sustainability, Renewables, Wave Energy Converters, Hinged Systems, Ansys Aqwa, Physical and Numerical Modeling.

RESUMO

A crescente necessidade de explorar novas fontes de energia, a fim de contribuir para os objetivos de descarbonização e manter o fornecimento de energia para uma população mundial em crescimento, torna crucial a investigação e desenvolvimento de diferentes fontes de energias renováveis que sejam fiáveis, acessíveis e abundantes. Com a energia das ondas não é diferente, apesar de ainda não ser uma opção de energia acessível. Para que se torne viável essa fonte de energia é necessário muita pesquisa e desenvolvimento. Esta dissertação pretende contribuir para o desenvolvimento das energias renováveis, especificamente com informações valiosas sobre o potencial de conversão da energia das ondas em quebra-mares utilizando dispositivos de sistemas articulados.

A tecnologia estudada nesta dissertação é do tipo *point absorber* e consiste em um corpo flutuante (neste estudo uma meia esfera) fixado a um quebra-mar por meio de um braço articulado. O movimento de subida e descida promovido pelas ondas faz com que o flutuador se mova para cima e para baixo. Esse movimento é então utilizado para gerar eletricidade limpa através de um sistema de power take-off.

O estudo centrou-se na modelação e posterior validação do dispositivo articulado nos molhes norte do Porto de Leixões e do Rio Douro, através de um modelo numérico e de um modelo experimental. Este estudo enquadra-se nos projetos PORTOS e WEC4Ports, que visam contribuir para a autossuficiência energética dos portos europeus, que são habitualmente grandes consumidores de energia. Para isso, inicialmente foram realizadas diversas simulações com o software ANSYS® AQWA. Posteriormente, com base nos resultados desse estudo numérico, foi construído um modelo experimental à escala geométrica de 1:14 e posteriormente testado no canal de correntes de ondas do Laboratório de Hidráulica da Secção de Hidráulica, Recursos Hídricos e Ambiente da FEUP.

O estudo numérico permitiu estimar produções anuais de energia na ordem dos 190MWh/ano e 135MWh/ano para quebra-mares inclinados (taludes) e para quebra-mares verticais, respetivamente. Assim, a tecnologia desenvolvida tem potencial para contribuir significativamente para a autossuficiência energética dos portos e para as metas de descarbonização. Por fim, o modelo experimental permitiu validar os resultados obtidos numericamente através de um erro relativo inferior a 21%.

PALAVRAS-CHAVE

Energia das Ondas, Sustentabilidade, Renováveis, Conversores de Energia das Ondas, Sistemas Articulados, Ansys Aqwa, Modelagem Física e Numérica.

INDEX

ACKNOWLEDGMENTS.....	v
ABSTRACT	vii
RESUMO.....	ix
INDEX	xi
FIGURE INDEX	xiii
TABLE INDEX.....	xv
ABBREVIATIONS	xvii
SYMBOLS AND UNITS	xix
1. INTRODUCTION.....	1
1.1. General Framework.....	1
1.2. Objectives.....	4
1.3. Dissertation Structure.....	5
2. WAVE ENERGY CONVERSION IN COASTAL STRUCTURES	7
2.1. Wave Energy and Breakwater Integration	7
2.2. Essential Features of a WEC.....	23
2.3. Wave Resource.....	24
2.4. Energy Production and CO ₂ Reduction.....	27
3. CASE STUDY	31
3.1. Port of Leixões	31
3.2. Power Take-Off Systems	38
3.3. Hinged Systems for Wave Energy Conversion.....	39
3.4. Final Considerations.....	42
4. NUMERICAL MODEL.....	43
4.1. Introduction.....	43
4.2. Body Definitions	44
4.3. Software Parameters.....	46
4.4. Best Damping Coefficient.....	47
4.5. Simulations.....	49
4.6. Expectable Power Matrix	51
4.7. Efficiencies and Breakwater Comparison	55
4.8. Expectable Electricity Production and CO ₂ Reduction	57
4.9. Numerical Model Limitations	59
5. EXPERIMENTAL MODEL.....	61
5.1. Body Concept and Construction	61
5.2. Scaling.....	63

5.3.	Wave Current Flume	64
5.4.	Damping Characterization.....	65
5.5.	Measuring and Working Equipment	69
5.6.	Experimental Tests.....	72
5.7.	Obtained Power Matrix	74
5.8.	Validation of Numerical Model	76
5.9.	Experimental Model Limitations and Recommendations	79
6.	CONCLUSIONS.....	81
6.1.	Conclusions	81
6.2.	Further Research	82
	BIBLIOGRAPHY	83
	APPENDIX I – MATLAB® CODE FOR DAMPING CHARACTERIZATION	87
	APPENDIX II – POWER VALUES OBTAINED FOR EXPERIMENTAL MODEL	89
	APPENDIX III – ANSYS® REPORT FOR THE NUMERICAL MODEL	91

FIGURE INDEX

Figure 1. Relation between electricity consumption and HDI [2].	1
Figure 2. Annual mean wave power density [7].	3
Figure 3. PORTOS - Ports Towards Energy Self-Sufficiency Project® [10].	5
Figure 4. Usual configuration of a rubble mound breakwater in Ria Alvor, Portimão [12].	9
Figure 5. Cross section with its constituent elements [12].	10
Figure 6. Example of a modern large vertical breakwater [13].	10
Figure 7. Two main categories of composite breakwaters [14].	11
Figure 8. Submerged breakwater cross section [15].	11
Figure 9. WaveRoller® (top) and Bombora® (down) technologies [16], [17].	12
Figure 10. Simple explanation on how OWC extracts wave energy [18].	13
Figure 11. Breakwater integrated with overtopping device scheme [20].	14
Figure 12. The heave motion of the buoy converts the energy in point absorbers [21].	15
Figure 13. Mutriku OWC breakwater integration [23].	17
Figure 14. Sakata OWC chamber in the breakwater [24].	18
Figure 15. EWP WECs placed in the Jaffa port [25].	19
Figure 16. EWP WECs placed in the Gibraltar old ammunition jetty [27].	19
Figure 17. PICO OWC located in Porto Cachorro, Azores [31].	21
Figure 18. WaveStar unit installed in Hanstholm, Denmark [33].	21
Figure 19. Port of Pecém WEC [36].	22
Figure 20. Power available versus average consumption annual mean power necessities [7].	26
Figure 21. Mean wave energy potential along the Brazilian and Portuguese coast [37], [40].	27
Figure 22. Scatter diagram for Viana – Porto showing the wave resource in hours [37].	28
Figure 23. The Port of Leixões, West – East view [44].	31
Figure 24. Location and representative diagram of the Port of Leixões [43].	32
Figure 25. Moveable bridge across the Leça River in the Port of Leixões [45].	33
Figure 26. Bathymetry heat map for the Port of Leixões influence area [44].	34
Figure 27. Wave regime for the nearest breakwater point [46].	35
Figure 28. Sites of deployment for both breakwaters.	36
Figure 29. GHG emissions for 2019 and 2020 in the Port of Leixões [47].	37
Figure 30. Direct drive PTO system used in a WCE prototype [53].	38
Figure 31. Scheme of a hinged system WEC [49].	39
Figure 32. Energy Conversion Unit from EWP [50].	41
Figure 33. Floater mechanism of EWP devices [50].	41
Figure 34. Computational time exponentially growing with mesh density.	43
Figure 35. CAD drawing with dimensions of the WEC prototype in a vertical breakwater.	44
Figure 36. CAD drawing of the vertical breakwater to be tested.	45
Figure 37. Free forces diagram applied to the body.	45
Figure 38. Joints and geometry in the ANSYS® environment (vertical breakwater).	47
Figure 39. Power curve showing the best <i>CD</i> .	48
Figure 40. Peak frequency versus power for all the <i>HS</i> .	52
Figure 41. Power surface for vertical breakwater.	54
Figure 42. Power surface for sloped breakwater.	54
Figure 43. CWR value versus peak frequency.	57
Figure 44. Map showing the length available for deploying WECs in the Port of Leixões.	59
Figure 45. Bicycle components used for experimental modeling.	61
Figure 46. Experimental WEC setup built.	62

Figure 47. Detailed view of the arm attachment zone and brake setup.....	63
Figure 48. Dimensions of the channel used.	65
Figure 49. Free torque diagram applied to the floater.	65
Figure 50. Typical damped pendulum decay graph.	67
Figure 51. Time that the system would take to completely stop according to the code.	68
Figure 52. Coordinates system adopted and name of the markers.	70
Figure 53. Qualisys® cameras setup and positioning.	70
Figure 54. The four probes and their distance in the channel.	71
Figure 55. HR Wallingford® wave maker and concrete blocks used.	72
Figure 56. Time-series for Top 1 marker.	74
Figure 57. RAO values compared for different regular waves amplitudes.	78

TABLE INDEX

Table 1. Examples of WEC integration into coastal structures [6]	16
Table 2. Population, wave power availability and annual mean power by continent [7] [39]	25
Table 3. Pelamis 750kW power matrix [42]	29
Table 4. Significant wave height versus wave period distribution [46]	35
Table 5. Significant wave height versus wave direction distribution [46]	35
Table 6. Energy consumption by source for the Port of Leixões in 2019 and 2020 [47].....	37
Table 7. Best damping coefficient values for the two breakwaters.....	49
Table 8. Sea States (SST) for each different simulation	50
Table 9. Power matrix obtained for the device under study attached in a vertical breakwater ...	51
Table 10. Power matrix obtained for the device under study attached in a sloped breakwater ..	51
Table 11. Enhanced power matrix with hypothetical ADO system in a vertical breakwater.....	52
Table 12. Enhanced power matrix with hypothetical ADO system in a sloped breakwater	53
Table 13. Actual power matrix of EWP device [50]	53
Table 14. Wave power available for different SSTs	56
Table 15. CWR values obtained in a vertical breakwater	56
Table 16. CWR values obtained in a sloped breakwater.....	56
Table 17. Wave resource matrix for the location under study	58
Table 18. Electricity matrix for different SST throughout the year for vertical breakwater	58
Table 19. Electricity matrix for different SST throughout the year for sloped breakwater	58
Table 20. Common scaling factors used in WECs studies [51]	64
Table 21. Damping type according to its damping factor	67
Table 22. Experimental tests <i>HS</i> and <i>TP</i> values	73
Table 23. Power matrix obtained from regular waves experimental simulations	75
Table 24. Power matrix obtained from irregular waves experimental simulations.....	75
Table 25. Enhanced power matrix from regular waves experimental tests.....	76
Table 26. CWR values for the experimental study	76
Table 27. Error matrix for model validation	77
Table 28. Power values for numerical and experimental models under regular waves	89
Table 29. Power values for numerical and experimental models under irregular waves	89

ABBREVIATIONS

HDI – Human Development Index

WEC – Wave Energy Converter

OTEC – Ocean Thermal Energy Conversion

IEA – International Energy Agency

PTO – Power Take Off

OWC – Oscillating Water Column

EWP – Eco Wave Power®

ZHL – Zero Hidrográfico de Leixões (Hydrographic Zero of Leixões)

NG – Natural Gas

GHG – Greenhouse Gases

CO₂eq – Carbon Dioxide Equivalent

APA – Agência Portuguesa do Ambiente (Portuguese Environment Agency)

MWL – Mean Water Level

SST – Sea State

PM – Pierson-Moscowitz

ADO – Active Damping Optimization Control Systems

SF – Scaling Factor

ODE – Ordinary Differential Equation

LCOE – Levelized Cost of Energy

R&D – Research and Development

RAO – Response Amplitude Operator

SYMBOLS AND UNITS

H – Wave Height [m]	C_{AD} – Angular Damping Coefficient [Nsm/°]
T – Wave Period [s]	P – Power [W]
H_S – Significant Wave Height [m]	P_W – Wave Available Power [W]
T_P – Wave Peak Period [s]	V – Velocity [m/s]
T_E – Wave Energy Period [s]	s – Scale [-]
T_Z – Wave Zero-Crossing Period [s]	λ – Scaling Parameter [-]
SF – Scaling Factor [-]	T_R – Resulting Torque [Nm]
g – Gravitational Acceleration [m/s ²]	α – Angular Acceleration [rad/s ²]
ρ_S – Fluid Density [kg/m ³]	ω – Angular Velocity [rad/s]
V_D – Volume of Water Displaced [m ³]	I_T – Total Moment of Inertia [kgm ²]
F – Buoyant Force [N]	L – Arm Length [m]
W – Weight [N]	β – Damping Factor
m_B – Body Mass [kg]	t – Time [s]
m_F – Floater Mass [kg]	θ – Angular Displacement [rad]
m_A – Arm Mass [kg]	θ_{MAX} – Max Angular Displacement [rad]
h – Water Height [m]	CW – Capture Width [m]
r – Body Radius [m]	CWR – Capture Width Ratio [-]
C_D – Damping Coefficient [-]	RAO – Response Amplitude Operator [-]
C_{LD} – Linear Damping Coefficient [Ns/m]	

1

INTRODUCTION

1.1. GENERAL FRAMEWORK

Energy plays an indispensable role in today's world. The majority of developed nations heavily depend on energy to fulfill various aspects of human life. Transportation, industrial processes, communication and information, food harvesting, medical applications, and human comfort are only a small sample of what energy is necessary for. This way, it is not hard to realize that energy consumption and development are closely related because energy is a crucial input for economic growth and development [1]. Countries that consume more energy per capita tend to have higher levels of development, as they are able to power their economies and provide their citizens with more access to goods and services. This relationship can be seen plotting the human development index (HDI) vs energy consumption (Figure 1). Where countries like Norway and Iceland consume a lot of electricity per capita and have a high HDI, whereas countries such as Mozambique and Congo consume way less but also have a significant lower HDI.

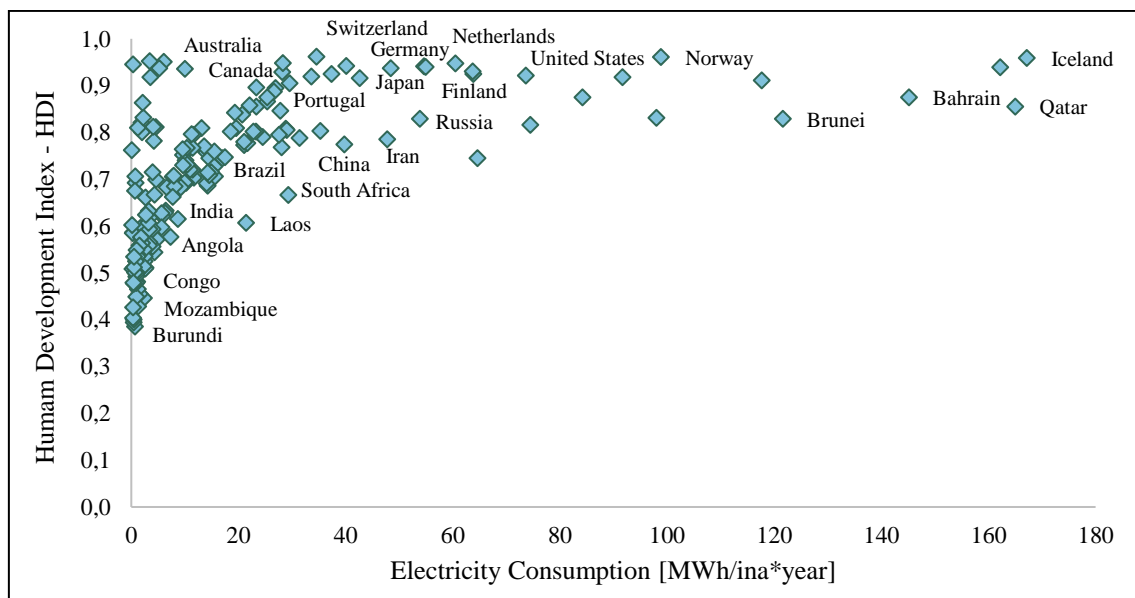


Figure 1. Relation between electricity consumption and HDI [2].

However, in addition to human development relations, there are two other major issues that crucially influence the need for development in the energy sector. The first, intrinsically linked to human behavior, is the constant increase in the world's population and, consequently, the growing demand for energy to meet the needs of the world's population. The second one, on the other hand, of an environmental nature, has to do with the growing concerns associated with the excessive

use of fossil fuels and their associated consequences [3]. These two factors together highlight the importance of developing the energy sector, not only in ways of generating electricity but also in ways of consuming, transmitting and even thinking about energy processes.

Thus, developing new technologies and innovative solutions to meet those challenges can help to improve energy efficiency, reduce greenhouse gas emissions, and enhance the reliability, affordability, and security of energy systems, as well as increase life quality. By studying energy and investing in research and development, it is possible to better understand the challenges and opportunities in this field, and work towards a more sustainable and equitable future. As such, the importance of studying energy and developing new technologies cannot be overstated, and it will be crucial for addressing the complex challenges of the 21st century.

1.1.1. MARINE ENERGY SOURCES

Renewable sources are fundamental to accomplishing the actual energy challenges. Renewable energies are defined as energy that comes from sources that are naturally replenished, such as sunlight, wind, rain, tides, waves, and geothermal heat. These energy sources are considered "renewable" because they can be replenished naturally and sustainably over time, as opposed to non-renewable energy sources like fossil fuels, which are finite and will eventually run out.

Marine energy sources aren't different. These sources include wave energy, tidal energy, ocean thermal energy, and offshore wind energy and all of them rely on an energy source that is naturally replenished. Wave energy is a form of renewable energy that is harnessed from ocean waves using devices such as wave energy converters (WECs). Tidal energy is generated from the rise and fall of tides and can be harnessed for example using tidal turbines. Ocean thermal energy is generated from the temperature difference between warm surface waters and cold deep waters and can be harnessed using ocean thermal energy conversion (OTEC) systems. Offshore wind energy is generated by wind turbines installed in offshore locations, where winds are typically stronger and more consistent, apart from not being affected by buildings, trees, or other obstacles.

The potential for marine renewable energy sources is significant, as oceans cover 71% of the Earth's surface and have a vast amount of energy available. Marine renewable energy sources have the potential to supply up to 20% of the world's electricity demand by 2050 [4]. Currently, most marine renewable energy technologies are still in their early stages of development, and several challenges need to be addressed before they can become a competitive source of energy. These challenges include high capital costs, technology reliability, and environmental impacts. However, recent advancements in marine renewable energy technology and increased investment in research and development have shown promising results.

The future role of marine renewable energy in the energy mix is expected to be significant, especially in coastal regions with high marine energy potential. In addition to reducing greenhouse gas emissions and increasing energy security, marine renewable energy can also provide economic benefits by creating job opportunities and stimulating local economies [5]. As a result, several countries have already implemented policies and incentives to support the development of marine renewable energy technology. In conclusion, marine renewable energy sources have a significant potential to contribute to the global energy mix, and their actual and future role depends on the continued development and deployment of advanced technologies, as well as supportive policies and incentives. This dissertation aims to contribute to the understanding and development of marine renewable energy technology, mainly wave energy with the goal of advancing its role in the energy transition.

1.1.2. WAVE ENERGY

Wave energy research gained widespread attention in the 1960s and 1970s during the global energy crisis, but interest in wave energy conversion technology has fluctuated over the years. Despite some progress, wave energy converters (WECs) remain relatively new, with only a few designs having undergone real-sea testing. Currently, wave energy is not yet economically competitive with other renewable resources, such as wind and solar energy. To become a viable source of renewable energy, capital, and operating expenditures must be reduced by 45%, and power production must increase by 200% [6]. Therefore, a significant improvement, rather than just incremental progress, is necessary for wave energy to achieve economic viability.

The global potential of wave energy is enormous, with estimates of over 2TW [7]. Unfortunately, many existing WECs cannot extract a significant portion of this potential. However, even with low conversion rates, the potential for wave energy is still substantial, and it could play a crucial role in the world's energy scenario in the coming years. World wave energy potential and dominant wave direction are shown in Figure 2. The figure indicates that South Oceania and America have tremendous potential, along with the western coast of Europe and the Pacific coast of North America.

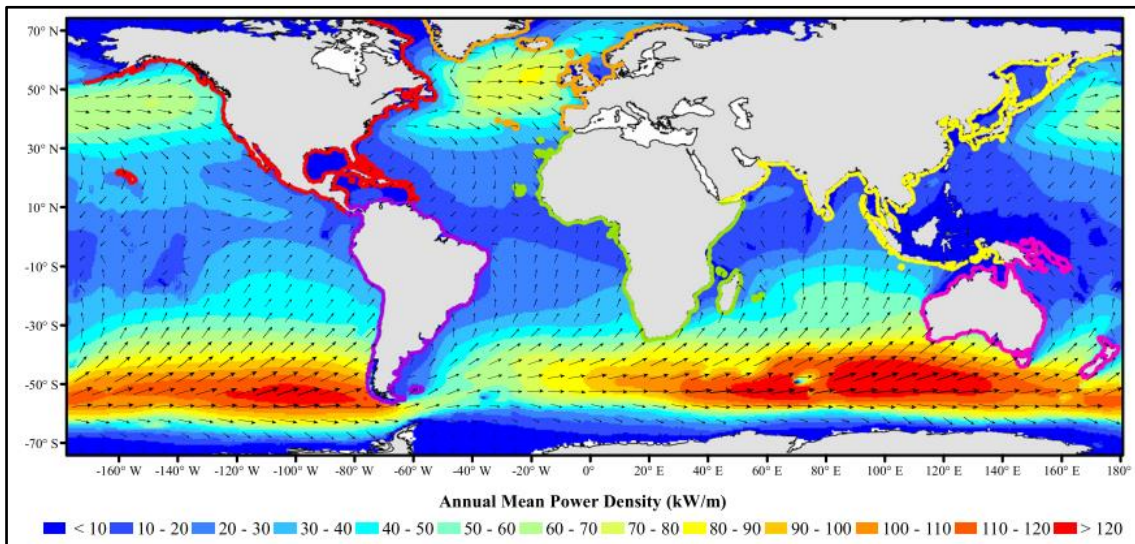


Figure 2. Annual mean wave power density [7].

Despite its vast potential, wave energy remains underdeveloped largely due to the high costs associated with it. The testing and deployment of WECs can be particularly expensive due to the harsh marine environment conditions, the need for significant transportation efforts, and the high labor requirements. Additionally, the awareness of the need to change the energy mix is relatively recent. In the past, fossil fuels were considered the most reliable solution for the energy sector, and it was only after the 2000s that significant changes began to occur. Along with the high costs previously mentioned, this fact has contributed to a lack of encouragement for the completion of wave energy projects.

Currently, the wave energy landscape is evolving rapidly, and significant progress is being made in this field every day. There are more than 1.000 different concepts for WECs, but only a few of them have advanced to the testing phase [8]. Generally, WECs can be classified into four main groups. Overtopping devices capture waves in a reservoir above the waterline and use the potential energy to generate electricity as the water flows through a turbine. Attenuators are composed of multiple segments connected perpendicular to the incident wave, utilizing the

relative motion between the segments to capture energy. Oscillating water columns (OWC) consist of a fixed structure with a turbine above the waterline, which generates electricity as waves push air through the turbine. Point absorbers, which are the most common type of WEC, are floating bodies with a power take-off (PTO) device attached, whose characteristic dimensions are much smaller than the incoming wavelength [5]. This dissertation aims to specifically study hinged point absorbers and their integration into pre-existing coastal structures.

1.1.3. ENERGY SELF-SUFFICIENCY AND CARBON NEUTRALITY IN PORTS

Energy self-sufficiency and carbon neutrality are becoming increasingly important goals for ports around the world, as they seek to reduce their environmental impact and meet global emissions reduction targets. According to the International Maritime Organization, the shipping sector accounts for around 3% of global greenhouse gas emissions [9], and this is expected to increase in the coming years. Ports are key players in the shipping sector and have a significant role to play in reducing emissions. Achieving energy self-sufficiency and carbon neutrality in ports can help to reduce global emissions and improve air quality in surrounding areas.

Wave energy is a promising solution for achieving energy self-sufficiency and carbon neutrality in ports. Ports are typically located in coastal areas with often significant, wave energy potential, making them ideal locations for wave energy technologies. Apart from that, ports usually already have breakwater structures built, which can avoid significant expenses when deploying an onshore WEC. In addition, wave energy is a predictable and reliable source of energy that can provide a stable power supply for port operations.

Some ports around the world have already implemented wave energy technology to move forward in achieving energy self-sufficiency and carbon neutrality. For example, the Jaffa Port in Israel has installed a WEC that generates electricity from the motion of the waves. This technology provides the equivalent energy to supply around 100 households and reduces its carbon footprint by approximately 300t of CO₂ per year.

In conclusion, energy self-sufficiency and carbon neutrality are important goals for ports around the world, and wave energy is a promising solution for achieving these goals. This dissertation aims to contribute to the understanding and development of a specific wave energy technology in ports, with the goal of advancing its role in achieving energy self-sufficiency and carbon neutrality in the port sector.

1.2. OBJECTIVES

Seaports consume a high amount of energy and are sometimes a significant source of pollution. Marine renewable resources, *e.g.*, wave energy, are promising alternatives to supply a significant part of the energy consumption of these infrastructures, thus contributing to the energy self-sufficiency of seaports, supporting their transition to a low carbon economy.

This dissertation aims to study, optimize and experimentally validate a new technology for producing electricity from wave energy, which is based on the conversion of energy from the movement of a floating body connected to an articulated arm fixed to a coastal structure (*e.g.*, breakwater port, jetty, breakwater).

This work is part of the activities of the European project PORTOS – Ports Towards Energy Self-Sufficiency (Figure 3), coordinated by FEUP, which has among its case studies the Port of Leixões and the Ports of the Azores, as well as the participation of the company Eco Wave Power, which owns the technology, that will be studied in detail in this dissertation. This research work is also part of the project WEC4Ports – A hybrid Wave Energy Converter for Ports (OCEANERA-NET COFUND).



Figure 3. PORTOS - Ports Towards Energy Self-Sufficiency Project® [10].

1.3. DISSERTATION STRUCTURE

This dissertation is structured in six chapters. The first one (Introduction) and the second one (Wave Energy Conversion in Coastal Structures) are mainly descriptive and present the state of the art of WECs, their main advantages, similar devices and some considerations about waves as an energy resource. Then, in chapter 3, the case study is presented, namely the Port of Leixões and the floating body (point absorber) type devices, as well as a broad discussion of local sea conditions and how to extract energy of the waves in that zone. Afterwards, Chapters 4 and 5 present, respectively, the numerical analysis carried out in a computer using the software ANSYS® AQWA and the experimental study carried out in the wave-current flume of the hydraulics laboratory of FEUP. In these sections, the main results obtained are shown and discussed. Finally, chapter 6 presents the main conclusions of the work, as well as points that could be improved and considerations for future studies.

2

WAVE ENERGY CONVERSION IN COASTAL STRUCTURES

As previously mentioned in the preceding section, there exist various types of WECs, including moored systems, floating systems, and onshore installations within coastal structures. Typically, the latter type of WEC is linked to lower installation and maintenance costs owing to the ease of accessing the device and its reinforced deployment structure. Nonetheless, it is clear that appropriate and suitable coastal structures, such as breakwaters, are desirable when planning to install a WEC. The present section aims to discuss and showcase the primary challenges and opportunities associated with the integration of WECs into coastal structures. In this dissertation, particular emphasis will be placed on the north breakwater of Port of Leixões and of Douro River, both in Portugal.

2.1. WAVE ENERGY AND BREAKWATER INTEGRATION

The integration of WEC devices with existing marine facilities has become increasingly prevalent, particularly in nearshore applications. This approach is driven by the enhanced economic viability achieved through shared costs for construction, installation, maintenance, and operation, aligning with the objectives of stand-alone WEC devices [6]. Additionally, the integration of WECs into breakwaters can help to overcome some of the environmental and social barriers that are often associated with stand-alone wave energy projects, mainly related to the affectation of coastal and marine ecosystems, fishing communities and also visual impact, with potential to disrupt the natural landscapes.

Furthermore, the integration of wave energy and breakwaters has other benefits, some of which are listed and discussed below:

- 1) Providing both electricity generation and coast protection: Integrating WECs into breakwater structures offers an innovative way to generate clean electricity from the power of ocean waves. By utilizing pre-existing breakwater structures, developers can harness the energy of the waves while protecting the coast from big waves events. This integration provides a unique opportunity to generate clean energy from the ocean while also contributing to the overall sustainability and safety of coastal communities;
- 2) Limiting negative environmental impacts by using pre-existing structures: By integrating WECs into pre-existing breakwater structures, developers can minimize the environmental impact of their installations. This is because the construction of standalone wave energy facilities can have negative impacts on marine ecosystems and coastal

habitats. Apart from that, the fixing structure also requires a significant amount of material and can have high environmental impacts. By using existing structures, developers can avoid disrupting marine environments and avoid the need for extensive construction activities;

- 3) Improved WEC reliability and lifetime: WECs are complex machines that are subject to significant wear and tear from the harsh marine environment. By integrating WECs into breakwater structures, developers can often improve their reliability by using the structural integrity of the breakwater to protect the WECs from wave impact during storm events. This can help to reduce the maintenance and repair costs associated with WECs, making them a more economically viable option;
- 4) Proximity to the electrical grid: Another significant consideration is the proximity of the integrated system to the electrical grid. Offshore WECs require long distance cables in order to transmit the electricity that is generated. Large cables under the ocean are not cheap and can have some environmental impacts as well. This way, by minimizing the need for long-distance power cables, the overall cost and complexity of the energy transmission can be reduced.

To correctly take advantage of all these benefits, it is crucial to meticulously develop WECs that are customized and adapted to each location. This entails having a comprehensive knowledge of the local wave climate and the physical features of the breakwater structure. Moreover, it is vital to contemplate the potential consequences of wave energy conversion on marine ecology and the surrounding environment. By carefully factoring in these elements, it becomes feasible to devise wave energy systems that are both efficient and ecologically sustainable.

Apart from the benefits listed above, wave energy also complements other renewables [11]. Waves carry a substantial amount of energy, particularly in regions approximately between 40 - 50 degrees latitude. Consequently, in countries blessed with abundant wave resources, the potential for harnessing solar energy tends to be relatively lower. On the other hand, the formation of waves depends on wind conditions, but their propagation occurs at varying speeds. As a result, wind and waves often occur at different times, enabling a more consistent electricity supply when these energy sources are combined.

However, apart from the benefits, there are also some main challenges for WECs to overcome. The main challenge is to find a suitable breakwater location [6]. The efficiency of WECs in converting waves is heavily dependent on their location of operation. Factors that contribute to optimal placement include the direction of incoming waves, tidal range, wave reflection, and underwater bathymetry. In addition, the strength of the breakwater must be taken into consideration, as waves, despite their seemingly innocuous appearance, can exert a powerful force that can compromise the integrity of the breakwater structure throughout its operation. Thus, it is fundamental to ensure that the stability and functionality of the breakwater is not affected.

2.1.1. TYPES OF BREAKWATERS

Breakwaters are coastal structures designed to provide protection from ocean waves and currents. The main function of breakwaters is to dissipate the energy of waves and to create a sheltered area for vessels inside ports, and harbors by means of several principles including: wave breaking, dissipation of wave energy through porous flow, wave energy reflection, as well as reducing transmission of wave by overtopping [6]. They are typically constructed as large concrete or stone

structures and are often designed to be visually appealing as well as functional. Usually, the choice between one type of breakwater or the other has to do with the depth of water, with the characteristics of the sea bottom, and with the energy of the waves. This sub-section provides an overview of the different types of breakwaters commonly used in coastal engineering, including their design principles, advantages, and limitations.

2.1.1.1. Rubble Mound Breakwaters

Rubble mound breakwaters are among the most common types of breakwaters used in coastal engineering. They consist of a layer of large stones or concrete blocks placed on top of a foundation of smaller rocks (Figure 4). The design of the rubble mound breakwater is based on the principles of hydraulic stability, which involves ensuring that the structure can withstand the forces of ocean waves and currents. The main advantage of rubble mound breakwaters is their flexibility, which allows them to adapt to changing coastal conditions.



Figure 4. Usual configuration of a rubble mound breakwater in Ria Alvor, Portimão [12].

Even though rubble mound breakwaters are a popular choice for coastal protection due to their flexibility and adaptability, regular maintenance is always required to ensure that the blocks used in their armor layer remain in place and the structure remains stable. This can be a challenge in some locations. Apart from that, the feasibility of proper installation should also be assessed, due to the porous nature of this type of breakwater, the fixing structure may be excessively expensive or unfeasible, especially in very deep waters.

Figure 5 displays a cross section of a typical rubble mound breakwater. As can be seen, the core is protected by a geo-filter and an underlayer. These geotextiles serve as a crucial barrier, effectively thwarting the erosion of the core and seabed by blocking the passage of sediment particles, while still allowing the flow of porewater. Beneath the geotextile, a granular underlayer assumes the role of a protective shield, shielding it from potential punctures caused by the overlying armor elements. Additionally, this underlayer mitigates hydraulic pressure differentials, diminishes lift forces exerted on the armor elements, and fosters interlocking to fortify the armor layer above [12]. Beyond this layer, the armor layer takes center stage, acting as a formidable defense against the damaging impact of wave action. Lastly, the toe of the structure plays a pivotal role in anchoring the armor elements and bolstering geotechnical stability against macroscopic failures, thereby preventing any potential undermining of the structure due to scouring.

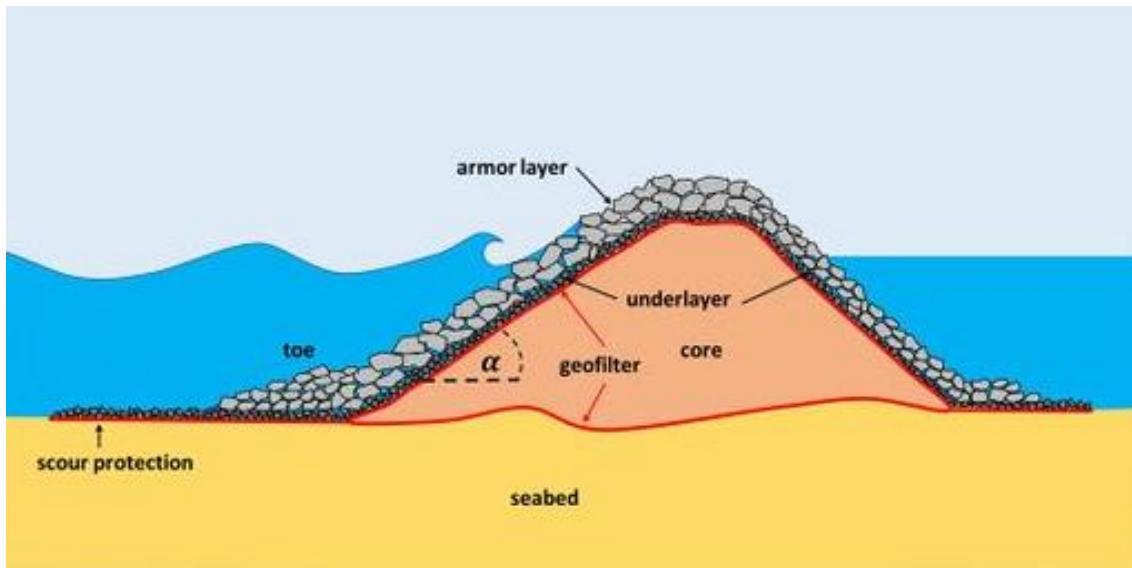


Figure 5. Cross section with its constituent elements [12].

2.1.1.2. Vertical Breakwaters

Vertical breakwaters are characterized by their high vertical walls, which provide excellent protection against waves and currents (Figure 6). These structures are typically made of concrete and are designed to resist the forces of the waves and currents through their mass and geometry. The main advantage of vertical breakwaters is their robustness, which makes them suitable for use in areas with high wave energy, causing big splashes and strong wave reflection effects in front of the breakwater structure [6]. However, they are more expensive to construct than other types of breakwaters and require extensive maintenance, apart from that, they also work as a barrier for sediment transportation which disturbs natural sediment dynamics [6].



Figure 6. Example of a modern large vertical breakwater [13].

The vertical walls of these structures can provide a stable foundation for WECs, and their solid construction can help to reduce the impact of the waves on the WECs. However, the high cost of construction and maintenance may make them less feasible for some projects. Furthermore, this type of breakwater requires a sea bottom with sufficient load supporting capacity. Apart from that, high wave reflections can occur, causing problems for ships entering the port.

2.1.1.3. Composite Breakwaters

Composite breakwaters are a combination of a vertical and a rubble mound breakwater, and can be divided into two categories: either horizontal or vertical composite breakwaters (Figure 7). These structures are designed to combine the advantages of both types of breakwaters while minimizing their disadvantages. The design of composite breakwaters is intended to provide maximum protection against the forces of the waves and currents. The main advantage of composite breakwaters is their flexibility, which allows them to adapt to changing coastal conditions. Despite that, they require careful design and construction to ensure that the different components of the structure work together effectively. Even so, the complex design and construction of these structures can increase the cost and complexity of the project, which may make them less feasible for some projects.

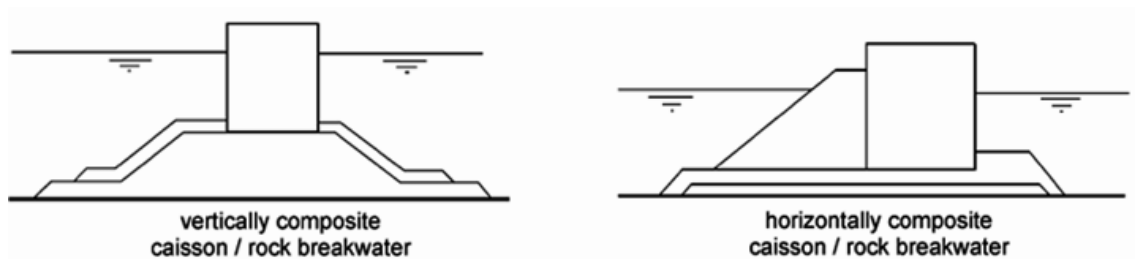


Figure 7. Two main categories of composite breakwaters [14].

2.1.1.4. Submerged Breakwaters

Submerged breakwaters are designed to be placed below the water (Figure 8). They are typically made of concrete or stone and are designed to resist the forces of the waves and currents through their mass and geometry. The main advantage of submerged breakwaters is their ability to reduce the energy of the waves and currents without creating a visual impact. However, they are difficult to construct and require careful design to ensure that they function effectively.

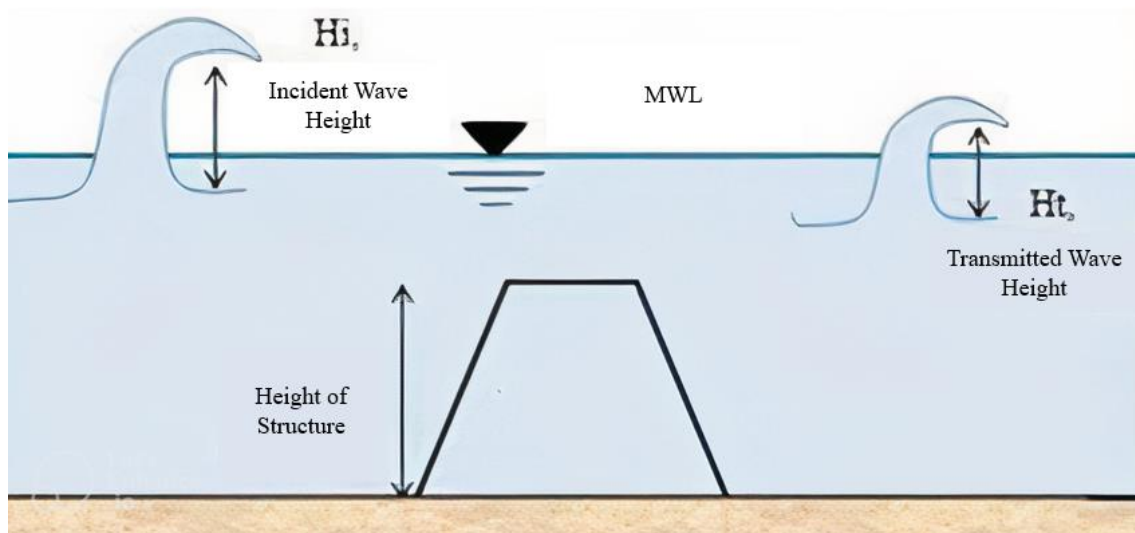


Figure 8. Submerged breakwater cross section [15].

Integrating a WEC in this type of breakwater depends on the type of technology since, after all, it will make the WEC to be also submerged or at least moored to the breakwater. It is interesting mentioning that some submerged devices such as the WaveRoller® (Figure 9) may also work as a submerged breakwater, since its operation consists mainly in a big plane wall that goes one side to another, acting as a barrier for water.

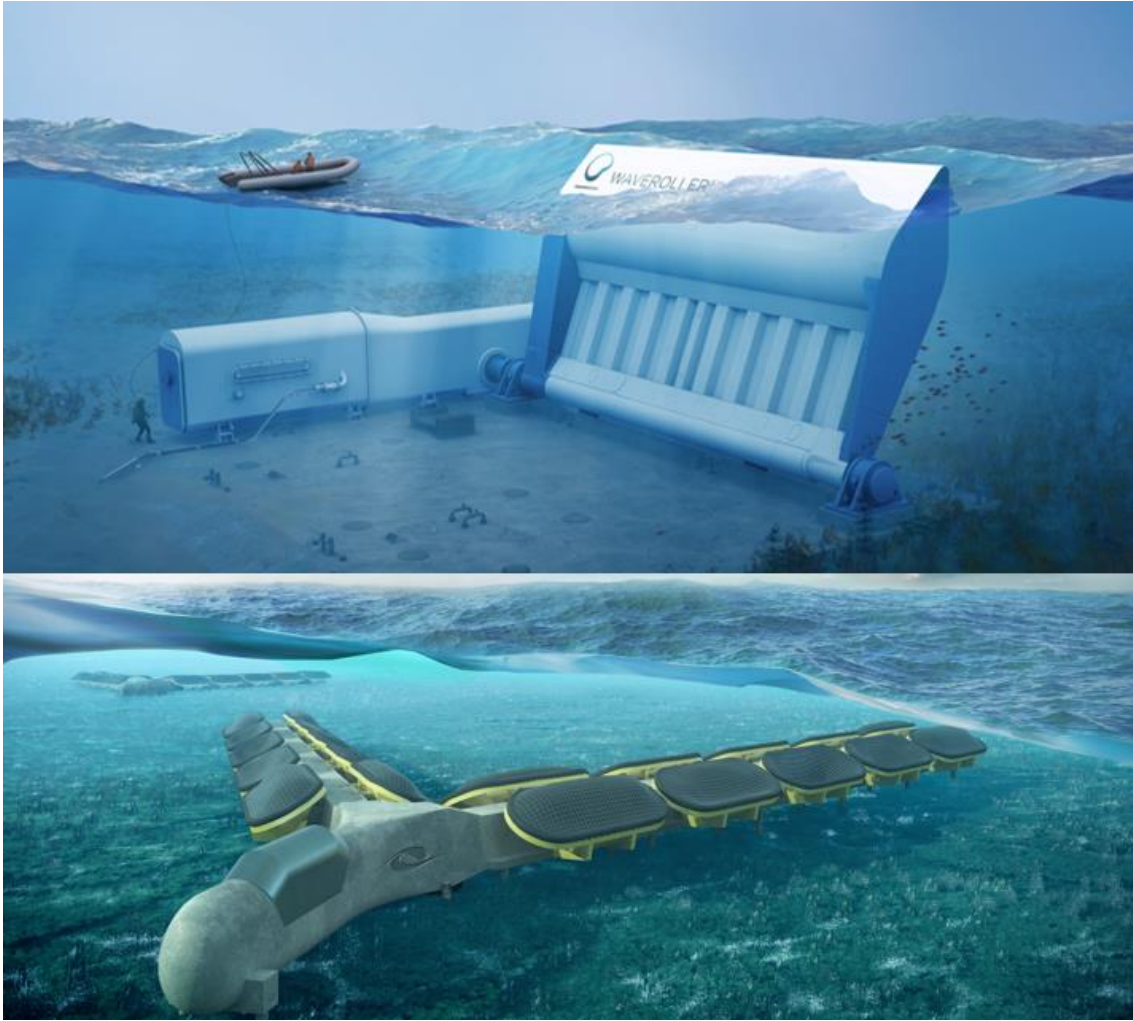


Figure 9. WaveRoller® (top) and Bombora® (down) technologies [16], [17].

Another interesting idea for submerged breakwaters integration with WECs is to take advantage of the pressure differential between the wave crest and trough. This is what the Bombora® (Figure 9) wave plant does. The plant consists of a series of submerged, air-filled chambers that are placed on the seabed or submerged breakwaters. As waves pass over the chambers, the air inside them is compressed, creating a hydraulic pressure that is used to power a turbine and generator. The generated electricity is then transmitted to shore via an underwater cable. The unique design of the Bombora wave energy plant allows it to capture energy from both the rising and falling waves, making it more efficient than traditional wave energy systems. Additionally, the plant operates silently and with minimal impact on the marine environment, making it an attractive option for marine renewable energy generation.

2.1.1.5. Final Considerations

In summary, breakwaters are essential coastal structures designed to provide protection against the action of ocean waves and currents. The type of breakwater used depends on the specific coastal conditions and the level of protection required. Rubble mound breakwaters are flexible and can adapt to changing coastal conditions, while vertical wall breakwaters provide excellent protection against high wave energy and are usually recommended for deep water applications, where the foundation characteristics of the seabed are sufficiently good. Composite breakwaters combine the advantages of both types of breakwaters, while submerged breakwaters are invisible and provide protection without creating a visual impact. The choice of breakwater type depends

on the specific coastal conditions and the level of protection required. Worldwide, most of the designs can be found, with some being significantly more common than others. This fact emphasizes the importance of considering the specific local wave, tide, and general marine characteristics to choose the most suitable type of breakwater.

2.1.2. SUITABLE WEC'S TYPES FOR INTEGRATION

Despite the hundreds of different configurations of WECs, not all of them are suitable for breakwater integration. In this section, only three of the actual most suitable designs will be explained and detailed. It is worth mentioning that only the third type of them is the main focus of this dissertation and will be further discussed in detail.

2.1.2.1. Oscillating Water Column

One of the most promising types of WECs for integration into breakwaters is the oscillating water column (OWC) device. Initially invented by Yoshio Masuda [6], OWCs operate by harnessing the energy of ocean waves and converting it into useful electrical power. OWCs are typically comprised of a partially submerged chamber that is open to the sea at the bottom and contains a column of air (Figure 10). As waves enter the chamber, they force air out through a pneumatic turbine (a), which generates electricity. When the waves recede, air is drawn back into the chamber through the turbine (b), creating a back-and-forth motion that drives the turbine and generates additional power. The location of the opening mouth is typically positioned below the minimal water level established during low tide conditions with some clearance. This strategic placement serves to eliminate the impact of tidal effects on the OWC structure and to avoid the entrance of air. By positioning the opening below the low tide mark, the OWC can operate independently of the tidal cycles, providing a more consistent and reliable performance [6].

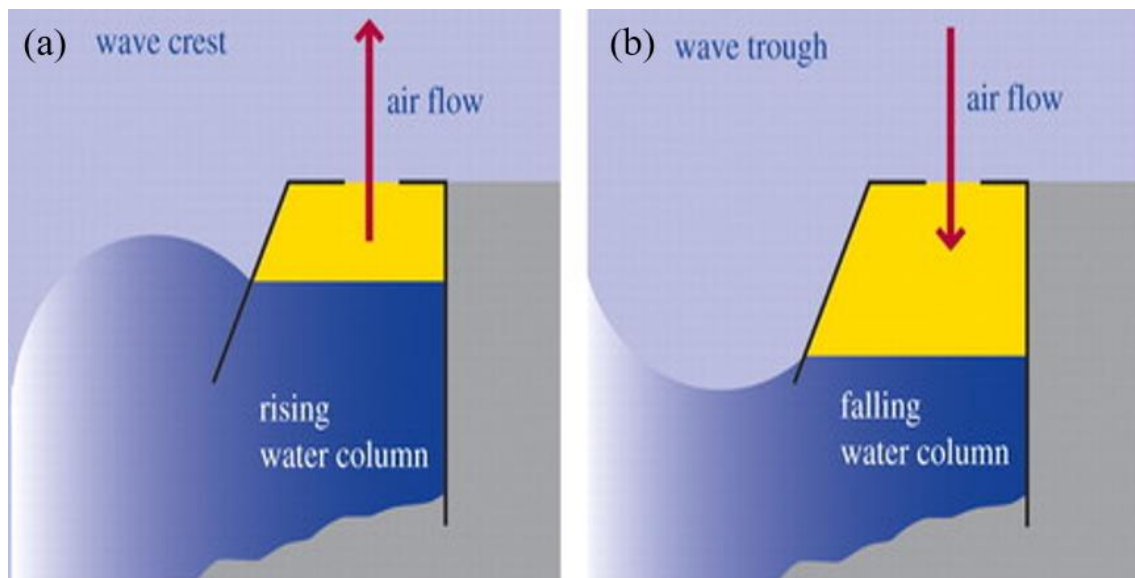


Figure 10. Simple explanation on how OWC extracts wave energy [18].

The key advantages of OWC devices are their simplicity and reliability, as they have no moving parts in contact with seawater, making them less prone to corrosion and fouling. Those WECs can also operate effectively in a wide range of wave conditions, making them suitable for deployment in a variety of locations.

OWCs have been successfully installed in several wave energy projects around the world, including the Mutriku Breakwater in Spain, which was the first commercial-scale wave power

plant to use OWC technology, as explained in the next section. In addition, several other OWC projects are currently under development or in operation in countries such as Scotland (Islay) and Japan (Sagata Port).

Furthermore, OWCs usually have one of the highest efficiencies among others WECs [19]. However, despite their promise, OWCs do have some limitations. They are typically more exposed to the harsh marine environment and must handle strong forces in their structures (there is no storm protection mode). Apart from that, they are also sensitive to changes in water level, which can affect their performance due to the change of their natural period [18]. However, ongoing research and development efforts are aimed at improving the efficiency and performance of OWC devices, as well as addressing these and other challenges to their deployment and commercial viability.

2.1.2.2. Overtopping

Overtopping wave energy converters are a type of WEC that converts the potential energy of spilling ocean waves into electrical energy. Overtopping devices use the kinetic energy of incoming waves to fill a reservoir or basin, which then spills over into a hydraulic turbine, generating electricity. The main components of an overtopping device include the ramp, the reservoir, the turbine, and the control system (Figure 11). The reservoir is designed to capture the water that overtops the device and channels it towards the turbine. The low-head turbine, which is connected to a generator, converts the energy of the falling water into electricity. The control system manages the flow of water and the operation of the turbine to ensure optimal power output.

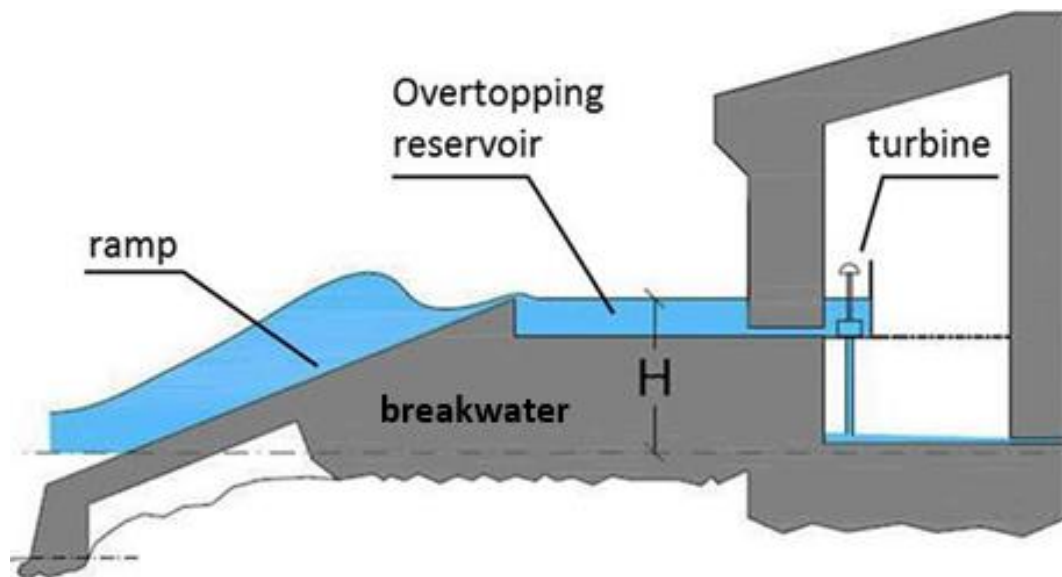


Figure 11. Breakwater integrated with overtopping device scheme [20].

The operation of an overtopping device can be divided into two stages: wave energy capture and electricity generation. In the first stage, the incoming waves approach the device, and the height of the wave crest increases as it moves towards the shore. As the wave crest reaches the overtopping device, it spills over the crest and enters the reservoir. The height of the water in the reservoir increases until it reaches a predetermined level, at which point it is released to flow towards the hydraulic turbine. In the second stage, the water that flows out of the reservoir drives the turbine, which is connected to a generator to produce electricity. The turbine is designed to operate efficiently over a range of water flow rates, and the generator is designed to produce a consistent voltage and frequency for the electrical grid.

One of the key design considerations for overtopping devices is the size of the reservoir. A larger reservoir can capture more water volume from incoming waves, but it also requires more material, and the construction costs are higher, as well as being more exposed to corrosion and fouling effects. Additionally, the efficiency of the turbine is critical in the electricity generation process. A well-designed turbine can maximize the amount of energy converted into electricity, while a poorly designed turbine can significantly reduce the power output. Usually, considering the characteristics of the turbine head, the most suitable ones are from Kaplan type [20].

Overtopping devices have several advantages over other types of WECs. They can be constructed in various sizes, ranging from small-scale devices for rural areas to large-scale installations for utility-scale power generation. They also have low visual impact, as most of the devices are located below the waterline.

In conclusion, overtopping WECs are a promising technology for harnessing the power of ocean waves to produce electricity. By capturing the energy of falling water, overtopping devices can generate renewable energy while minimizing the environmental impact. The efficiency and reliability of the turbine and control system are critical factors in maximizing the power output of overtopping devices, and further research and development in this field will be key to unlocking the full potential of this technology.

2.1.2.3. Point Absorbers

Point absorber devices (Figure 12) are also a kind of technology that enables the transformation of wave energy from the ocean into electrical energy, taking advantage of their natural up and down movement (wave crest and trough). These devices can be constructed both in onshore and offshore locations with high wave energy potential. Those WECs consist of a buoyant structure that moves up and down with the wave motion. The movement of the buoy drives a generator, which converts the kinetic energy of the waves into electrical energy that can be used to power homes and businesses. The buoyant structure of a point absorber device is typically a cylinder or floating buoy that is attached to a mooring system anchored to the seafloor. As the waves pass by, the buoy or cylinder moves up and down along the tether, which in turn drives a PTO system to generate electricity.



Figure 12. The heave motion of the buoy converts the energy in point absorbers [21].

These devices employ different types of PTO systems, including hydraulic, pneumatic, and mechanical systems. In hydraulic systems, the buoy's motion generates hydraulic pressure, which is utilized to operate a hydraulic motor that generates electricity. Pneumatic systems work similarly but use compressed air instead of hydraulic fluid to produce power. Mechanical systems directly drive a mechanical generator using the motion of the buoy.

Furthermore, this type of device has some advantages, such as their small and compact design, making them feasible for deployment in a variety of locations, including shallow waters and near-shore areas. They are also less affected by the direction of the incoming waves compared to other WECs, thereby improving energy capture efficiency. However, point absorber devices have their own set of challenges. They experience significant mechanical stress and fatigue due to constant oscillations induced by wave motion, which can cause wear and tear on the device.

Moreover, the tethers or mooring systems used to anchor the device to the seafloor may be subject to degradation, which can impair the device's performance and lifespan. In spite of the challenges, point absorber devices remain an attractive technology for harvesting renewable energy from ocean waves. On-going research and development efforts aim to enhance the efficiency and reliability of these devices while addressing the technical and economic challenges of their deployment and operation in real-world conditions.

2.1.3. EXAMPLES OF WEC INTEGRATION INTO COASTAL STRUCTURES

There are already some WECs concepts integrated into coastal structures, such as breakwaters. This section aims to present and briefly discuss some of these examples. Table 1 shows several examples of projects and real installations of WEC integration into, not only breakwaters, but coastal structures in general. As can be seen, most of them rely on OWC technology due to the benefits previously discussed [6].

Table 1. Examples of WEC integration into coastal structures [6]

WEC - Breakwater	Type	Water Depth (m)	Output Power (kW)
Sakata Port Breakwater	OWC	18	27,3
Stellenbosh Wave Energy Converter (SWEC)	OWC	14	5.000
Shore Wave Energy Converter (ShoreSWEC)	OWC	14	6
Mutriku Wave Energy Plant	OWC	5	68,5
Siadar Wave Energy Project 1	OWC	8	4.000
Siadar Wave Energy Project 1	OWC	8	30.000
Land Installed Marine Power Energy Transmitter (LIMPET)	OWC	6	113
PICO, Azores, Portugal	OWC	8	31,7
Trivandrum, India	OWC	12	125
Sea Slot-Cone Generator (SSG)	Overtopping	6-18	49-62
Overtopping Breakwater for Energy Conversion (OBREC)	Overtopping	25	-
Piston-Type Porous Wave Energy Converter (PTPWEC)	Piston	-	-

2.1.3.1. Mutriku Port OWC - Spain

Mutriku Port, situated on the northern coast of Spain in the Basque Country, serves as both a fishing port and a notable site for WEC development. The WEC project in Mutriku Port is the result of dedicated efforts by Ente Vasco de la Energía (EVE), the Basque energy company committed to advancing renewable energy initiatives. The Mutriku WEC project is one of the world's first grid-connected wave energy projects and has been operational since 2011.

The Mutriku WEC project consists of ten Wells turbines that are integrated into a section of 100m of the breakwater of the port (Figure 13). The Wells turbine is a type of turbine designed to operate in unidirectional air or water flows, making it well-suited for wave energy applications. Usually, the efficiency of this turbine is lower (50-60%) that of conventional turbines, but higher than achievable with conventional turbines in alternating mode [22]. The turbines are driven by the motion of the waves, which hit the breakwater and cause air to flow back and forth through the turbines. The airflow drives the turbines, which in turn drives generators to produce electricity. The project has a peak power output of 296kW and generates enough electricity to power around 250 homes. This pilot power plant has been successful in demonstrating the viability of wave energy as a source of renewable energy and has helped to advance the development of WEC technology.



Figure 13. Mutriku OWC breakwater integration [23].

However, the Mutriku WEC project has also faced some challenges. The project has experienced significant downtime due to the harsh ocean conditions and the wear and tear on the equipment. The turbines and generators require regular maintenance and replacement, which can be costly and time-consuming. Despite these challenges, the Mutriku WEC project has provided valuable insights into the potential of wave energy as a renewable energy source and has helped to pave the way for future WEC projects around the world.

2.1.3.2. Sakata Port OWC - Japan

The Sakata Port breakwater (Figure 14) stands as a pioneering and highly successful example of integrating breakwater and WEC technology, with its initial testing conducted in 1989 [6]. This innovative structure, situated in Japan at a water depth of 18m, employs the OWC concept and is specifically designed for shallow water applications. It demonstrates exceptional wave resistance capabilities, withstanding waves of up to 5m in height.

To harness wave energy, the breakwater incorporates a 7m wide opening that directly connects to an OWC unit positioned at the center of the structure. This configuration ensures both stability and safeguarding for the OWC component [6]. The energy conversion process within the device utilizes two Wells turbines, enabling the conversion of wave energy into electricity. Preliminary estimations indicate a power output of approximately 60kW. The Sakata Port breakwater exemplifies the successful integration of WEC technology within breakwater structures, showcasing its potential for sustainable energy generation.

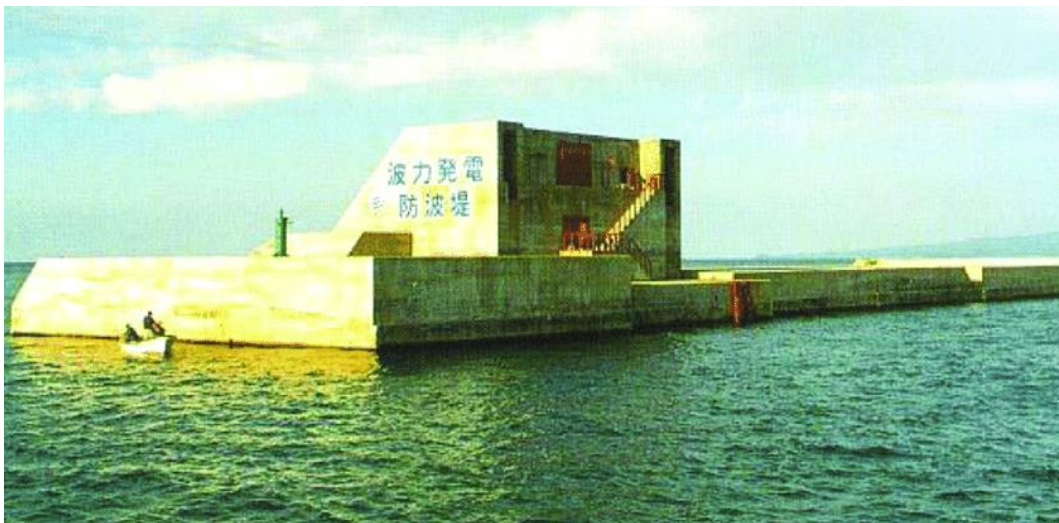


Figure 14. Sakata OWC chamber in the breakwater [24].

2.1.3.3. Jaffa Port - Israel

The Jaffa Port, located in Tel Aviv, Israel, has recently integrated the Eco Wave Power (EWP) technology to generate electricity from wave energy (Figure 15). EWP technology is a point absorber system that uses a float on the water surface to capture the energy of waves and convert it into electricity. The Jaffa Port project consists of a series of EWP units installed on the breakwater structures, with a total capacity of 100 kW. The motion of the floaters drives a hydraulic pump that pressurizes a fluid, which is then used to generate electricity through a hydraulic motor and a generator. The generated electricity is then fed into the local grid for consumption.

The Jaffa Port project started in 2016 and has been operational since 2018. The project has been successful in generating electricity and reducing greenhouse gas emissions. It has also created new job opportunities and promoted the development of the local renewable energy sector. The integration of EWP technology at Jaffa Port is a significant step towards the promotion of clean and renewable energy sources. It serves as an example of how wave energy can be harnessed to generate electricity in an efficient and environmentally friendly manner. The Jaffa Port project has attracted attention from other coastal regions around the world, and it is expected that more projects using EWP technology will be developed in the future.



Figure 15. EWP WECs placed in the Jaffa port [25].

2.1.3.4. Gibraltar World War II Ammunition Jetty - Gibraltar

The establishment and implementation of the EWP wave energy power station in Gibraltar (Figure 16) symbolize a notable advancement in the commercialization of EWP technology. This initiative received co-funding from the EU Regional Development Fund and private investment groups, underscoring the collaborative efforts and driving its development [26]. In 2014, EWP entered into a 5MW agreement with the Government of Gibraltar and the Gibraltar Electricity Authority, which paved the way for the construction of the initial 100KW phase of the 5MW power station situated on the eastern side of Gibraltar. The power station was officially opened in May 2016 and is currently operating through a power purchase agreement (PPA). This pioneering project demonstrates the potential of wave energy technology to provide a reliable and renewable source of electricity while highlighting the importance of continued research and development to improve its efficiency and reduce its environmental impact.



Figure 16. EWP WECs placed in the Gibraltar old ammunition jetty [27].

Unfortunately, EWP has recently announced plans to move its wave energy power plant from Gibraltar to AltaSea's premises in the Port of Los Angeles citing its increasing interest in the US market and the condition of the Ammunition Jetty as primary reasons [28]. With almost six years of operational experience and over 49,632 grid connection hours in Gibraltar, EWP is trying to get ready to expand its pioneering technology to larger scales and new regions, in line with its new agreements.

2.1.3.5. Overtopping Breakwater for Energy Conversion - Italy

The concept of the overtopping breakwater for energy conversion (OBREC) device capitalizes on wave energy by utilizing the overtopping phenomenon of existing breakwaters. It captures the overtopped water and channels it to drive a low-head turbine, thereby generating clean energy. OBREC devices are adaptable to various breakwater shapes and structures and are currently undergoing development. This integration concept is particularly intriguing as it effectively enhances the functionality of standalone breakwater devices, enabling them to simultaneously serve as wave breaking and wave energy extraction systems [6].

An exemplary instance of an OBREC device is the Naples harbor prototype, which represents the world's first fully integrated overtopping wave energy converter within an existing breakwater. In this prototype, a section of the rubble mound armor layer is replaced by a front reservoir specifically designed to capture the overtopping waves for electricity production [29]. The prototype comprises a concrete structure with a sloping impermeable front ramp that directs the overtopping waves into a reservoir situated behind it. To harness the energy, low-head turbines are employed, capitalizing on the difference in water levels between the reservoir and the mean sea level. The project received full funding from Italian and European authorities, reflecting their keen interest in research and development in this field.

2.1.3.6. PICO OWC - Portugal

The Pico OWC (Figure 17), situated on Pico Island in the Azores, serves as a noteworthy European pilot project that reached completion in 1999, thanks to funding from the European Commission, Portuguese utilities, and the Portuguese State. Notably, despite lacking attachment to any breakwater, the PICO plant showcases a successful integration between WECs and coastal structures. Initially overseen by the scientific coordination of Instituto Superior Técnico (IST) in Lisbon, the ownership of the plant was later transferred to WavEC in 2007 [30]. Enclosed within a 1050m³ chamber, the OWC plant incorporates a Wells® turbine with a peak power output of 400kW (operating at 1475rpm) and an outer diameter of 2,3m [31].

Although the Pico Plant enjoyed initial success, it eventually encountered structural deficiencies, leading to various initiatives aimed at its recovery and promotion. In February 2016, a decision was made to close the plant due to wear and tear on the submerged section of the structure. The closure aimed to ensure safe and environmentally friendly conditions. However, due to the Regional Government's interest in a feasibility analysis for the plant's recovery, the decision was temporarily suspended. Unfortunately, conclusive assessment of its viability was unattainable, resulting in the subsequent dismantling of the plant. Following a partial collapse in April 2018, the plant was disconnected from the grid, and necessary security measures were implemented.

The Pico Plant made a substantial contribution to wave energy research, development, and innovation. It played a role in two European networks dedicated to testing infrastructure for wave energy technologies, providing international teams with access to valuable resources. Throughout its lifespan, the Pico Plant attracted funding exceeding 35 million euros, with 11 projects directly

contributing approximately 2 million euros toward its operation, maintenance, and research activities. Moreover, the plant served as a platform for over 8 doctoral theses, numerous master's theses, and scientific internships. While its closure is regrettable, the Pico Plant remains a pivotal reference for the advancement of wave energy technology and its future implementation [30].



Figure 17. PICO OWC located in Porto Cachorro, Azores [31].

2.1.3.7. WaveStar® - Denmark

The Wavestar® device (Figure 18) is an example of a WEC that utilizes multiple bodies combined into a larger structure. The device consists of aligned rows of round floats, called point absorbers, attached to a bridge structure that is fixed to the seabed using steel piles cast into concrete foundations. The structural bridge supporting the floats is positioned in the direction of the dominant wave direction. As waves pass, the floats move up and down, pumping hydraulic fluid into a common hydraulic manifold system (hydraulic PTO), due to the proximity between floaters, the hydrodynamics interaction should also be considered when studying this type of WEC [32].



Figure 18. WaveStar unit installed in Hanstholm, Denmark [33].

This system produces a flow of high-pressure oil into a hydraulic motor that directly drives an electric generator. A prototype with two floaters, each with a diameter of 5m, has been undergoing sea trials at DanWEC in Hanstholm, Denmark [5]. This device is an excellent example of a WEC that utilizes multiple floating bodies and can generate electricity by harnessing wave energy.

The WaveStar® test unit at Hanstholm was installed in September 2009. Starting from May 2010 the converter was running in unmanned continuous operation. The WEC has survived several storms with no damage. The first measurements of the power production agreed with expectations. In order to minimize the risk of damage, the WaveStar engineers chose to start the initial testing using a very simple control strategy. Hereby the peaks in forces, motions and powers would only apply moderate load to the PTO. Calculations show that a new optimized PTO control will increase the power production significantly [34].

2.1.3.8. Porto do Pecém - Brazil

The first national wave power plant in Brazil was developed by COPPE/UFRJ in order to diversify the national energy mix. It was installed in 2012 at the Pecém port in Ceará, 60km away from Fortaleza, to contribute to the port energy self-sufficiency. The region's characteristics, such as the prevalence of low waves (between 1 and 2m high) and their frequency due to the trade winds, were crucial for defining the project location. The simulations were done in the COPPE's Oceanic Tank, the world's deepest artificial tank, with more than 23 million liters of water [35].

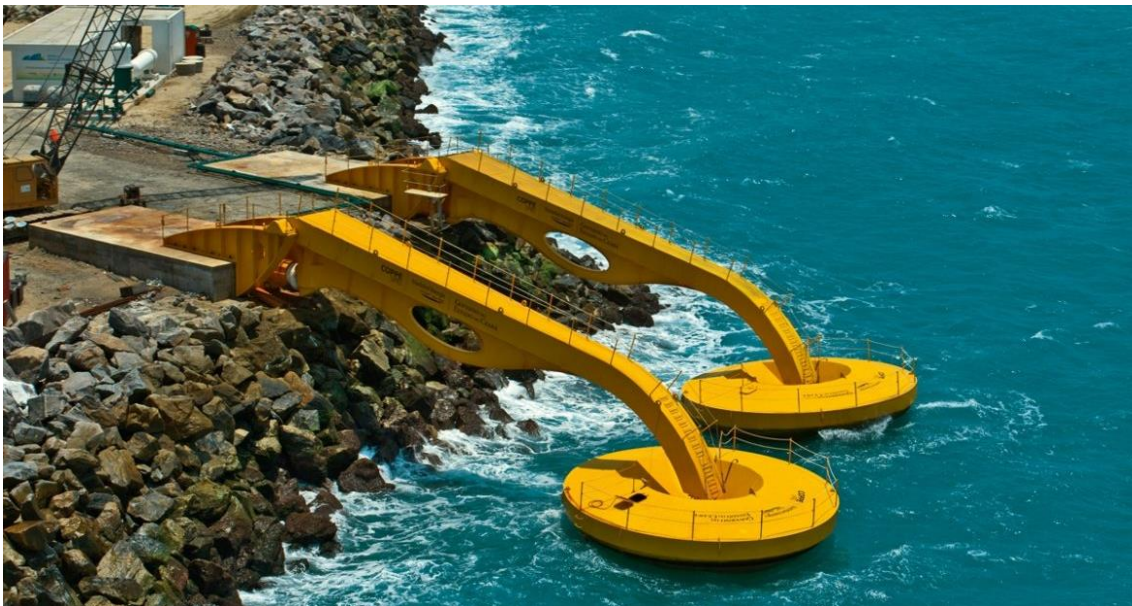


Figure 19. Port of Pecém WEC [36].

The Brazilian wave power plant project developed by COPPE stands out for using a high-pressure system to move the turbine and generator, a concept patented by the institution. The device consists of two large floating mechanical arms fixed on articulated horizontal structures, as seen in Figure 19. These structures move with the action of waves, operating as lever arms with circular buoys at one end that move according to the alternating and repetitive motion of the waves. This movement activates a hydraulic pump at the other end, which compresses the fluid to maintain the pressure of the hyperbaric chamber. The pressurized hyperbaric chamber, initially filled with water and nitrogen, releases a jet of water whose pressure is equivalent to a 400m high waterfall, generating rotation in the turbine's axis, which is then transmitted to the generator to convert mechanical energy into electrical energy [35].

2.2. ESSENTIAL FEATURES OF A WEC

Valuable and detailed information about the main “rules of thumb” for WEC design and characteristics can be found in specific literature. These “rules” can set an array of fundamental parameters that should be kept in mind when planning the installation of a WEC. Most of them come from theoretical concepts and demonstrations that set limits for energy capture efficiency and others are based on expertise from previous models and prototypes. The ocean, as already mentioned, is a very harsh environment and a good WEC device should be able to survive in that environment producing significant amounts of energy and not being excessively expensive. Some of the basic “rules” that a WEC designer should consider when designing a device like this are:

1) **Survivability:** WEC devices are exposed to a range of ocean forces, including waves, tides, and currents. Therefore, these devices must be designed to withstand these forces and ensure that they remain functional during their operational life. The survivability of a WEC depends on its size, shape, and materials used. Devices that are not properly designed may experience damage or even failure during operation, leading to costly repairs and replacements. By considering survivability during the design phase, WEC devices can be designed to ensure their safety, longevity, and optimal performance, which is essential for their overall feasibility;

2) **Reliability and Maintainability:** The reliability of a WEC device is essential to ensure that it can operate over an extended period, generating consistent energy output with minimal maintenance requirements, mainly because they are often located in remote areas, and maintenance and repair activities can be challenging and expensive. A reliable device can also help reduce the cost of ownership, making WEC projects more feasible. By designing WEC devices with reliable components and materials, and ensuring that they undergo regular maintenance and inspections, the overall feasibility of the project can be enhanced.

Another interesting point to be highlighted under the maintainability scope is the necessity of bringing offshore WECs back to shore to perform maintenance and repair activities. This is tremendously expensive and has significant implications for the WECs environmental aspects as well as in its overall performance. Smaller and more assembled components should be considered in order to promote in-situ operations;

3) **Performance:** The performance of a WEC device is affected by several factors, including wave characteristics, device design, and operational conditions. A well-designed device can capture as much wave energy as possible and convert it efficiently into electrical power. Traditionally, it is often stated that a proficient wave absorber also possesses the ability to generate waves. This implies that when an object moves through the water, it produces a wave in accordance with its motion, commonly referred to as a radiated wave [5]. The effectiveness of such a body in absorbing an incoming wave is directly linked to how closely the radiated wave aligns with the characteristics of the incoming ocean wave. In essence, the greater the resemblance between the radiated wave and the incoming wave, the higher the efficiency of the body in wave absorption. By optimizing the performance of a WEC device, the overall feasibility of the project can be improved, as more energy can be generated, and the cost of energy production can be reduced.

Apart from that, designers should also be aware that designing a WEC to operate efficiently over sea conditions that provide the largest contributions to annual productions (optimal conditions) are highly more desirable than designing it for the most common sea

state, in which, most of the times will not contribute as much to the overall energy production [37];

- 4) Scalability: After testing the prototype several times the design must be scalable to real size dimensions, otherwise, the project will never make to be a multi-MW device as it should in order to be economically feasible [5]. Apart from that, the design should also be open to further enlargement projects, increasing its deployment possibilities;
- 5) Environmental Sound: WEC devices have the potential to reduce the world's population's dependence on fossil fuels and contribute to the reduction of carbon emissions. However, there are some environmental concerns related to the installation and exploration phase that should be taken into account when planning a WEC deployment. Proper environmental impact assessments should be carried out during the design phase to ensure that the devices are able to mitigate the environmental damage they created by not emitting pollutants.

It should be noted that there exists an infinite number of other rules of thumb that can be followed when designing WECs, particularly with regard to economics and energy conversion systems. However, for the purposes of this dissertation, only fundamental concepts and general guidelines were deemed necessary to provide the foundational understanding for the subsequent sections.

2.3. WAVE RESOURCE

Wave energy can be seen as a concentrated form of wind energy and even, ultimately, of solar energy. In fact, if there was no sun shining on the earth's surface there wouldn't be winds blowing above ocean surfaces and the waves would never be formed [37]. Said that, just like wind and solar or any other source for energy conversion, wave energy potential evaluation also relies on quantifying the available resource. The resource, in this case, is of course the energy carried by the waves. Several studies were carried out in order to quantify the wave resource through the world's coastline and most of them provided enthusiastic results, showing up the potential of wave energy as a renewable source of energy.

Although it is still underdeveloped, wave energy has several particularities that strongly encourage researchers and investors. First, and as already said, wave energy is a renewable and clean source of energy, avoiding harmful emissions to generate electricity. Another advantage is its predictable output, with power levels possibly being forecasted 1-2 days in advance. Additionally, wave energy has no specific timing, *i.e.*, the waves are always there, with more or less power of course, but the generation of electricity is continuous, different from solar for example, which is only available for production during the day. The seasonal load of wave energy also correlates with electricity consumption in the northern hemisphere, providing an important source of energy when demand is the highest (winter). Moreover, in terms of power density, wave energy has a higher density than wind and much higher than solar, making it a more efficient option for generating electricity. Finally, wave energy is a vast available resource, capable of providing up to 10-20% of worldwide electricity consumption [38].

The wave power density represents the amount of wave energy transmitted per unit length of wave crest along the water column in the direction of wave propagation [37]. For deep waters irregular waves, this power can be estimated as the following:

$$P_w [W/m] = \frac{g^2 \rho H_s^2 T_E}{64\pi} \quad (1)$$

where ρ represents the density of the seawater (in this text always considered as 1025kg/m^3), g the acceleration of gravity ($9,81\text{m/s}^2$), H_s the significant wave height (m), and T_E the wave energy period (s). This formula allows for rough estimations of the wave energy potential for a specific location. However, the formula only allows estimations for available power. The converted power requires more detailed and complex analyses to be properly estimated. In this section, firstly a global approach is presented, indicating the world hotspots for wave energy conversion, after that, a more detailed sub-section is destined for Portuguese and Brazilian situations.

2.3.1. GLOBAL SITUATION

Figure 2 was an output of the work developed by Gunn K and Stock-Williams [7]. Their work significantly changed the previous estimations made regarding wave energy potential by making more accurate assumptions and considering important factors when working on the estimations. They estimated the world's global available wave power in 2,11TW, in which, a massive share would be disregarded due to non-extractable conditions. When using the Pelamis® device power matrix, the extractable power showed to be only 5% of the total power, but this fact is strongly affected by the type of device utilized.

Despite the visual strength that the southern hemisphere might seem to have (Figure 2), the quantities of wave power reaching the south and north hemisphere's coastlines are almost equal: 1,07TW for the north and 1,05TW for the south. This highlights the fact that high wave power results from long fetches and no coastline to work as a barrier, whenever there is a barrier (coastline) the wave power is strongly reduced [7]. When looking at the continents, North America is the top one with more available resources, followed by Oceania and South America, however, when comparing with the continent electricity consumption the scenario inverts, and North America together with Asia and Europe would be the only continents that wouldn't be able to be entirely supplied by wave energy in an ideal and unrealistic scenario. Oceania on the other hand has significantly more power available than it consumes. Table 2 together with Figure 20 displays useful data for the six different continents.

Table 2. Population, wave power availability and annual mean power by continent [7] [39]

Continent	Population	Power Available (GW)	Annual Mean Power (GW)
North America	376.000.000	427 ± 18	577
Oceania	44.800.000	400 ± 15	142
South America	660.000.000	374 ± 16	127
Africa	1.417.600.000	324 ± 12	84
Asia	4.760.000.000	318 ± 14	1.488
Europe	741.600.000	270 ± 20	438
Total	8.000.000.000	2113	2.855

The power availability map also allows drawing conclusions about countries leading wave energy research. After all, there is no reason to support the development of a technology that isn't feasible in a specific country. Said that, countries such as the United States, Canada, Japan, and mainly Australia and Atlantic European countries are the ones with more research and development activities related to wave energy exploration.

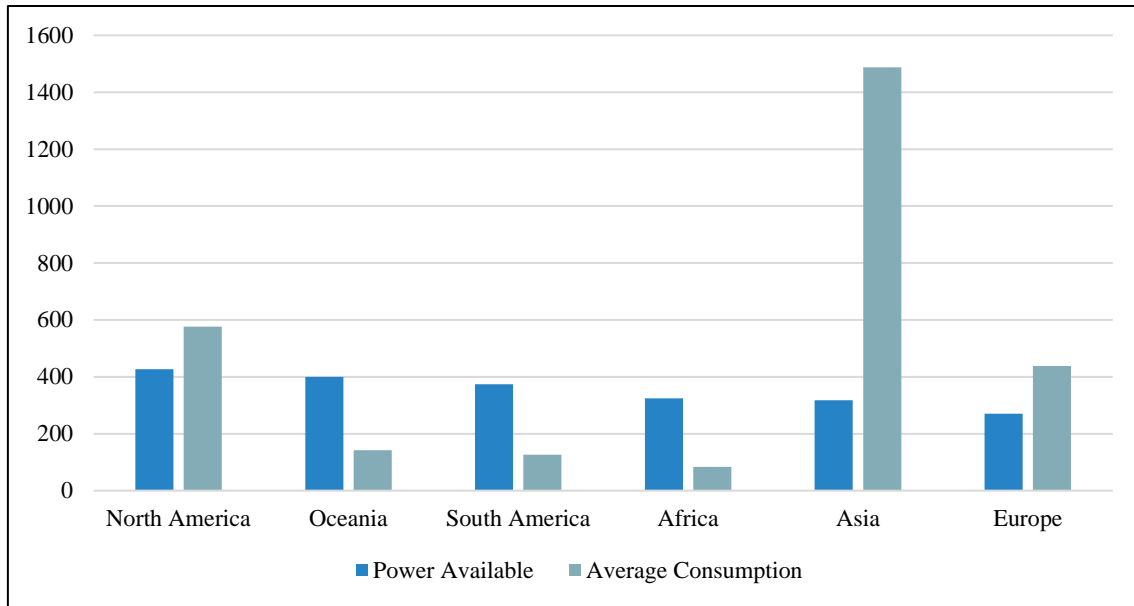


Figure 20. Power available versus average consumption annual mean power necessities [7].

2.3.2. PORTUGAL SITUATION

Portugal lies directly on the Atlantic Ocean, along the western coast of Europe. This location offers great potential for harnessing wave energy, as shown in Figure 21. Upon analyzing the figure, it is possible to identify two main regions along the Portuguese coast that offer different wave energy power resources. The northern and central coastal regions have the highest values, while the southwestern coast has less potential.

Although offshore locations offer significant wave energy potential, most devices are not designed to be deployed far from the coast. Therefore, it is more informative to look at the values of power nearshore. Figure 21 displays both offshore and nearshore wave energy potential throughout the Portuguese coast, with the nearshore potential represented by color bars next to the coast.

Analyzing the nearshore potential can yield interesting conclusions. For instance, while the region between Porto and Viana do Castelo may appear the most promising due to its high offshore power value, its nearshore potential experiences the biggest reduction. This is because the shape of the coast in that region does not face the dominant wave direction coming from the ocean, as indicated by the arrows on the map [37]. On the other hand, the region between Peniche and Nazaré exhibits the highest potential for nearshore applications, as it is aligned with the dominant wave direction.

Finally, the total nearshore (inner continental shelf at a depth of 50m off the coast of Portugal) offers a total annual omni-directional available wave energy resource of approximately 77TWh, which represents a 14% reduction compared to the offshore value of 90TWh [37]. The sea states that offer significant wave heights between 3 and 4m and energy periods between 9 and 10s, are the ones that most contribute to the total annual production, with winter events being responsible for 75% of the occurrences [37]. These findings suggest that there is significant potential for harnessing wave energy in Portugal, particularly in the north and during the winter season, and that further exploration of this resource could lead to significant advancements in renewable energy production to the country scenario. Further information regarding specific ports in Portugal that are the aim of this thesis will be given in the coming chapters.

2.3.3. BRAZIL SITUATION

Brazil has a significant coast extension facing directly the Atlantic Ocean with strong wave energy potential, however, there are some big differences among the regions. The southern coast of Brazil exhibits higher values of wave energy, with some coastal areas reaching almost 2m of average significant wave height, while in the north, the average significant wave height is only 1m. When talking about wave power, the difference in magnitude is even greater, with nearshore values up to 11kW/m at the south and 5 to 8kW/m at the north [40]. This variation can be graphically seen in Figure 21.

The values show that the highest energy flux is found in the states of Rio Grande do Sul, Santa Catarina, and São Paulo, all divisions situated in the south. Conversely, the smallest values were observed off the coast of Bahia and Pernambuco which are all located in the Northeast. The larger variation in magnitude can be attributed to the angle at which the swell approaches, which in the southern regions is predominantly south oriented, and by the varying wind regimes in the respective regions [41]. Information regarding the average significant wave height and the wave periods are strongly varying throughout the coastline, again, it is worth remembering that Brazil's coastline has 7.491km of extension.

These numbers suggest that the southern coast of Brazil is more suitable for the implementation of WECs. However, additional studies are required to determine the most appropriate specific regions for such implementation as a function of technologies.

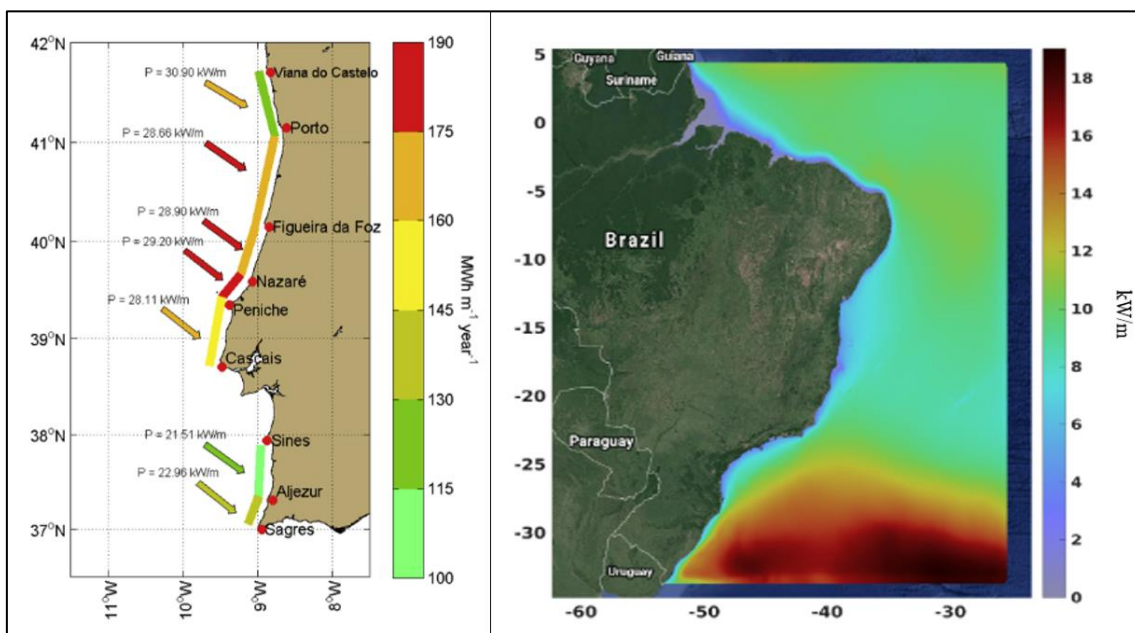


Figure 21. Mean wave energy potential along the Brazilian and Portuguese coast [37], [40].

2.4. ENERGY PRODUCTION AND CO₂ REDUCTION

As soon as the wave resource is fully characterized it is time to evaluate energy production. This can be easily done by just crossing the wave resource matrix with the WEC power matrix. As previously discussed, each different type of WEC has a different working principle and thus has a different power matrix configuration. This can lead to different energy production values for the same energy resource at site. Said that, for a high-quality wave energy production estimation, a reliable and adequate power matrix should be used.

The wave resource matrix (also known as joint probability distribution), for a particular area displays the frequency of occurrence (usually how many hours in a year) of a specific sea state characterized by a significant wave height and a peak wave period [42]. The matrix is typically created by combining data from various sources, including satellite data, oceanographic models, and direct measurements, to provide a comprehensive picture of the wave resource in a particular region. Figure 22 shows, as an example, the offshore wave resource matrix for the coast between the northern cities of Porto and Viana do Castelo in Portugal. It is not hard to realize that the most common sea state has between 3 to 5m of significant wave height and 8 to 12s of energy wave period. In a real sea state, not all combinations of height and period are present or feasible, resulting in numerous empty cells within the scatter plot. To obtain a comprehensive overview, a scatter diagram was generated for the entire year by aggregating the cell points for each month. This cumulative analysis accounted for a total of 8760h throughout the year (or 8784h in a leap year) [42].

On the other hand, the power matrix (Table 3) displays the power output expected for a specific sea state. The power matrix considers various factors that affect the WEC's performance, such as the WEC's geometry, hydrodynamic properties, control system, and the characteristics of the waves it is exposed to. By simulating the WEC's behavior in different wave conditions, the power matrix can provide an estimate of the WEC's power output, as well as its efficiency and performance characteristics.

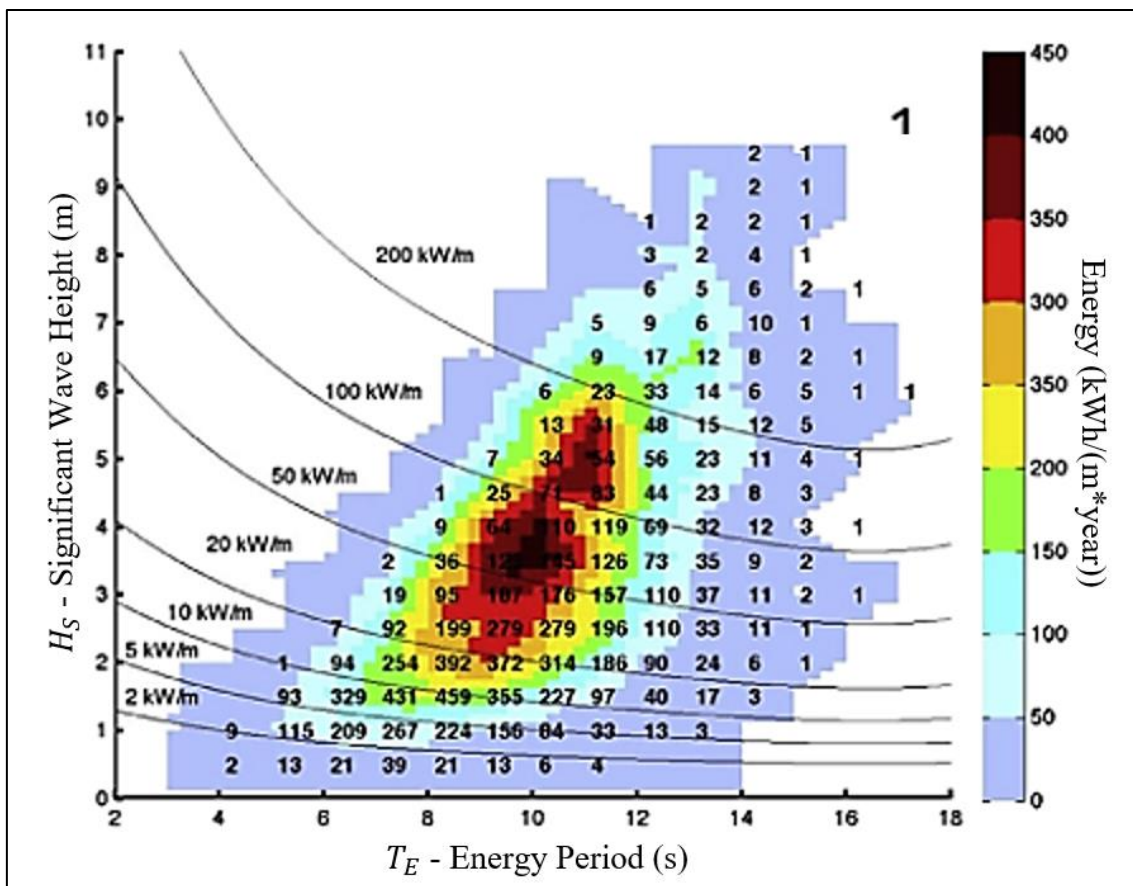


Figure 22. Scatter diagram for Viana – Porto showing the wave resource in hours [37].

Table 3. Pelamis 750kW power matrix [42]

PELAMIS 750 kW Output (kW)		T_E - Energy Period (s)												
		1	2	3	4	5	6	7	8	9	10	11	12	13
H_S Significant Wave Height (m)	0,5	0	0	0	0	0	0	0	0	0	0	0	0	0
	1,0	0	0	0	0	0	29	37	38	35	29	23	0	0
	1,5	0	0	0	0	32	65	83	86	78	65	53	42	33
	2,0	0	0	0	0	57	115	148	152	138	116	93	74	59
	2,5	0	0	0	0	89	180	231	238	216	181	146	116	92
	3,0	0	0	0	0	129	260	332	332	292	240	210	167	132
	3,5	0	0	0	0	0	354	438	424	377	326	260	215	180
	4,0	0	0	0	0	0	462	540	530	475	384	339	267	213
	4,5	0	0	0	0	0	544	642	628	562	473	382	338	266
	5,0	0	0	0	0	0	0	726	707	670	557	472	369	328
	5,5	0	0	0	0	0	0	750	750	737	658	530	446	355
	6,0	0	0	0	0	0	0	750	750	750	711	619	512	415
	6,5	0	0	0	0	0	0	750	750	750	750	658	579	481
	7,0	0	0	0	0	0	0	0	750	750	750	750	613	525
	7,5	0	0	0	0	0	0	0	750	750	750	750	686	593
	8,0	0	0	0	0	0	0	0	0	750	750	750	750	625
	8,5	0	0	0	0	0	0	0	0	0	750	750	750	750
9,0	0	0	0	0	0	0	0	0	0	0	750	750	750	
9,5	0	0	0	0	0	0	0	0	0	0	0	750	750	
10,0	0	0	0	0	0	0	0	0	0	0	0	0	750	
10,5	0	0	0	0	0	0	0	0	0	0	0	0	0	

Finally, in a world with growing environmental awareness, the next step is to calculate the CO₂ reduction achieved by using a WEC to generate electricity. The CO₂ emissions avoided can be directly calculated by multiplying the energy output of the WEC by the CO₂eq emissions per kilowatt-hour of electricity generated from traditional sources. These values take into account the specific energy mix of the country and can strongly vary according to the country's energy policies. Countries like China, India, and Iran have high values of CO₂eq emission per kWh (531, 632 and 494gCO₂eq/kWh in 2022) of electricity produced due to few penetrations of renewables in the mix, however, on the other hand, countries like Brazil and Canada (107 and 128gCO₂eq/kWh) have way smaller values because of intense use of renewables.

For instance, if a WEC generates 190MWh of electricity (as it will be shown later) and the CO₂eq emissions per kWh of traditional electricity are 0,5kg [3], the CO₂ reduction would be:

$$CO_2 \text{ Reduction} = \text{Electricity Generated} \times CO_2 \text{ eq Factor} \quad (2)$$

$$CO_2 \text{ Reduction} = 190 \text{ MWh} \times 500 \frac{\text{kgCO}_2\text{eq}}{\text{MWh}} = 95 \text{ tCO}_2\text{eq} \quad (3)$$

Therefore, using a WEC to generate 190MWh of electricity would result in a CO₂ reduction of 95tCO₂eq compared to generating the same amount of electricity using traditional methods. In conclusion, calculating the CO₂ reduction achieved by using a WEC to generate electricity involves determining the WEC's power and energy output, calculating the CO₂ emissions from traditional electricity generation, and subtracting the CO₂ emissions avoided by using a WEC. By using this process, we can determine the positive impact that WECs can have on reducing greenhouse gas emissions and mitigating climate change.

3

CASE STUDY

The main sites of interest in this study were the Port of Leixões and the Port of Azores. However, due to the physical proximity and greater knowledge of the structures of the Port of Leixões as well as the possibility of visiting the sites in person, this dissertation focused on studying the Port of Leixões only. The northern breakwater of the Port of Leixões is of the sloped type and served as the basis for the numerical analysis. For the vertical breakwater, the north breakwater at the mouth of the Douro River was used. This chapter presents the location and the technology principle under study.

3.1. PORT OF LEIXÕES

3.1.1. HISTORY AND DEVELOPMENT

The Port of Leixões (Figure 23), located on the northern Portuguese coast, is an important commercial and fishing port covering an area of circa 180ha. Located at the mouth of the Leça River in the municipality of Matosinhos, the Port of Leixões has become the largest port infrastructure in the northern region of Portugal. The construction of the artificial port began in July 1884 with the North and South Breakwaters built on existing rocks outcrops using 50t granite block [43]. In 1890, a submerged breakwater extended the North Breakwater by a few meters. These structures were mostly completed in 1892. However, it wasn't until 1914 that the construction of a commercial harbor commenced, featuring a docking berth on the South Breakwater.



Figure 23. The Port of Leixões, West – East view [44].

Amidst national political instability and financial constraints during the period of economic downturn, construction endeavors experienced a halt until 1932 [43]. However, the escalation in maritime activities and challenges arising from mooring issues, exacerbated by intensified wave forces, necessitated a new expansion of the Port. In response, expansion efforts turned inward, utilizing the Leça estuary, resulting in the establishment of Dock 1 and the extension of the north breakwater to mitigate wave-induced impacts within the harbor. Subsequent expansion initiatives from 1956 to the 1960s further progressed inland with the addition of Dock 2 (spanning 0,5km).

In the 1960s, the Port of Leixões underwent a significant expansion phase, which included various infrastructure developments. These encompassed the establishment of a dedicated fishing harbor, the construction of a terminal to accommodate oil tankers, and the elevation of the north breakwater extension beyond submersion levels. Subsequent advancements included the north container terminal (1974-1979), the extension of Dock 2 (1974-1983), and the subsequent expansion of Dock 4. In the late 1980s, further enhancements were made to the breakwater, while the Marina and South Container Terminal were added in the 1990s. For a visual representation of the port's facilities, refer to Figure 24, which presents a straightforward and user-friendly layout [45].

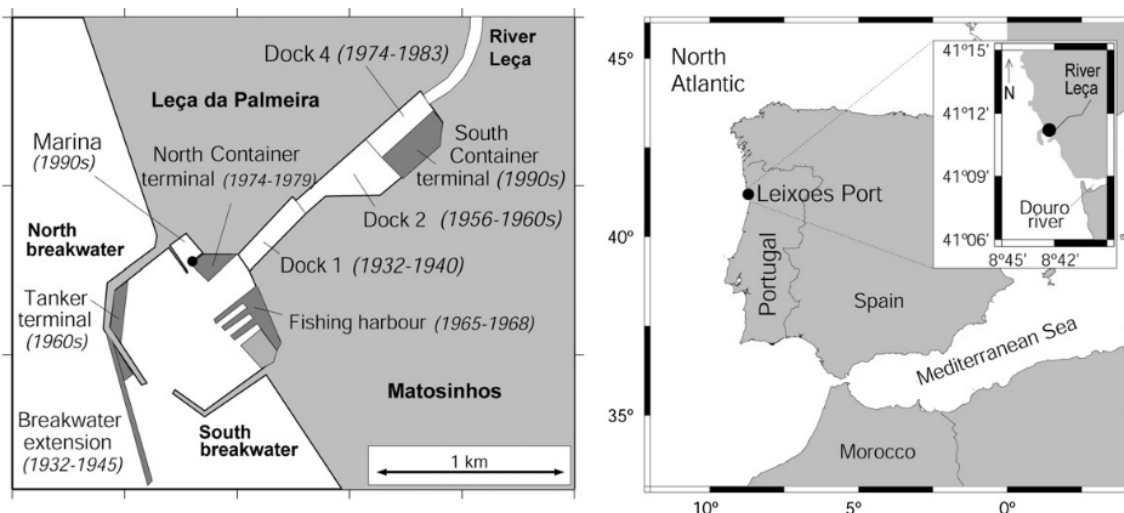


Figure 24. Location and representative diagram of the Port of Leixões [43].

The sheltering effect is achieved by two breakwaters, with the northern one being about 1800m long and the southern one about 950m. Each of these breakwaters has a section perpendicular to the coastline and another roughly parallel to the same line, connected by curves of great radius and delimiting an almost square surface. The width of the entrance channel to the port, between the heads of the sheltering breakwaters, is 220m [44].

The port is a key transportation hub in Portugal, handling a significant portion of the country's international trade. It is the second-largest artificial port in the country after the Port of Sines, with a rich history of expansion and development that has transformed it into the thriving port it is today. With 5km of quayside and a total of 120ha covered by water, the port has modern equipment and advanced ship management computer systems that ensure seamless handling of cargo. It enjoys good maritime, road, and rail accessibility, making it a versatile and competitive port in Portugal.

The Marina of Leixões, also known as Marina Porto Atlântico, is located on the North Pier of the port and is a popular destination for boat enthusiasts and tourists. Every year, the Port of Leixões

handles around 14 million tons of goods, representing 25% of Portuguese international trade [45]. The port's strategic location and rich hinterland make it a vital link in the European port system. It operates 365 days a year with high levels of productivity and reduced ship downtime at the quay. The movement of goods in the port is handled by concessionaire companies that have access to the most modern equipment, while the port authority provides piloting, towing, and mooring services.

The main access channel to the port has a depth of 14 meters, which ensures a permanently open bar to port traffic without access restrictions due to tides. Leixões deals with a wide range of goods, including clothes, granite, wines, cars, cereals, containers, scrap metal, iron and steel, alcoholic beverages, brandy, sugars, oils, petroleum products, and even accommodates cruise ship passengers. With about three thousand ships passing through Leixões every year, the port is a crucial hub for both regional and international trade.

One of the distinctive features of the Port of Leixões is the moveable bridge that connects the North and South parts of the port (Figure 25). The bridge was inaugurated in 2007 and was designed by the Portuguese architect João Motta Guedes. The bridge has a free span of 78m and a width of 10,7m, and its central section can be lifted to allow the passage of larger ships. The bridge is not only a functional element of the port's infrastructure but also a landmark of the city of Matosinhos, attracting tourists and locals alike.



Figure 25. Moveable bridge across the Leça River in the Port of Leixões [45].

3.1.2. BATHYMETRY

The topo-hydrography of the seabed of the Port of Leixões is essentially determined by the dredging operations carried out to ensure navigability and by the subsequent distribution of sediments, mostly originating from the river flow of the Leça River and the transport carried out by the tidal currents to its interior [46].

Recent bathymetric surveys show that the mouth of the Port of Leixões is at levels ranging between -15 and -16m at hydrographic zero of Leixões (ZHL. All the following bathymetry values will be given in relation to ZHL standards). Along the entire area adjacent to the north breakwater,

due to the permeability of the infrastructure and the passage of sands from the coastal transit to the interior of the Port of Leixões, the bathymetry ranges from -15 to -6m. Also, the opposite area, the south of the interior breakwater, has shallower depths than the entrance zone, with the bathymetry ranging from -15 to -8m.

As the channel moves upstream of the old north breakwater of the port, the anteport area, followed by the docks access channel, is at elevations between -11 and -12m. Elevations between -11 and -12m are also reached in the area of the bulk, multipurpose, and south container terminals. In the area of pier B and the cruise terminal, bathymetric elevations are between -10 and -11m. At pier C, elevations vary between -6 and -7m. In the fishing harbor and marina area, the depths are significantly lower, varying between -3 and -7m.

Finally, outside the Port, bathymetric depths gradually decrease towards the open sea domain. In the area of the breakwater extension, the bathymetry varies between -12 and -19m. Approximately 20m around the breakwater extension area, 77,5% of the area has bathymetric depths below -14m, with 50% of the area below the -17m bathymetric zone [44]. Figure 26 displays the heat map of the bathymetry for the Leixões Port influence area.

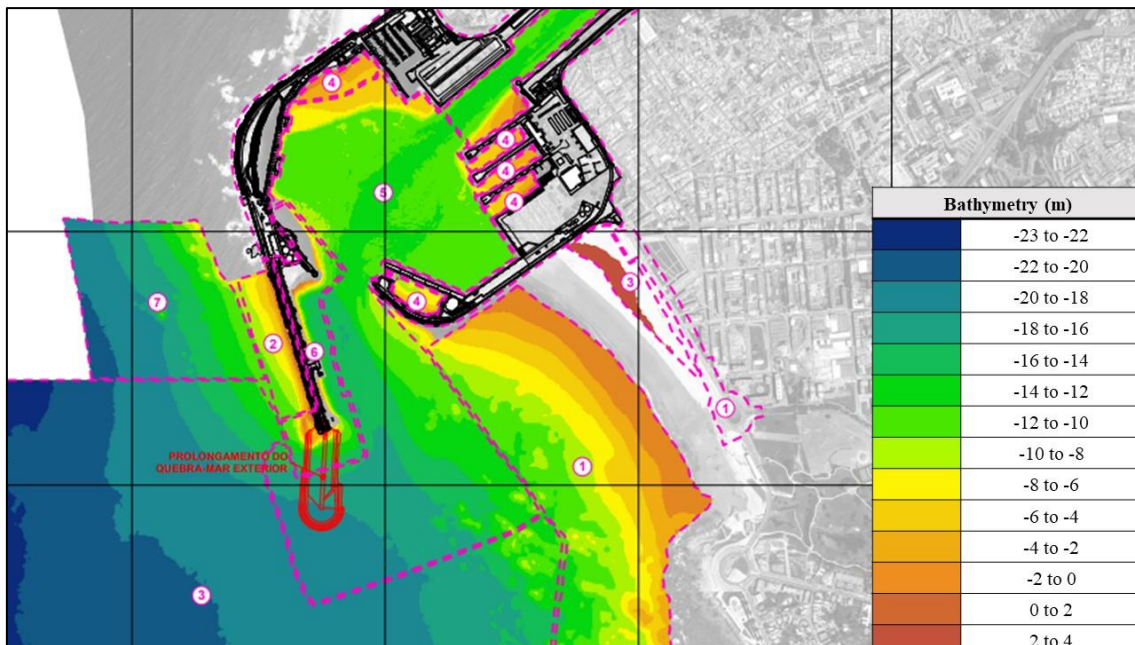


Figure 26. Bathymetry heat map for the Port of Leixões influence area [44].

3.1.3. WAVE RESOURCE

WECs must be exposed to waves with sufficient energy throughout the year to fulfill their function. Therefore, the planning and construction of WECs for zones protected by breakwaters or any other wave energy dissipation structure are of little interest. Therefore, the areas of the Port of Leixões with the greatest interest for the conversion of wave energy are on the outside of the north breakwater, directed perpendicularly to the dominant direction of the waves. In this sense, the characterization of the wave resource is necessary for the area outside the breakwaters.

There are many factors influencing the wave resource for a particular location. Therefore, the wave resource characterization can give a good indication of whether or not to install a WEC in a particular site. The following figures will show some of these wave parameters for the Port of Leixões outside area. This outside zone can be considered as the pink number 3 (Figure 26).

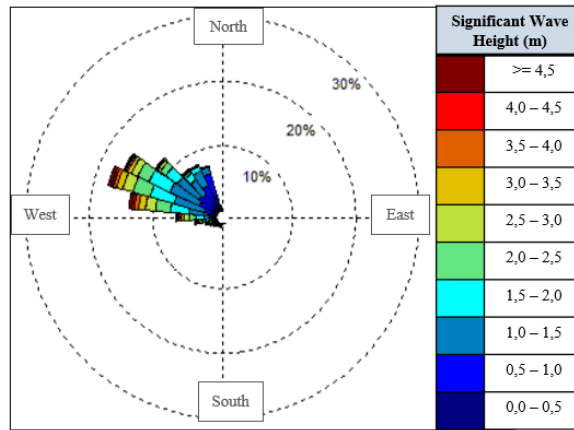


Figure 27. Wave regime for the nearest breakwater point [46].

Table 4. Significant wave height versus wave period distribution [46]

Wave Resource Port of Leixões	T _z - Zero Crossing Period (s)												Total
	4	5	6	7	8	9	10	11	12	13	14	15	
6,0	0%	0%	0%	0%	0%	0%	0%	0%	0%	0%	0%	0%	0%
5,0	0%	0%	0%	0%	0%	0%	0%	0%	0%	0%	0%	0%	0%
4,0	0%	0%	0%	0%	0%	1%	1%	1%	1%	1%	1%	0%	7%
3,0	0%	0%	0%	0%	1%	3%	4%	4%	3%	2%	1%	0%	18%
2,0	0%	0%	2%	6%	9%	10%	8%	6%	3%	1%	0%	0%	45%
1,0	0%	1%	6%	8%	7%	4%	1%	0%	0%	0%	0%	0%	27%
0,0	0%	0%	0%	0%	0%	0%	0%	0%	0%	0%	0%	0%	2%
Total	1%	2%	8%	14%	18%	18%	14%	11%	7%	4%	2%	1%	100%

54959 records

Table 5. Significant wave height versus wave direction distribution [46]

Wave Resource Port of Leixões	Mean Wave Direction (°)									Total
	180	203	225	248	270	293	315	338	360	
6,0	0%	0%	0%	0%	0%	0%	0%	0%	0%	0%
5,0	0%	0%	0%	0%	0%	1%	0%	0%	0%	1%
4,0	0%	0%	0%	0%	1%	4%	1%	0%	0%	7%
3,0	0%	0%	0%	1%	2%	9%	6%	0%	0%	18%
2,0	0%	0%	0%	1%	3%	14%	21%	6%	0%	45%
1,0	0%	0%	0%	0%	1%	3%	8%	16%	0%	27%
0,0	0%	0%	0%	0%	0%	0%	0%	0%	0%	2%
Total	0%	1%	1%	2%	7%	31%	36%	22%	0%	100%

54959 records

To conclude, the wave characteristics of the given dataset indicate that the significant wave heights range between 0 and 8,98m, with an average value of 1,63m. The majority of the recorded values lie between 0 and 4m, with the most common range being between 1 and 2m. Similarly, the average zero-crossing periods range from 3,9 to 17,3s, with an average value of 8,7s. Most of the recorded values fall within the range of 5 to 12s, with the most frequent range being between 6 and 11s. Lastly, the average wave directions fall between 182° and 342° , with an average value of 295° . Many of the recorded values lie within the ranges of $247,5^\circ$ to $337,5^\circ$, with the most common ranges being between 270° and $337,5^\circ$, corresponding mainly to the NW direction [46]. Overall, these statistics provide valuable insights into the typical wave characteristics at the site of interest.

3.1.4. SITES OF DEPLOYMENT

The main sites of interest for the application of the technology under study in this dissertation focus on locations with good exposure to waves. As will be presented in chapter 4, two breakwater configurations were studied. The first is of vertical type and the second is of sloped type. Both the north breakwater and the south breakwater of Port of Leixões are of the sloped type (Figure 28a). In this way, the northern breakwater of Port of Leixões was used as a deployment point for the numerical study of the behavior of sloped breakwaters. On the other hand, to study the behavior of vertical breakwaters, the northern breakwater at the mouth of the Douro River was used, which is approximately 2,5km from the Port of Leixões (Figure 28b). The latter was used as the basis for the numerical and experimental model due to the impossibility of building and testing two different breakwater configurations in a timely manner. Figure 28 shows both sites of deployment for the devices under study in this dissertation.



Figure 28. Sites of deployment for both breakwaters.

3.1.5. ENERGY AND CO₂ EMISSIONS SCENARIO

For a given commercial establishment (supermarket, car factory, port...) to achieve energy self-sufficiency, it must produce the amount of energy it will consume, thus avoiding buying energy from the national grid. This concept, when put into practice together with clean and renewable energies, also contributes to achieving carbon neutrality, which in the current world scenario is a highly desirable goal for commercial entities. The technology under study in this dissertation will allow to produce clean of emissions and renewable electricity, thus it can strongly contribute both to the energy self-sufficiency of the Port of Leixões and also to the reduction of CO₂ emissions.

Table 6 shows the energy consumption by source for the Port in 2019 and 2020. As can be seen, both electricity and combustion fuels (natural gas NG and diesel) contribute the same to the total annual consumption. This means that efforts are not only necessary in clean energy production, but also in electrification, *i.e.*, incorporate the use of electricity instead fossil fuels. In fact, only in this way the clean energy generated can be decently used, otherwise, the Port will remain with a significant portion of its energy consumption related to non-renewable energy sources.

Table 6. Energy consumption by source for the Port of Leixões in 2019 and 2020 [47]

Energy Consumption (GJ)	2019	2020
Diesel	54.170,6	54.170,6
Natural Gas	608,3	1.121,9
Total Fuel Energy	54.778,9	55.292,5
Low-Voltage Electricity	7.980,7	7.837,8
High-Voltage Electricity	44.151,7	44.317,5
Total Electricity Energy	52.132,4	52.155,3
Total Energy	106.911,3	107.447,8

GHG emissions are also not low for the Port of Leixões (Figure 29). This is mainly due to the fact that diesel has a high CO₂ emission factor. According to the Portuguese environment agency (APA), for each gigajoule (GJ) of energy released by diesel, around 74,1kg of CO₂eq are emitted. On the other hand, the Port of Sines, located south of Lisbon, processes 2,5 times more cargo than the Port of Leixões but even so emits only 561,5 tons of CO₂eq [48], a value that is 7,2 times lower than the registered for the Port of Leixões. This great disparity demonstrates that the Port of Sines is significantly closer to being energy self-sufficient and reach carbon neutrality than the Port of Leixões, as its processes are already much more electrified and willing to receive clean and renewable energy. Overall, the Port of Leixões has significant work to do before it gets 100% energy self-sufficient.

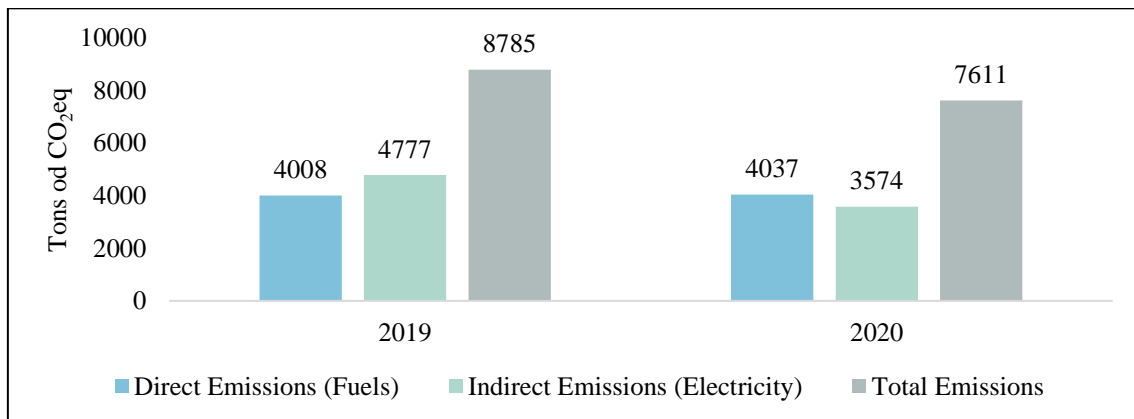


Figure 29. GHG emissions for 2019 and 2020 in the Port of Leixões [47].

3.2. POWER TAKE-OFF SYSTEMS

Wave energy converters are devices that capture energy from ocean waves and convert it into electricity. However, most WECs require a mechanism to convert the motion of the waves into rotational or linear motion, which can then be used to generate clean electricity. Such mechanism is a power take-off (PTO) system.

A PTO system is a mechanism that converts the mechanical energy of a moving shaft into electrical energy. In the case of a pivoted hinged WEC, the PTO system is used to convert the rotational motion of a wave-driven device into electrical energy that can be cleanly fed into the electrical grid. Although several types of PTO systems can be utilized in hinged WECs, each one with its advantages and disadvantages, some of the most common types of PTO systems are hydraulic systems, pneumatic systems, and direct drive systems [51].

Hydraulic systems are one of the most common types of PTO systems used in hinged WECs. In a hydraulic PTO system, the rotational motion of the wave-driven device is used to compress a hydraulic fluid, which in turn drives a generator to produce electricity. Hydraulic PTO systems offer an advantage in that they can be engineered to handle high torque and low rotational speeds, making them a suitable choice for hinged WECs. However, it should be noted that these systems are also significantly complex and their operation in harsh oceanic environments can necessitate high levels of maintenance. Furthermore, hydraulic PTO systems can be designed to be highly efficient, with some systems achieving conversion efficiencies of up to 90% [52].

Pneumatic systems are another type of PTO system that can be used in hinged WECs. In a pneumatic PTO system, the motion of the wave-driven device is used to compress air, which is then used to drive a turbine to generate electricity. One of the advantages of pneumatic PTO systems is that they are relatively simple and can be designed to be highly reliable. Moreover, pneumatic PTO systems can also have good efficiencies values, with some systems achieving conversion of up to 70% [31].

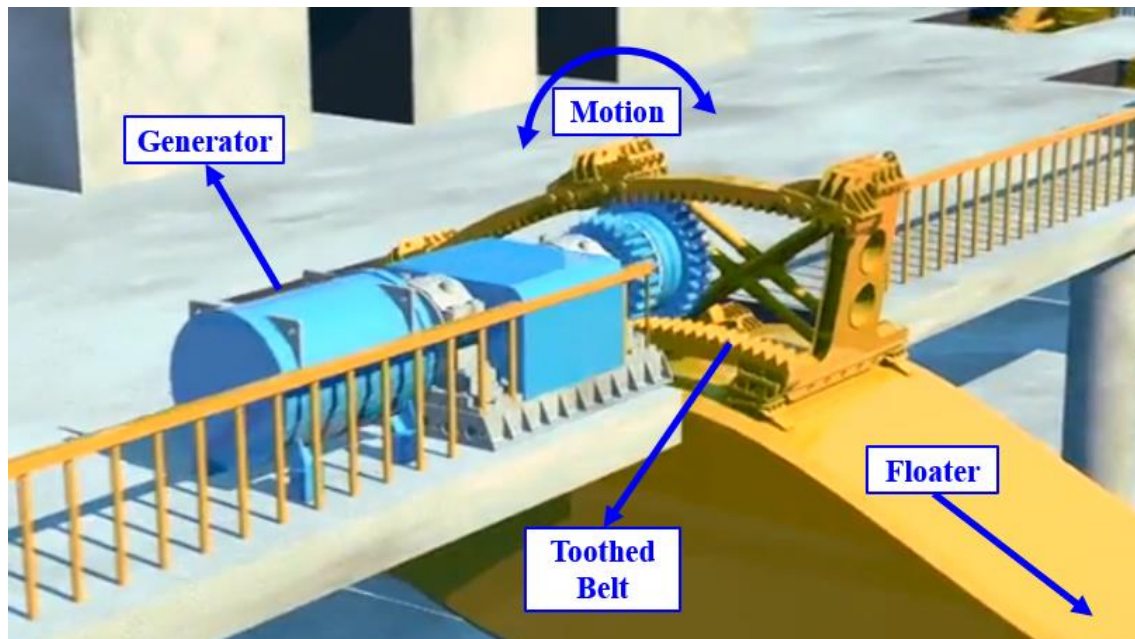


Figure 30. Direct drive PTO system used in a WCE prototype [53].

Lastly, direct drive systems are a third type of PTO system that can be used in hinged WECs. In a direct drive PTO system, the rotational motion of the wave-driven device is used to directly drive a generator to produce electricity (Figure 30). The biggest advantage of direct drive PTO systems is that they are relatively simple and can be designed to be highly efficient, as well as the fact that they can be better scalable [51]. Additionally, direct drive PTO systems do not require any additional components, such as hydraulic or pneumatic systems, which can make them more reliable.

While each type of PTO system has its own advantages and disadvantages, the choice of which system to use in a hinged WEC will depend on a variety of factors, including the specific design of the device, the expected operating conditions, and the desired efficiency and reliability of the system. Regardless of the type of PTO system used, it is clear that these devices will play an increasingly important role in the development of wave energy as a viable source of renewable energy.

3.3. HINGED SYSTEMS FOR WAVE ENERGY CONVERSION

3.3.1. WORKING PRINCIPLE

As the name already describes, hinged, articulated or pivoted WECs rely somehow on hinged motion. This is, these WECs absorb the energy associated with the relative motion of the adjacent bodies. In the case of this dissertation, the adjacent body is a half sphere floater (better described in Figure 31), and the hinged motion happens to be relative to the breakwater. The natural oscillation of the incoming waves makes the body move up (when hit by waves) and then move down (after the wave passes). This up and down movement drives the hinged system, making the arm move together with the floater.

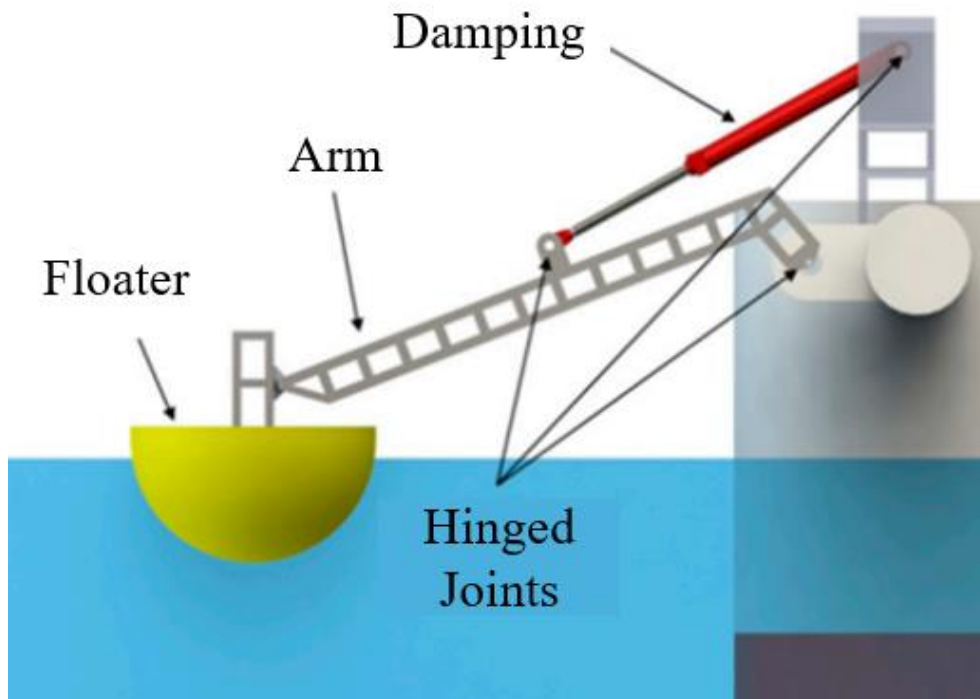


Figure 31. Scheme of a hinged system WEC [49].

Without any sort of damping, the system would just move freely, and no useful energy could be extracted from its movement. That is the reason why a damping mechanism is always necessary in order to extract energy. The damping mechanism can be easily explained with an analogy to a traditional bicycle brake system. If a person is mounted on the bicycle, pressing the brakes moderately, they will only be able to move if they pedal very hard, this happens because the brake is blocking the movement and a lot of energy that the person is doing on the pedal is being dissipated by the brake. On the other hand, when the person is not using the brakes, none of their pedal energy is wasted and the bicycle can move forward freely. The same happens with WECs, when there is no damping, the system can move freely, and no energy can be converted by the PTO in order to generate electricity. However, when there is some resistance to movement, it takes more force to move the floater and more energy will be converted by the PTO, generating more electricity.

The damping that will be applied to the system is usually described through the damping coefficient parameter, in this text C_D , and should be carefully chosen. High values for C_D will make it harder to the floater to move and low values C_D will let it too soft. The study to find the ideal value is commonly done by running several simulations for different C_D values and then, checking each of them drives for the highest power output. Section 4.4 better describes those aspects and displays the analysis done for the device under study.

The power take-off system (PTO) is then responsible for converting this energy dissipated into useful energy. Due to their strong importance in WEC feasibility, section 3.2 detailed more types of PTO systems that can be used for hinged WECs.

3.3.2. ECO WAVE POWER DEVICES

EWP is still consolidating their technology. Some small scales devices were already tested, and some others are still being tested. However, no real scaled device undergone real sea conditions at the date of this dissertation [50]. The EWP devices can be divided into three fundamental components for better functioning explanations:

- 1) Coastal Structure: As previously stated the device can be attached to a multitude of coastal structures. Those structures include breakwaters, piers, jetties and many others that can support the loads and also have a section available for attaching the devices;
- 2) Energy Conversion Unit: The complete conversion unit (Figure 32), encompassing hydraulic and electrical conversion equipment, is meticulously crafted and put together within a standard-sized shipping container, strategically positioned on land. This ingenious, compact, and portable design streamlines the process of transporting it to the desired location with remarkable ease and efficiency. Additionally, all operational and maintenance tasks are conducted exclusively from the land, eliminating the necessity for divers, marine vessels, underwater mooring, cables, and other expensive marine installation, operational, and maintenance procedures that are typically required for offshore solutions [50].

The floaters up and down movement compress a hydraulic fluid that is stored in the hydraulic fluid tank. This compressed fluid feeds the accumulators that then drives the hydraulic motor, generating clean electricity. The fluid operates in a closed circuit and the valves regulates the flows in order to optimize production;

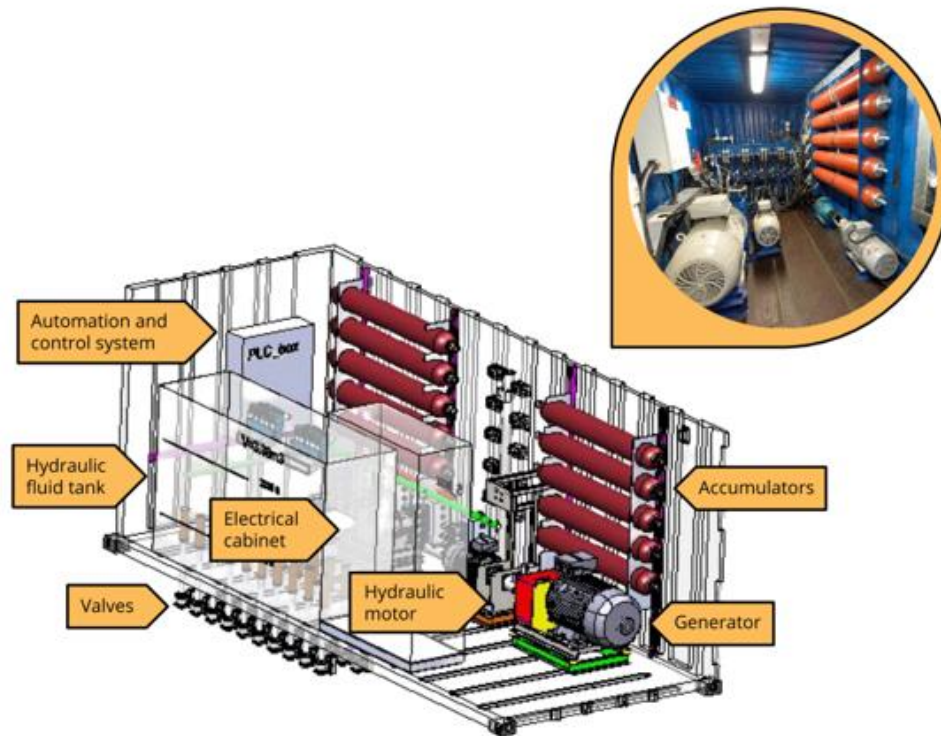


Figure 32. Energy Conversion Unit from EWP [50].

- 3) Floater Mechanism: The real scale EWP floater has a length of 3,6m, a width of 2,8m and a height of 1,5m. This device can generate up to 1MW under good sea conditions operation and can withstand waves up to 4m height. Even higher waves make the device to enter in storm protection mode, using the lock mechanism and making the device to be on vertically on place while the storm passes [50]. Figure 33 shows the floater mechanism and its components. It is also possible to see the hydraulic cylinder responsible for compressing the hydraulic fluid.

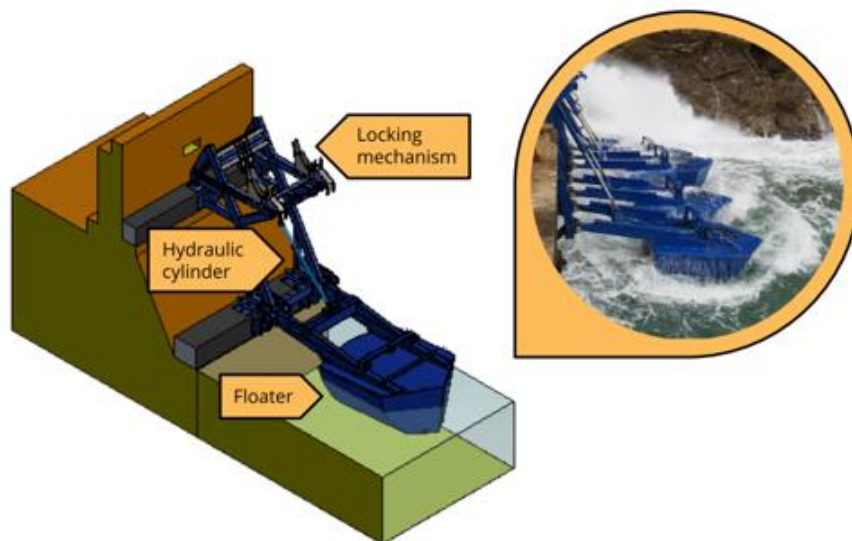


Figure 33. Floater mechanism of EWP devices [50].

3.4. FINAL CONSIDERATIONS

Chapter 3 aimed to present the case study that will be developed in the following chapters. The WEC to be tested is of the point absorber type and is based on the device developed by EWP. There are two locations where the feasibility and extracted power tests will be carried out. The first one is on the north breakwater of Port de Leixões due to its sloped configuration, and the second is on the north breakwater of the Douro River due to its vertical configuration. Both numerical and experimental studies will be performed in incoming chapters.

Furthermore, different PTO configurations and systems were presented, namely hydraulic, pneumatic and direct. Even though EWP uses a hydraulic PTO in its devices, in this study there will be no PTO system. As will be explained later, there are other ways to measure the extractable power of a device without the need to measure its absolute value. A functional PTO system would greatly increase the complexity of the experimental and numerical study and for this purpose the power value was estimated based on physical relations.

4

NUMERICAL MODEL

4.1. INTRODUCTION

Once the state of art and the case study are presented, it is time to move forward to the numerical model presentation. The main aim of the numerical model study was to simulate how the hinged WEC would move and behave under the action of realistic sea conditions. As previously explained, predicting sea motions and their effects in the surroundings structures can be quite challenging and time consuming. However, there are some techniques that can be used to simplify the calculations and provide a reasonable estimation of the body movements and yet, on its power output.

The software used for the numerical simulations was ANSYS®, in particular the module called AQWA. ANSYS® is a powerful simulation software used for different applications within engineering fields such as chemistry, thermodynamics, structures analysis, and of course, hydrodynamic analysis. The software operates with the engineering famous mesh concept, where the user defines a reasonable mesh and then, the software solves the governing equation for each partition of the mesh, providing a general view of the results in the object under study. Of course, the denser the mesh, the better will be the approximations. However, the larger will be the computational time required (Figure 34). This way, it is recommended to find a good balance between accuracy and computational time.

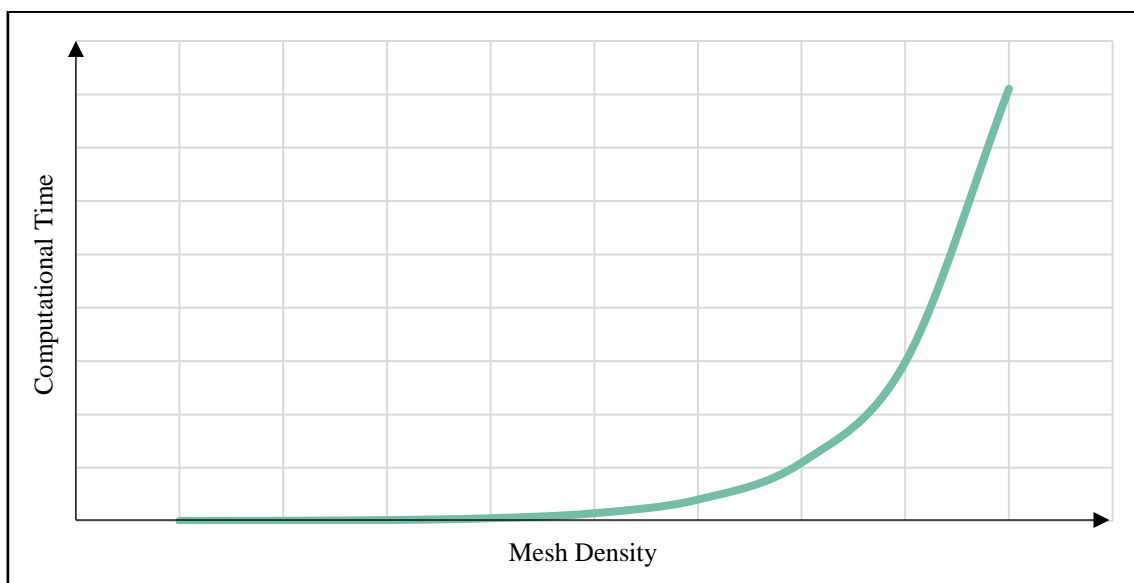


Figure 34. Computational time exponentially growing with mesh density.

In this chapter, a detailed description of the numerical model used is given, from the body sizing definitions to the expectable electricity production matrix. Two versions of the hinged WEC were modeled and tested in this study, both using the same floating body and conditions. The only difference was the breakwater type. In the first set of simulations a vertical breakwater was used to support the WEC (along the text identified with the “V” letter) whereas in the second set of simulations a sloped breakwater was used (identified as “S” letter). The objective of testing two different configurations of breakwaters was to compare and evaluate the effects that those structures might have on the electricity output of the WEC.

4.2. BODY DEFINITIONS

The first step to take in the numerical model analysis was to set up the body parameters and definitions, *i.e.*, the body weight, the body dimensions, the mean water height and so many other parameters that were fundamental to the analysis to run.

As previously said, the body consists of a floating half sphere connected to the breakwater through a moveable and rigid arm. The up and down movement of the floating body allows the conversion of wave energy into useful electricity. Detailed size information was extracted from EWP® technical brochures available online and allowed for the 3D drawing of the WEC. Figure 35 displays the AutoCAD® drawing of the main dimensions of the real scale WEC according to EWP® devices. Those devices were shown both in Figure 15 and Figure 16.

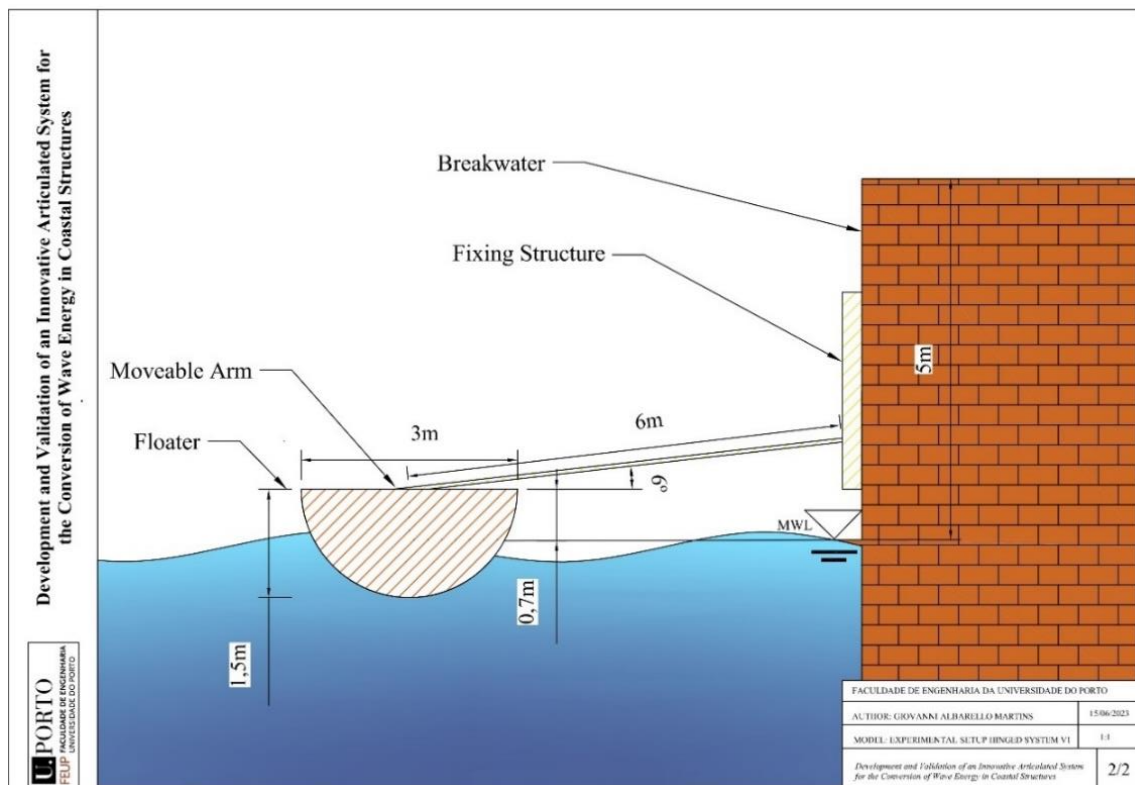


Figure 35. CAD drawing with dimensions of the WEC prototype in a vertical breakwater.

As can be seen in Figure 35, the body is a 3-meter diameter half sphere, connected through a 6-meter rigid arm to the breakwater. For the mean sea water level, the arm is 6-degree inclined horizontally and the water height in the body can be considered as almost half of its radius (0,7m). Finally, the vertical breakwater considered in this study has an approximate height of 5m from the mean water level (MWL) and the bathymetry in that region suggests that the depth is about

8m. The sloped breakwater tested has the same height and was considered to be placed over the same bathymetry, however, it follows a trapezoidal shape, sloping 56° with the horizontal plane, as shown in Figure 36.

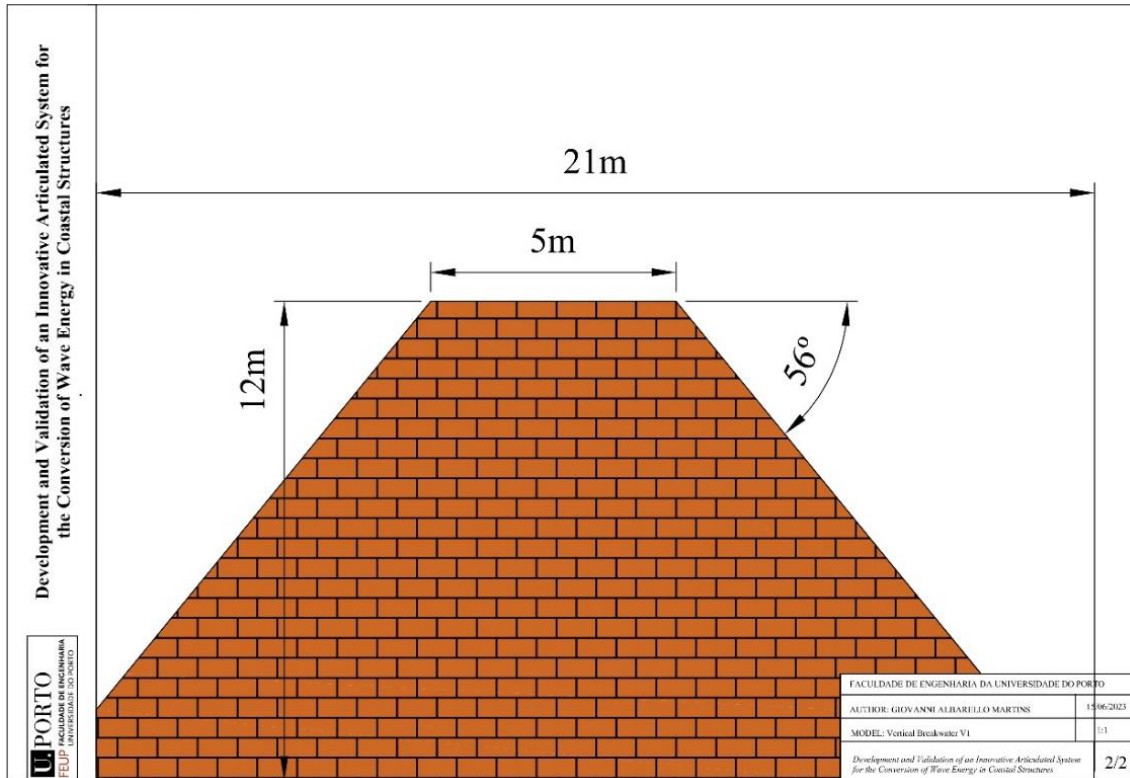


Figure 36. CAD drawing of the sloped breakwater to be tested.

Before proceeding to the 3D drawing, it is important to explain how the total mass of the floating body and its density were calculated. The Archimedes principle states that when a body is immersed in a fluid, it will encounter an upward buoyant force equivalent to the weight of the fluid it displaces. This principle can be translated by the equation below, in which ρ_S represents the fluid density (1025 kg/m^3 for seawater), V_D the volume of water displaced, g the gravitational acceleration ($9,81 \text{ m/s}^2$) and F the buoyant force.

$$F = \rho_S * V_D * g \quad (4)$$

Applying a simple free forces diagram (Figure 37) to the body it is easy to realize that the buoyancy force (F) should be equal to the weight of the body (W) in order to achieve equilibrium. Therefore, it is only necessary to know the water height in the body to set up the equations in order to calculate the mass of the body. The equation development is shown below.

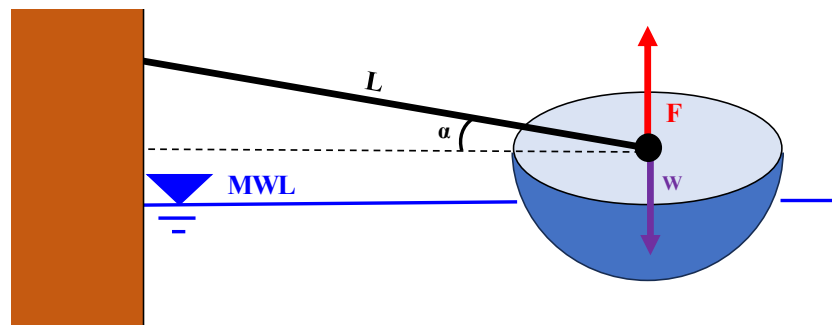


Figure 37. Free forces diagram applied to the body.

Applying the equilibrium principle:

$$F = W \quad (5)$$

Where W is the weight. Replacing:

$$\rho_S * V_D * g = m_B * g \quad (6)$$

Where m_B is the body mass. Taking both g out of the equation:

$$m_B = \rho_S * V_D \quad (7)$$

The volume displaced is given by the spherical cap volume formula:

$$m_B = \frac{\rho_S * \pi * h^2 * (3 * r - h)}{3} \quad (8)$$

Where h is the water height in the body and r is the body radius. Finally, the mass comes as:

$$m_B = \frac{1025 * \pi * 0,7^2 * (3 * 1,5 - 0,7)}{3} \cong 2000 \text{ kg} \quad (9)$$

And the body density:

$$\rho_B = \frac{m_B}{V_B} = \frac{1999}{7,07} = 283 \frac{\text{kg}}{\text{m}^3} \quad (10)$$

Lastly, the 3D drawing of the hinged WEC was done using SOLIDWORKS®. ANSYS® has its own 3D modeler called Design Modeler, but unfortunately it is poorly developed. Therefore, considering the possibility of importing the geometry from SOLIDWORKS®, which performs automatically all the moments of inertia calculations, it was chosen to draw the geometry of the hinged WEC outside the working environment of ANSYS® and then importing it. Furthermore, it was especially interesting using this software due to its capabilities of automatically calculating some of the body parameters that are necessary in the further ANSYS® simulations. In fact, it was just necessary to set up the body density and then the needed parameters were all calculated.

4.3. SOFTWARE PARAMETERS

Once the dimensions and main parameters of the body are defined, it is time to proceed to set up the analysis settings within the software. First, after importing the geometry it is necessary to define the joints. Joints are basically the connections between the body and the breakwater that will define the degrees of freedom for the body movement. Thus, it was necessary to make a hinged joint of the body in the breakwater, allowing only the Z movement (up and down), not any movement in Y direction, and second, a rigid joint to the breakwater in order to set the breakwater as immovable structure. Figure 38 shows the geometry and the joints within the ANSYS® environment.

The next step was to define the mesh (grid). ANSYS® usually tends to set the same mesh for the whole geometry, however, in this case, this wouldn't be a good solution due to the breakwater size, *i.e.*, a good mesh for the body would be too small to the breakwater (excessive resolution), and a good mesh to the breakwater would be too big (few representative) to the body. To address this situation, it was necessary to define the mesh separately, one denser mesh to the floating body and a less representative mesh to the breakwater.

To set up the hydrodynamic diffraction (frequency domain) of the study, a wave direction range of -180° to 180° with an interval of 45° was selected, providing hydrodynamic coefficients data

for 7 different waves directions. Apart from that, the frequencies ranged from 2,4 to 65s. The frequency domain is a mandatory step before running the time domain analysis. It is also useful to have an overview of the body in function of different frequencies.

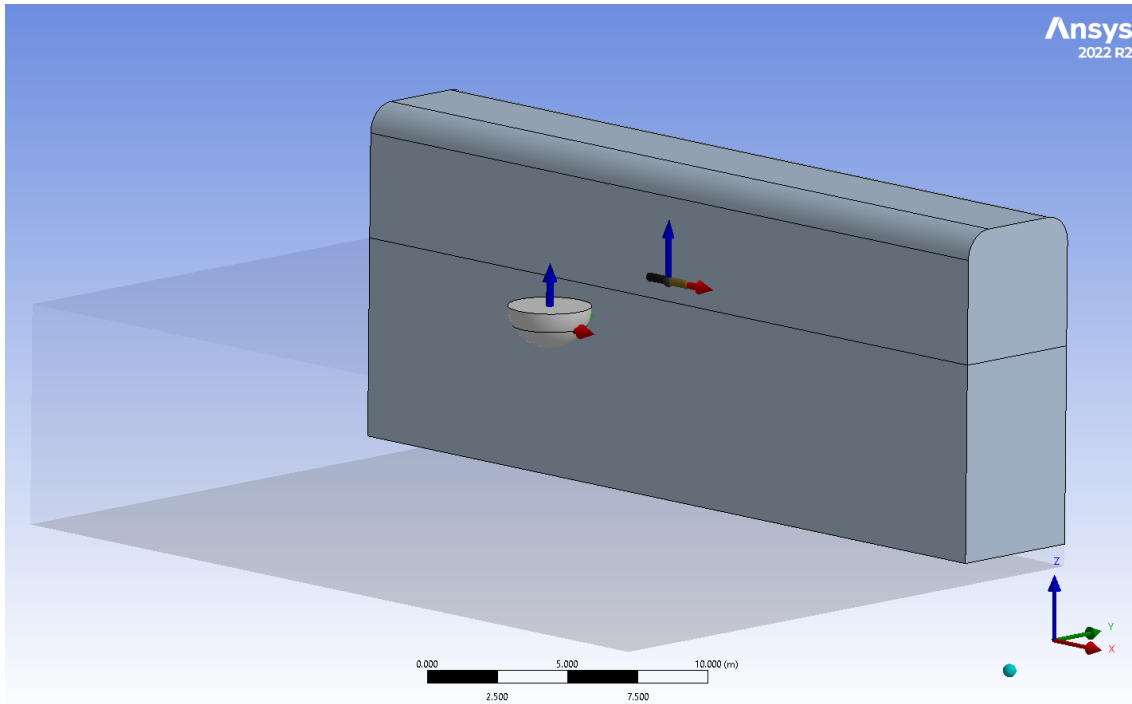


Figure 38. Joints and geometry in the ANSYS® environment (vertical breakwater).

Lastly, the hydrodynamic response of the hinged WEC (time domain) was simulated for a duration of 1.000s with 0,05s of time-step interval in order to avoid errors. The wave spectra used was the JONSWAP (Joint North Sea Wave Project) because of its suitability with the area under study and improved accuracy. The gamma value, or enhancement factor, defined as the ratio between the JONSWAP energy peak and the Pierson-Moskowitz spectra (PM), was selected to be 3,3. This value is considerate adequate for most engineering applications, even though recent studies suggest that the gamma value should be adapted for different locations and conditions [54]. More information about the irregular wave settings, *i.e.*, significant wave height, peak wave period, and direction is given further in the simulation sections.

Regarding the sloped breakwater tests, it can be said that there were absolutely no differences related to the software parameters. It was just necessary to update the geometry in the designer modeler and then set up a new mesh for the new breakwater geometry.

4.4. BEST DAMPING COEFFICIENT

The power output in a WEC is of utmost importance, after all, the main and only purpose of a WEC is to produce electricity. The equation that allows the estimation of the power output for a point absorber body is:

$$P = C_{LD} * V^2 \quad (11)$$

where P represents the power output, C_{LD} the linear damping coefficient and V the body velocity (in this case, towards the Z axis). Consequently, there is a strong relationship between the body velocity and the damping coefficient. One might think that increasing the C_D will always lead to a larger power output, which would be highly desirable, however, the C_D works like a “brake” for

the WEC and then, the larger this value the less the body velocity. Therefore, the best C_D value is the one that leaves the body neither too tight nor too loose, maximizing the power output.

Considering the importance in the general WEC efficiency of this value, is highly recommended to perform a study in order to find the best value. This is done through simulations for different C_D values and evaluating its power output values. At the end of this study, it is possible to plot the power curve, graphically showing where the power reaches its peak.

The procedure adopted to find the best C_D value consisted in running 26 different simulations for different C_D values. The SST used for running those simulations was the most representative one, *i.e.*, 2m of H_S and 9s of T_P (according to Table 4). The C_D value ranged from 1 to 130kNsm $^\circ$ and the method used was the bisection method, reducing the range after every simulation.

Finally, Figure 39 shows the power curve obtained for this study. It is graphically possible to observe that the best C_{AD} value is somewhere between 20 to 30kNsm $^\circ$ for the vertical breakwater and between 37 to 42kNsm $^\circ$ for the sloped breakwater. Hence, the C_{AD} value that was chosen to be used in the simulations was 25kNsm $^\circ$ for vertical breakwater and 40kNsm $^\circ$ for sloped breakwater, because these values maximize the power output generated by the device under normal operation.

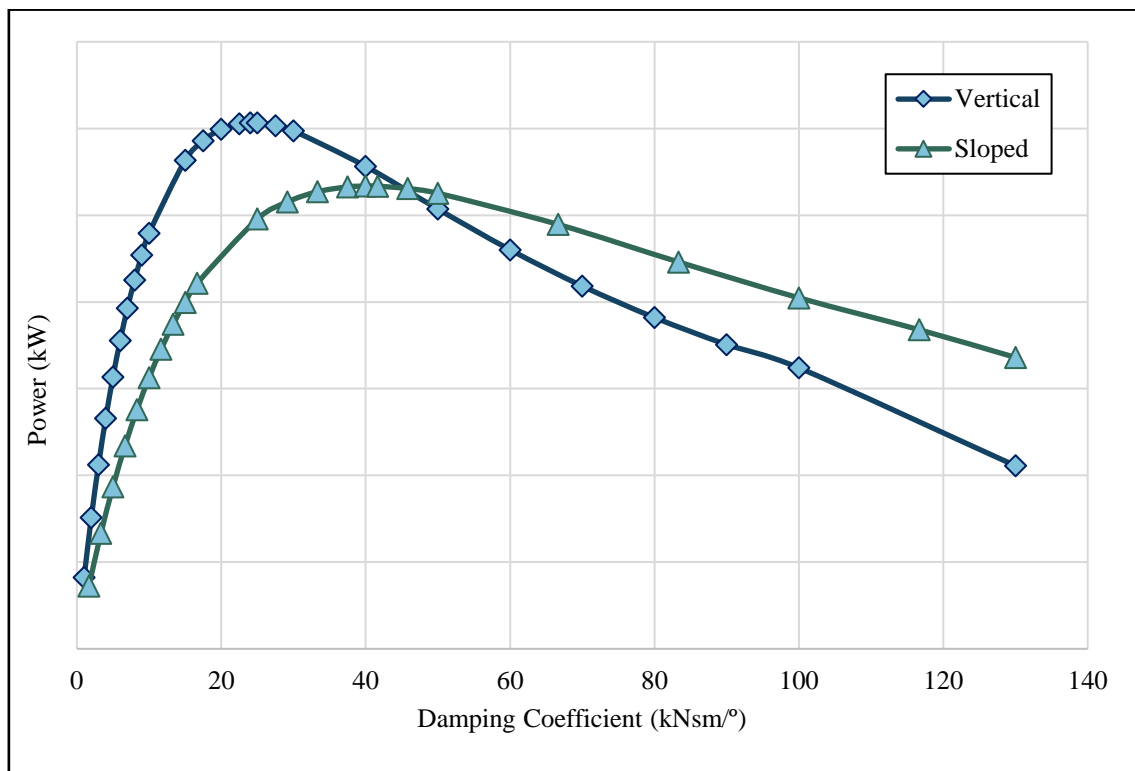


Figure 39. Power curve showing the best C_D .

It is important noting that angular C_{AD} (kNsm $^\circ$) and linear C_{LD} (kNs/m) are two things strictly connected but different. In order to convert one into another it is necessary to take into account the radius of the damping effect, in this case the length of the arm. It is also necessary to use linear damping instead of angular damping while calculating the power. Table 7 displays the best damping coefficients values for both breakwaters' configurations. The relation between them can be expressed as:

$$C_{LDV} [kNs/m] = \frac{C_{AD} [kNsm/^\circ] * 360}{2 * \pi * r^2} \quad (12)$$

For the best C_{AD} the equivalent C_{LD} can be calculated through:

$$C_{LDV} = \frac{25 * 360}{2 * \pi * 6^2} = 39,79 \text{ kNs/m} \quad (13)$$

Table 7. Best damping coefficient values for the two breakwaters

Damping Coefficient	Vertical	Sloped
Angular Damping (Nsm ^o)	25.000	40.000
Linear Damping (Ns/m)	39.789	63.662

4.5. SIMULATIONS

After setting up the simulation parameters and defining the best damping coefficient, it was necessary to start running simulations. In order to do that, the most common sea states (SST) near the installation site at the Port of Leixões were selected accordingly to what was shown in Table 4. Fortunately, the sea states do not vary significantly, actually, the range between 1 – 3m of H_S and 6 – 12s of T_p encompass more than 7.100 yearly hours, *i.e.*, more than 80% of the year. Thus, the simulations were set in order to accommodate all those SST. Apart from that, the most commons wave directions, shown in Figure 27, happens to be between 280 – 315° and were also incorporated in the simulations.

Table 8 displays all the 42 simulations that were made for each type of breakwater. The letter “N” in front of the simulation represents numerical simulation. There are 14 different SST, and for each, 3 wave directions were tested for 2 different breakwater configurations, totalizing 84 simulations. Furthermore, it is also possible to see the occurrence for each SST. Regarding the simulation duration time, 1.000s (about 100 waves per test) with 0,05s time-step was selected in order to assure that the WEC would experience significant exposure to the sea state.

ANSYS® would take about 25min to run each simulation. This number times 84 is equivalent to 35h of computational time. The computer used was a special computer with 32 treads (8+8 cores) Intel Xeon and 64GB of RAM memory within the hydraulics and water resources division of the civil engineering department. This computer allowed the simulations to be significantly faster than with normal computers. The simulations were complete after two weeks since the first simulation to run.

Table 8. Sea States (SST) for each different simulation

Simulation	SST	H_S (m)	T_P (s)	Direction (°)	Occurrence (%)
N01	SS1.1	3,00	9,00	280	
N02	SS1.2	3,00	9,00	290	3%
N03	SS1.3	3,00	9,00	315	
N04	SS2.1	3,00	10,00	280	
N05	SS2.2	3,00	10,00	290	4%
N06	SS2.3	3,00	10,00	315	
N07	SS3.1	3,00	11,00	280	
N08	SS3.2	3,00	11,00	290	4%
N09	SS3.3	3,00	11,00	315	
N10	SS4.1	3,00	12,00	280	
N11	SS4.2	3,00	12,00	290	3%
N12	SS4.3	3,00	12,00	315	
N13	SS5.1	2,00	7,00	280	
N14	SS5.2	2,00	7,00	290	6%
N15	SS5.3	2,00	7,00	315	
N16	SS6.1	2,00	8,00	280	
N17	SS6.2	2,00	8,00	290	9%
N18	SS6.3	2,00	8,00	315	
N19	SS7.1	2,00	9,00	280	
N20	SS7.2	2,00	9,00	290	10%
N21	SS7.3	2,00	9,00	315	
N22	SS8.1	2,00	10,00	280	
N23	SS8.2	2,00	10,00	290	8%
N24	SS8.3	2,00	10,00	315	
N25	SS9.1	2,00	11,00	280	
N26	SS9.2	2,00	11,00	290	6%
N27	SS9.3	2,00	11,00	315	
N28	SS10.1	2,00	12,00	280	
N29	SS10.2	2,00	12,00	290	3%
N30	SS10.3	2,00	12,00	315	
N31	SS11.1	1,00	6,00	280	
N32	SS11.2	1,00	6,00	290	6%
N33	SS11.3	1,00	6,00	315	
N34	SS12.1	1,00	7,00	280	
N35	SS12.2	1,00	7,00	290	8%
N36	SS12.3	1,00	7,00	315	
N37	SS13.1	1,00	8,00	280	
N38	SS13.2	1,00	8,00	290	7%
N39	SS13.3	1,00	8,00	315	
N40	SS14.1	1,00	9,00	280	
N41	SS14.2	1,00	9,00	290	4%
N42	SS14.3	1,00	9,00	315	

4.6. EXPECTABLE POWER MATRIX

The concept of power matrix is of utmost importance in the WEC studies. This matrix allows for a quick understanding of how the device will perform under specific conditions. Once the matrix is set, it is only necessary to know the wave resource matrix at the site of interest showing the occurrence frequency of different sea states variation to predict the electricity generated. This process, known as matrix crossing, is done for different locations and applications worldwide in order to analyze the feasibility of a specific WEC in that place. Of course, this process was also done in this study as explained below.

At the end of each simulation, it was possible to generate a CSV file containing the value of each selected variable for each time-step of the simulations. Using an Excel® spreadsheet that was previously adjusted it was just necessary to copy and paste the values obtained into the spreadsheet to get the power output. This way, it was possible to slowly populate the power matrix for both breakwaters' configurations.

Table 9 and Table 10 displays the power matrix generated after running all SST simulations. The value displayed for each SST is the average for the three directions analyzed, and the cells without results (-) were not analyzed due to few occurrences throughout the year.

Table 9. Power matrix obtained for the device under study attached in a vertical breakwater

Vertical - Power Matrix Obtained (kW)		T_P (s)								
		5	6	7	8	9	10	11	12	13
H_S (m)	4,0	Storm Protection Mode								
	3,0	-	-	-	-	38,9	35,6	32,4	28,9	-
	2,0	-	-	15,2	16,7	17,7	15,6	13,7	11,8	-
	1,0	-	4,1	4,0	4,1	4,0	-	-	-	-
	0,0	No waves								

Table 10. Power matrix obtained for the device under study attached in a sloped breakwater

Sloped - Power Matrix Obtained (kW)		T_P (s)								
		5	6	7	8	9	10	11	12	13
H_S (m)	4,0	Storm Protection Mode								
	3,0	-	-	-	-	51,7	50,6	50,0	47,5	-
	2,0	-	-	18,3	20,8	23,8	23,1	22,3	21,2	-
	1,0	-	4,5	4,7	5,2	5,8	-	-	-	-
	0,0	No waves								

As can be seen, higher values of H_S leads to higher values of power, the inverse happens to the T_P value, in which, a lower value leads to higher power. This is strictly related to the natural period of oscillation of the floater and can be explained with a simple analogy to the operation of a children's swing. When swinging their child on the swing, parents usually apply force by pushing them forward. However, this force will bring better results (in this case more speed and height) only if it is applied at the right moment, that is, only if the force application frequencies (parents pushing) and the swing frequency are the same. This phenomenon is also observed with oscillating hinged WECs. When the frequency of the incident waves is synchronized with the natural oscillation frequency of the device, the amplitude of the movement will be greater, consequently the velocity and ultimately the power will also be greater. Therefore, it can be said

that the hinged WEC under study has a natural oscillation period of about 8 to 10s, since those are the period values that the WEC produces more power for a given H_S . Figure 40 shows how the power value is always higher for frequencies between 0,1 to 0,12Hz (8 to 10s) for all the three H_S analyzed.

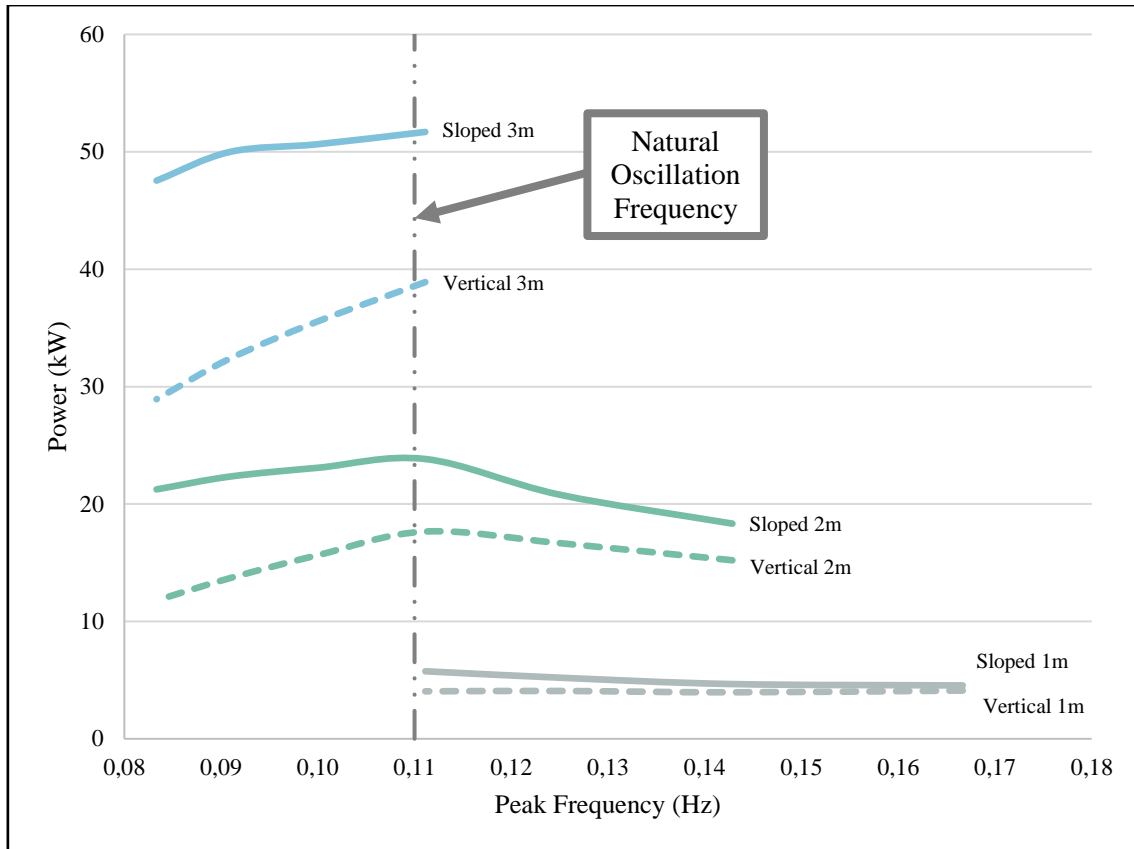


Figure 40. Peak frequency versus power for all the H_S .

During the section about the definition of the best damping coefficient, the concept of active damping optimization control systems (ADO) was not discussed. Those systems aim to maximize the power output of a WEC by applying the best C_D for each SST that is currently happening. Basically, there is a microcomputer that receives the current sea information, *i.e.*, the H_S and the T_P , and with this information the damper will apply a specific C_D for that specific SST, thus, the WEC will be always operating with the best C_D possible. In this study, the C_D used is the best for only one SST, which is the most frequent SST, however, for other SSTs this value would certainly vary. Therefore, it is fair to apply an enhancing factor in the power outputs values obtained, considering that there would be also damping optimization control. Many research and development has been done in this field and the enhancement can reach up to 300% [55]. For the purpose of this work a good value was considered to be 125% or 1,25 (Table 11 and Table 12).

Table 11. Enhanced power matrix with hypothetical ADO system in a vertical breakwater

Vertical - Power Matrix Enhanced (kW)		T_P (s)								
		5	6	7	8	9	10	11	12	13
H_S (m)	4,0	Storm Protection Mode								
	3,0	-	-	-	-	48,5	44,3	40,4	36,0	-
	2,0	-	-	18,9	20,8	22,0	19,5	17,0	14,7	-
	1,0	-	5,1	4,9	5,1	5,0	-	-	-	-
	0,0	No waves								

Table 12. Enhanced power matrix with hypothetical ADO system in a sloped breakwater

Sloped - Power Matrix Enhanced (kW)		T_P (s)								
		5	6	7	8	9	10	11	12	13
H_S (m)	4,0	Storm Protection Mode								
	3,0	-	-	-	-	64,4	63,1	62,3	59,2	-
	2,0	-	-	22,8	25,9	29,7	28,8	27,8	26,5	-
	1,0	-	5,7	5,8	6,5	7,2	-	-	-	-
	0,0	No waves								

Finally, in order to have a comparison reference, the power matrix of an actual EWP device was used. The power matrix was available in a technical brochure from the company, and it was generously handed out for the purpose of this study. Table 13 shows the actual power matrix of the EWP device.

Table 13. Actual power matrix of EWP device [50]

Power Matrix EWP (kW)		T_P (s)								
		5	6	7	8	9	10	11	12	13
H_S (m)	4,0	Storm Protection Mode								
	3,0	-	-	-	-	41,7	37,5	34,1	31,3	-
	2,0	-	-	26,8	23,5	20,8	18,8	17,1	15,6	-
	1,0	-	7,8	6,7	5,9	5,2	-	-	-	-
	0,0	No waves								

When comparing both power matrices the results were exciting. Considering that the shape of the devices is different and the fact that the power moves at the power of 3,5 with the Fourier scale, it is acceptable to not get exactly equal values. In this case, the average relative difference does not exceed 17%, showing a nice coupling between the numerical model and real-world applications, such as EWP device and improving the confidence of the results obtained.

One interesting way of graphically showing the power matrix is using a surface, this way, it is possible to display all the three variables (H_S , T_P and Power) in the same figure. The steeper the surface the more sensible is the device to handle different SST. The perfect surface should never be something like a high flat plateau, where all the SST provides good values of power output, otherwise, in SSTs with less available wave power (P_W) the efficiency (further called capture width ratio) would be enormously high, and unfortunately this cannot happen. The WEC under study showed itself to be a sensible WEC due to large difference in the power output for small differences in the SST. Figure 41 and Figure 42 displays the power matrix surface for the WEC under study.

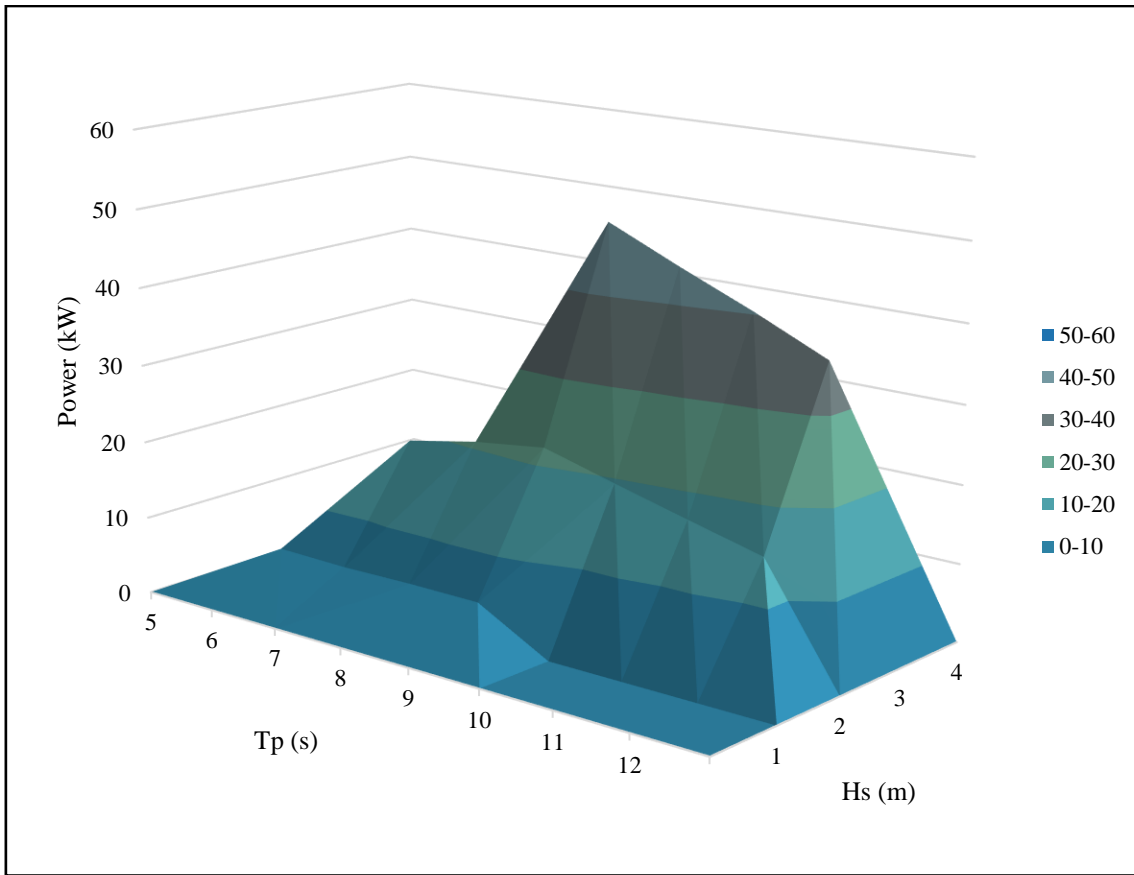


Figure 41. Power surface for vertical breakwater.

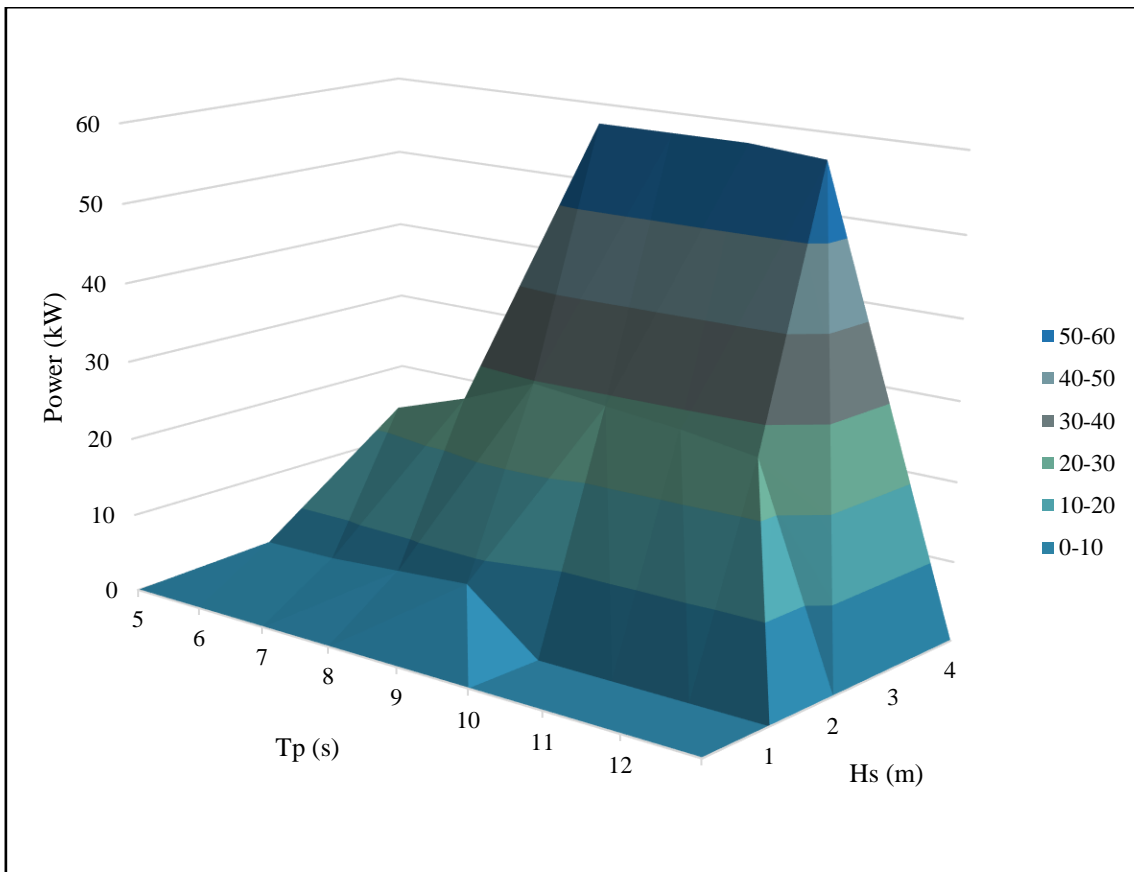


Figure 42. Power surface for sloped breakwater.

4.7. EFFICIENCIES AND BREAKWATER COMPARISON

In wave energy, when referring to efficiency there are mainly two parameters to express those values. Both are closely related and interconnected. The first one is the capture width (CW) and the second is the capture width ratio (CWR). The only difference from the first to the second is that the first does not consider the length available for power capture. Their formulas can be seen below:

$$CW = \frac{P}{P_W} \quad (14)$$

$$CWR = \frac{P}{P_W * L} \quad (15)$$

Where P is the power absorbed, P_W the wave power available and L the length of the device, that in this case is the diameter of the floater. This study would not be complete without a CWR analysis. In every power productor device, engineers are always worried about efficiency. Ultimately, the efficiency represents the work that was usefully extracted in comparison to the maximum extraction possible. The higher the efficiency values the better, meaning that more useful energy was converted given the same available power.

To calculate the WEC CWR for both breakwaters is necessary to estimate the wave available power (P_W). As already explained in section 2.3, the P_W can be estimated using Equation 1. However, for that equation to be used the period should be the energy period (T_E). Thus, it is necessary to work on the conversion between periods before proceeding to calculations. Using the JONSWAP spectrum ($\gamma = 3,3$) the relations are as following [5]:

$$T_P = 1,12 * T_E = 1,29 * T_Z \quad (16)$$

T_P , T_E , and T_Z are all wave period representations, but with different scales. T_E , or Energy Period, represents the time it takes for wave energy to pass a point and helps in understanding wave energy availability. T_P , or Peak Period, is the time interval between the highest peaks of waves and signifies the most energetic wave component in a spectrum. T_Z , or Zero-Crossing Period, is the average time between zero up-crossings of the wave profile and provides information about the average wave period. Having multiple wave periods is necessary because each of these parameters conveys different aspects of the wave's behavior, and together, they provide a comprehensive understanding of the ocean wave environment.

Once the T_E is calculated the P_W can be easily estimated. Table 14 shows the P_W for all the 14 SSTs analyzed. A quick look in Equation 1 allows to understand why the P_W value grows so quick with H_S . That happens because H_S is squared, and larger values of it will lead to even higher values of P_W . It is also interesting to note the contribution of T_E to the power, because despite it might look, the power increases with the period, *i.e.*, less waves crossing a vertical plane in the ocean will carry more power than when there are lots of waves crossing the same plane. This happens because when the period is higher, the wave celerity (velocity) is also higher, increasing the power available.

Table 14. Wave power available for different SSTs

Power Available (kW)		Periods								
		T_P (s)	6,0	7,0	8,0	9,0	10,0	11,0	12,0	13,0
		T_E (s)	5,4	6,3	7,1	8,0	8,9	9,8	10,7	11,6
H_S (m)	4,0	Storm Protection Mode								
	3,0	-	-	-	-	106	118	130	142	-
	2,0	-	-	37	42	47	53	58	63	-
	1,0	-	8	9	11	12	-	-	-	-
	0,0	No waves								

However, those values are meaningless for this study if the CWR is not assessed. Table 15 and Table 16 displays the CWR values for both breakwaters. In this study, the value was almost constant for H_S variations, while for T_E variations the CWR varied significantly, averaging 42% for vertical breakwaters and 57% for sloped breakwaters. Those variation can be graphically seen in Figure 43.

Table 15. CWR values obtained in a vertical breakwater

CWR		Periods								
		T_P (s)	6,0	7,0	8,0	9,0	10,0	11,0	12,0	13,0
		T_E (s)	5,4	6,3	7,1	8,0	8,9	9,8	10,7	11,6
H_S (m)	4,0	Storm Protection Mode								
	3,0	-	-	-	-	46%	37%	31%	25%	-
	2,0	-	-	51%	49%	47%	37%	29%	23%	-
	1,0	-	65%	54%	48%	43%	-	-	-	-
	0,0	No waves								

Table 16. CWR values obtained in a sloped breakwater

CWR		Periods								
		T_P (s)	6,0	7,0	8,0	9,0	10,0	11,0	12,0	13,0
		T_E (s)	5,4	6,3	7,1	8,0	8,9	9,8	10,7	11,6
H_S (m)	4,0	Storm Protection Mode								
	3,0	-	-	-	-	61%	53%	48%	42%	-
	2,0	-	-	62%	62%	63%	55%	48%	42%	-
	1,0	-	72%	63%	62%	61%	-	-	-	-
	0,0	No waves								

One interesting aspect to be discussed is the differences between the two breakwaters configurations. The sloped one showed itself to be more power producter than the vertical one in every simulation. This was even expected as vertical breakwaters suffer from greater energy losses in non-useful ways, such as splashing. While on sloped breakwaters, the wave enters more smoothly, allowing more energy to be converted in a useful way, in this case, through the WEC's PTO. However, it is important to mention that real life sloped breakwaters suffer from several others energy dissipations phenomena that were not considered in the model, such as porosity, roughness and turbulence. Those effects might lead to lower power values than vertical breakwaters. More detailed and complex numerical models would be required in order to evaluate those effects.

Besides that, CWR values averaged around 25% for the WEC under study. This value matches the expectable with others similar heaving devices, in which the CWR value ranged between 4 to 36% [55]. Within the wave energy world, OWCs devices are usually the ones with higher CWR, reaching up to 65% in some cases [55]. However, those values are still attached to high CAPEX and OPEX values, which still makes wave energy not preferable.

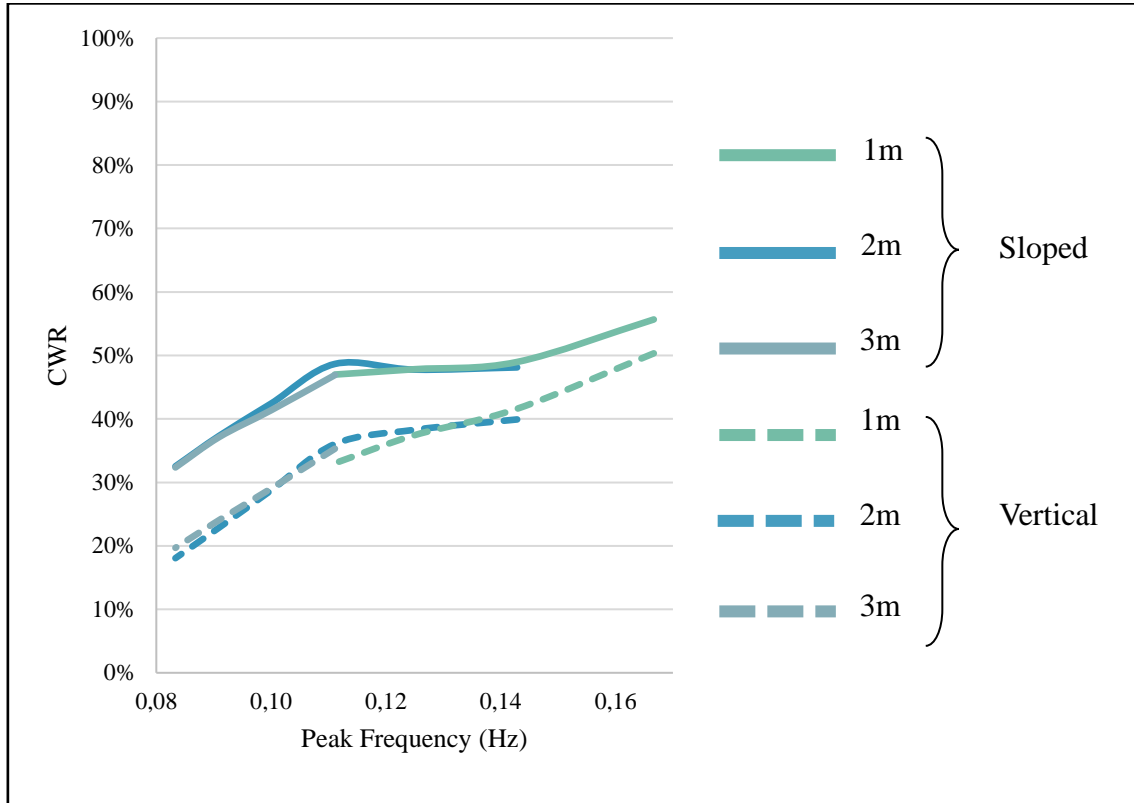


Figure 43. CWR value versus peak frequency.

4.8. EXPECTABLE ELECTRICITY PRODUCTION AND CO₂ REDUCTION

Energy can exist in numerous forms such as thermal, mechanical, kinetic, potential, electric, magnetic, chemical, and nuclear [56]. However, most of this energy can't be fully converted into work. Work is the energy transfer associated with a force acting through a distance, and the work done per unit of time is called power [56]. Energy that cannot be fully converted into work is usually denoted by disorganized energy, such as heat, but electricity for instance, can be fully converted into work, therefore, is the best way of energy people can have, *i.e.*, is the most organized and valuable type of energy. The WEC under study operates exactly under this principle. It converts disorganized energy (motion of the waves) into organized and useful energy (electricity), and the price it pays for it is low efficiency. However, until the date of this dissertation and until the validity of the second law of thermodynamics continues, the world will continue without devices capable of converting 100% of disorganized energy into organized energy. After all, the entropy of the world should always keep increasing.

The prediction of the disorganized energy effects on the body was already done. Now it is time to estimate what is the organized energy converted or the electricity output. To do that, the power matrix obtained should be crossed with the wave resource matrix, thus, the power in kW will be multiplied per the SST occurrence in hours and then the final value will be energy (kWh). Table 17 displays the same wave resource matrix for the Port of Leixões showed in Table 4, however, for only the SST analyzed and with hourly values, not percentage.

Table 17. Wave resource matrix for the location under study

Wave Resource Matrix (h)		T_P (s)								
		5	6	7	8	9	10	11	12	13
H_S (m)	4,0	-	-	-	-	88	88	88	88	88
	3,0	-	-	-	88	263	351	351	263	175
	2,0	-	175	526	789	877	701	526	263	88
	1,0	88	526	701	614	351	88	-	-	-
	0,0	No waves								

The electricity matrix output, shown in Table 18 and Table 19, suggests some interesting conclusions. First, it is evident that the most powerful SST (3m of H_S and 9s of T_P) is not the one that most contributes to the electricity generation. This is because this SST happens significantly less in a year than other SSTs. The biggest contributor for the electricity output happens to be the most common SST (2m H_S and 9s T_P), meaning that when designing WEC it is crucial to take into account not only the best performance but also the average performance. Secondly, when summing up all the values of the matrix it is possible to predict the production in a year. In this case, the value reaches up to 190MWh for sloped breakwater applications and 135MWh for vertical breakwater application for a single device placed in the Port of Leixões and in Douro River. These values might seem low at first view, however, it is mandatory to consider that those WEC can be installed one next to the other, making the final electricity production way larger.

Table 18. Electricity matrix for different SST throughout the year for vertical breakwater

Vertical - Electricity Output Matrix (MWh)		T_P (s)								
		5	6	7	8	9	10	11	12	13
H_S (m)	4,0	Storm Protection Mode								
	3,0	-	-	-	-	12,7	15,5	14,1	9,5	-
	2,0	-	-	10,0	16,4	19,3	13,7	9,0	3,9	-
	1,0	-	2,7	3,5	3,1	1,8	-	-	-	-
	0,0	No waves								

Table 19. Electricity matrix for different SST throughout the year for sloped breakwater

Sloped - Electricity Output Matrix (MWh)		T_P (s)								
		5	6	7	8	9	10	11	12	13
H_S (m)	4,0	Storm Protection Mode								
	3,0	-	-	-	-	16,9	22,1	21,8	15,6	-
	2,0	-	-	12,0	20,4	26,0	20,2	14,6	7,0	-
	1,0	-	3,0	4,1	4,0	2,5	-	-	-	-
	0,0	No waves								

The deployment length available at Port of Leixões is large and goes up to 542m (Figure 44). Considering a spacing of 5m for each WEC, the total numbers of WEC can be calculated dividing the total length by the individual WEC length, summing up to 108 places available. Multiplying this value by the total electricity produced it is possible to estimate a total of incredible 14.643MWh/year and 20.628 MWh/year for vertical and sloped respectively. Which, according to Table 6, is enough to supply all the electricity demand of the Port.

The carbon intensity in Portugal in 2022 was 234g of CO₂ for each kWh produced of electricity. This means that 3.426t of CO₂ would be avoided to be released into the atmosphere for vertical breakwaters and 4.827t of CO₂ for sloped breakwaters, strongly contributing to the European decarbonization schedules and of course, for slowing down the global warming. Apart from that, the Port would be more energy independent and self-sufficient. To put this into perspective, it is the equivalent of going around the globe 896 times using an average commercial airplane (considering 115gCO₂eq/km*passenger).



Figure 44. Map showing the length available for deploying WECs in the Port of Leixões.

4.9. NUMERICAL MODEL LIMITATIONS

While the numerical simulations conducted in ANSYS have provided valuable insights into the behavior of the hinged WEC fixed to vertical and sloped breakwaters, it is crucial to acknowledge the limitations and assumptions inherent in the modeling process. These limitations may affect the accuracy and applicability of the results. The following items outlines the key limitations of the numerical model:

- 1) **Idealized Fluid Dynamics:** The numerical model assumes idealized fluid flow behavior. It simplifies the complex interactions between the WEC and the surrounding fluid by employing fluid dynamic equations that may not capture all intricacies. For instance, turbulent effects, wave breaking, and boundary layer effects near the breakwater were not fully considered in the simulations. Real-world conditions may introduce additional complexities;
- 2) **Idealized Structural Response and Breakwaters:** The structural response of the articulated WEC is assumed to be linear and elastic in nature. In reality, the device may exhibit non-linear behavior due to material properties, fatigue, or structural complexities. These non-linear effects can impact the device's performance and fatigue life, which the model does not fully account for. Apart from that, several energy dissipation phenomena in the breakwater are also not considered. Roughness, holes between rocks and many other effects that may affect energy production should be considered;

- 3) **Computational Resources and Mesh Sensitivity:** Due to computational constraints, the model may use a coarser mesh or simplified settings. Thus, the model might not have been fully and completely represented in the numerical model. Mesh sensitivity studies to ensure the model's accuracy under various conditions might not have been exhaustively conducted;
- 4) **Site-Specific Variability:** The model may not fully account for site-specific variations in wave characteristics, bathymetry, seabed properties, and environmental conditions. Results may not be directly transferable to different locations or scenarios.

It is important to recognize these limitations when interpreting the results of numerical simulations. Future research and development should aim to address these limitations for a more accurate representation of real-world conditions and a more robust assessment of the articulated WEC's performance and feasibility.

5

EXPERIMENTAL MODEL

The numerical study would not be complete without any experimental validation. In order to do that, a physical model was built and tested in a wave flume. The tests were conducted at the FEUP Hydraulics Laboratory, and all the measures were taken using high-tech equipment. This chapter aims to explain the procedures behind those tests and to display and discuss the main results obtained.

5.1. BODY CONCEPT AND CONSTRUCTION

The biggest challenge was to find a concept that kept the device completely still with respect to lateral movement (later presented as the Y axis) but allowed free movement in the Z axis (up and down). In addition, it was also necessary to find a way to create a damping with a known value, since as already discussed here, it is always necessary to apply a resistance to the movement in order to extract power.

After some discussion and a lot of research it was decided that the best setup would be something like a disc brake bicycle wheel, where the bicycle fork would act as the WEC support, providing zero lateral movement and the hydraulic disc brake would be the damping. The components used from a bicycle can be better visualized in Figure 45.



Figure 45. Bicycle components used for experimental modeling.

To do so, it was necessary to buy three fundamental new parts. First, the bicycle fork that would support the device, then a set of hydraulic disc brakes and finally a front hub to allow the angular movement of the device.

The floater itself is nothing more than a spherical marine signal buoy cut in half with a wooden top. For the arm, two metal bars were used, which were cut to 44cm in length and screwed to the floater using six screws and nuts (Figure 47b). The angle of the arm with the floater was established using a piece of wood cut with the necessary inclination.

The floater assembly plus the metal arm was connected to the bicycle hub by means of small lateral screws. The fitting of the hub with the fork of the bicycle is perfect due to the wide use of this concept in the world of bicycles and allows for almost completely frictionless rolling (Figure 46).

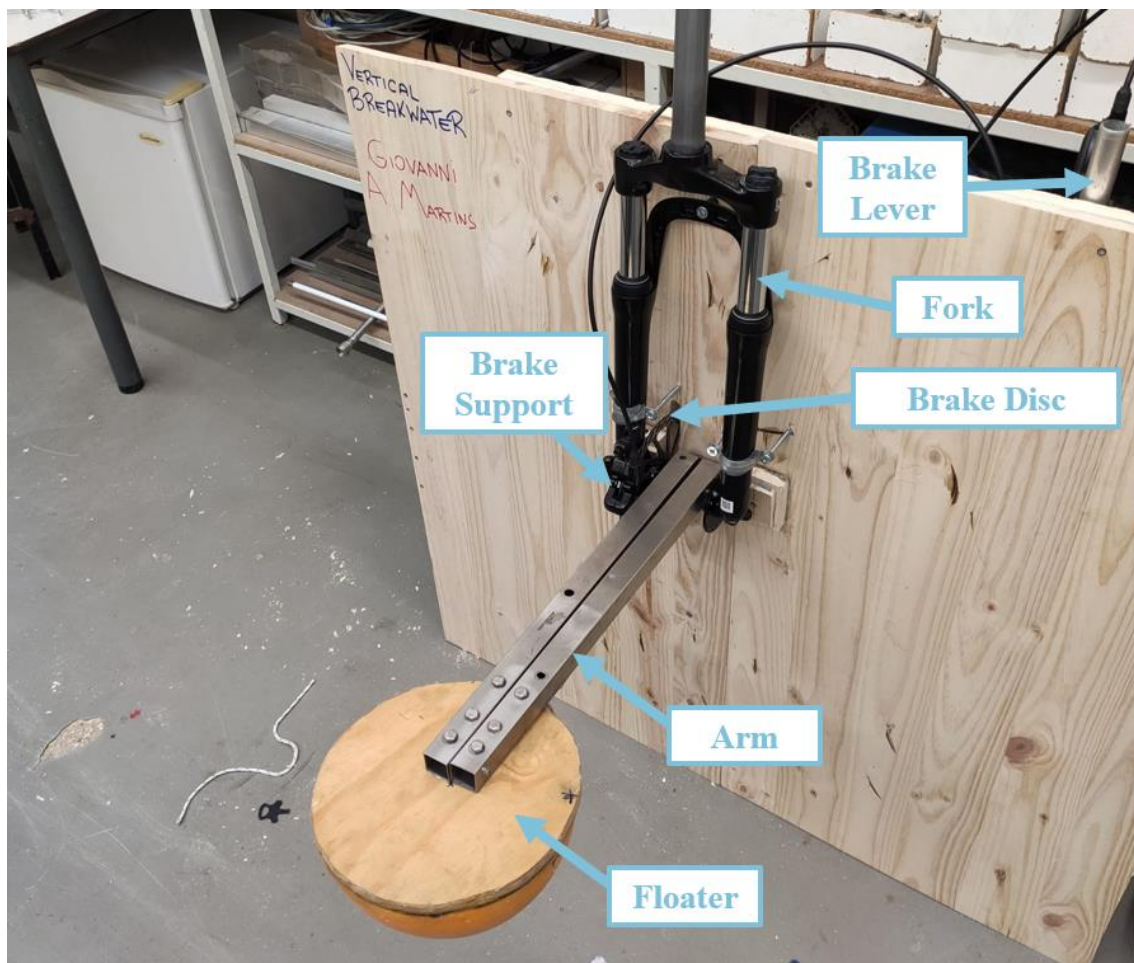


Figure 46. Experimental WEC setup built.

For the damping, a hydraulic brake system was used where a known preload would be applied to the brake, allowing to keep the damping coefficient constant. The bike fork purchased was already designed to have brake support, so the brake disc would be perfectly aligned and without friction. The brake lever was connected to a metal bar and then a system of threads and screws was made so that a specific damping value could be applied depending on how tight the brake was (Figure 47a).

Finally, after assembling everything, it was only necessary to build a wooden breakwater and attach the bicycle fork to the breakwater. The breakwater used was 1m by 1m and had to be drilled in the middle so that the disc would fit into the structure. Two lateral wooden supports were also built to support the force of incident waves. Reinforced concrete blocks (2500kg/m^3) were used to give strength and robustness to the breakwater to stand the waves generated. More than 750kg of blocks were placed behind the breakwater using the crane of the laboratory. Those blocks are shown later in Figure 55b.

Unfortunately, there was not enough time available for testing both breakwaters' configurations (sloped and vertical) due to tied laboratory schedules. The configuration chosen was the vertical breakwater due to the easiness of building. However, it was considered that if the numerical vertical model was properly validated by the experimental setup, so would the sloped breakwater, that followed absolutely the same parameters and rules as the vertical one.



Figure 47. Detailed view of the arm attachment zone and brake setup.

5.2. SCALING

Scaling while studying engineering devices is a common approach. Usually testing real scale projects can cost a significant amount of money and the results may not be worth it. Thus, it is usual to test something little, that will not have a huge cost, and in the case it fails, the losses are not severe. The same concept was applied in this study, with the aim of validating the numerical model and not costing a huge amount of money.

There are many scales used in engineering. However, within marine studies, people are usually interested in a good representation of the forces of inertia and gravity. For this purpose, the Froude scale (William Froude 1810-1879) is used, which was also applied in this experimental study. All relevant parameters, such as the damping and the power absorbed, are related and must be scaled according to proper scaling factors (SF) derived from the Froude scaling law. These factors are presented in Table 20.

Therefore, all values calculated for the experimental study as well as for their subsequent comparison with the numerical study had to undergo conversions between scales, most of them will not be even mentioned in this text. The equation that allows this conversion to be carried out only considers the scale to be used (s), the SF and the parameter to be converted (Equation 17).

Table 20. Common scaling factors used in WECs studies [51]

Quantity	Scaling Factor
Linear Displacement	s
Angular Displacement	1
Translational Velocity	$s^{0,5}$
Angular Velocity	$s^{-0,5}$
Translational Acceleration	1
Angular Acceleration	s^{-1}
Mass	s^3
Force	s^3
Torque	s^4
Power	$s^{3,5}$
Linear Damping	$s^{2,5}$
Angular Damping	$s^{4,5}$
Wave Height and Length	s
Wave Period	$s^{0,5}$
Wave Frequency	$s^{-0,5}$
Power Density	$s^{2,5}$

$$\lambda_{realScale} = \lambda_{scaleDown} * SF \quad (17)$$

5.3. WAVE CURRENT FLUME

The channel where the tests were performed is a large wave-current flume that works in a closed circuit (Figure 48), located within the Hydraulics Laboratory of FEUP. The water of the channel is pumped from 2 reservoirs, located at a lower level (under the floor of the laboratory zone), by 4 associated pumps in parallel. However, the installation is prepared for the placement of two more pumps if necessary. The connection to the channel is made by a duct of 500 mm in diameter that feeds the top reservoir [57]. In this reservoir there is a "trop-plein" structure that keeps the water level constant, thus allowing the channel's feeding flow to be constant.

The first section of the channel consists of an area 7,4m long, 1,6m wide and 3m high, has a flat bottom part of length 1,8m and another with inclined bottom, 3,5m long, from which the bottom level of the section of these of the channel is reached. The channel, discovered above, has a bottom with slope of 0,5%, length of 32,3m and rectangular cross-section with 1m wide and 1,33m high. The test section has 7 glass windows, 2m long and 1m high, to allow easy visualization of the flow and measurements using optical equipment. Downstream, a vertical flat gate, acting as a discharger, allows to regulate the height of the flow [57].

Figure 48a displays the side view of the tank with the observation glass windows and Figure 48b the top view, with main dimensions and components of the channel used. As can be seen, the workstation is on the top, allowing the user to check simultaneously the computer and the channel. This is especially interesting to understand the behavior of some particular SSTs.



Figure 48. Dimensions of the channel used.

5.4. DAMPING CHARACTERIZATION

Characterizing the damping was a specially challenging task. In order to calculate the extractable power, according to Equation 11, it is necessary to previously know the damping coefficient (C_D) to be used. This value can be calculated by running some tests with the experimental model and then trying to understand its behavior. The damping characterization done in this study consisted in a first theoretical and mathematical understanding of the damped pendulum equations, and then a MATLAB® code to simulate the desired effect. Those procedures are presented below.

First, it was necessary to set up the floater and arm parameters because those were fundamental for moments of inertia calculations that will be further used. The mass of the floater (m_F) was measured to be 0,475kg and the mass of the arm (m_A) 1,233kg. Apart from that, the arm had to be 0,443m long in order to match the scale.

Figure 49 shows the free torque diagram of the system. As can be seen, there are mainly three torques to be considered, the first one is related to the floater, the second one is related to the arm and should be considered to have half of the arm length, and the third one is the damping torque, or the resistance to the movement torque that should be also considered. Applying the equilibrium principle allows to develop equations that can estimate the damping coefficient value.

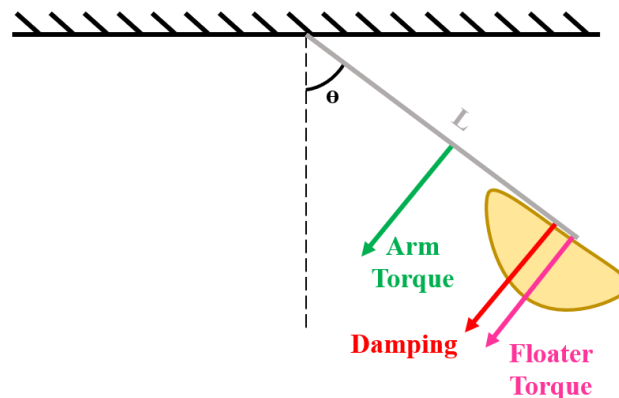


Figure 49. Free torque diagram applied to the floater.

The formula for resulting torque (T_r) is:

$$T_r = I_T * \alpha \quad (18)$$

Where I_T is the total moment of inertia and α is the angular acceleration. Applying the equilibrium principle to the system (arm plus floater), it is possible to develop:

$$m_F * g * L * \sin(\theta) + m_A * g * \frac{L}{2} * \sin(\theta) + C_D * \omega + I_T * \alpha = 0 \quad (19)$$

Where L is the arm length (Figure 49), ω is the angular velocity and θ is the angle with the vertical. The total moment of inertia is then given by:

$$I_T = m_F * L^2 + \frac{m_A * L^2}{3} \quad (20)$$

In which the floater uses the normal equation for moments of inertia and the arm uses the rod about axis equation, that can be numerically demonstrated that is 1/3 of the main value. Then, organizing Equation 20 and diving by I_T :

$$\alpha + \frac{C_D * \omega}{I_T} + \frac{(m_F * L + \frac{m_A * L}{2}) * g * \sin(\theta)}{I_T} = 0 \quad (21)$$

For simplicity it is defined that:

$$\lambda = \frac{C_D}{I_T} \quad (22)$$

$$U = (m_F * L + \frac{m_A * L}{2}) \quad (23)$$

The characterization equation then becomes:

$$\varphi^2 + \varphi * \lambda + \frac{U * g}{I_T} = 0 \quad (24)$$

Solving using complex ordinary differential equations (ODE) solvers:

$$\varphi = -\frac{\lambda}{2} \pm \frac{\sqrt{\lambda^2 - \frac{4 * U * g}{I_T}}}{2} \quad (25)$$

Assuming $\beta = \lambda/2$:

$$\varphi = -\beta \pm \sqrt{\beta^2 - \frac{U * g}{I_T}} \quad (26)$$

In which the damping can be categorized in three different types according to its β value:

Table 21. Damping type according to its damping factor

Damping factor	Damping Type
$\beta^2 > \frac{U * g}{I_T}$	Overdamped
$\beta^2 = \frac{U * g}{I_T}$	Critical
$\beta^2 < \frac{U * g}{I_T}$	Underdamped

Considering the damping mechanism used in this study, the third type is the one that best fits. Therefore, the equation that better describes the angle displacement with time comes as:

$$\theta(t) = e^{-\beta * t} * (A * \cos(\omega_* * t) + B * \sin(\omega_* * t)) \quad (27)$$

This equation has two components as shown in Figure 50. The exponential term that drives the decay and the oscillating term, which is a sinusoidal function. For characterizing a damper, it is just necessary to analyze the exponential component since only the absolute difference is needed.

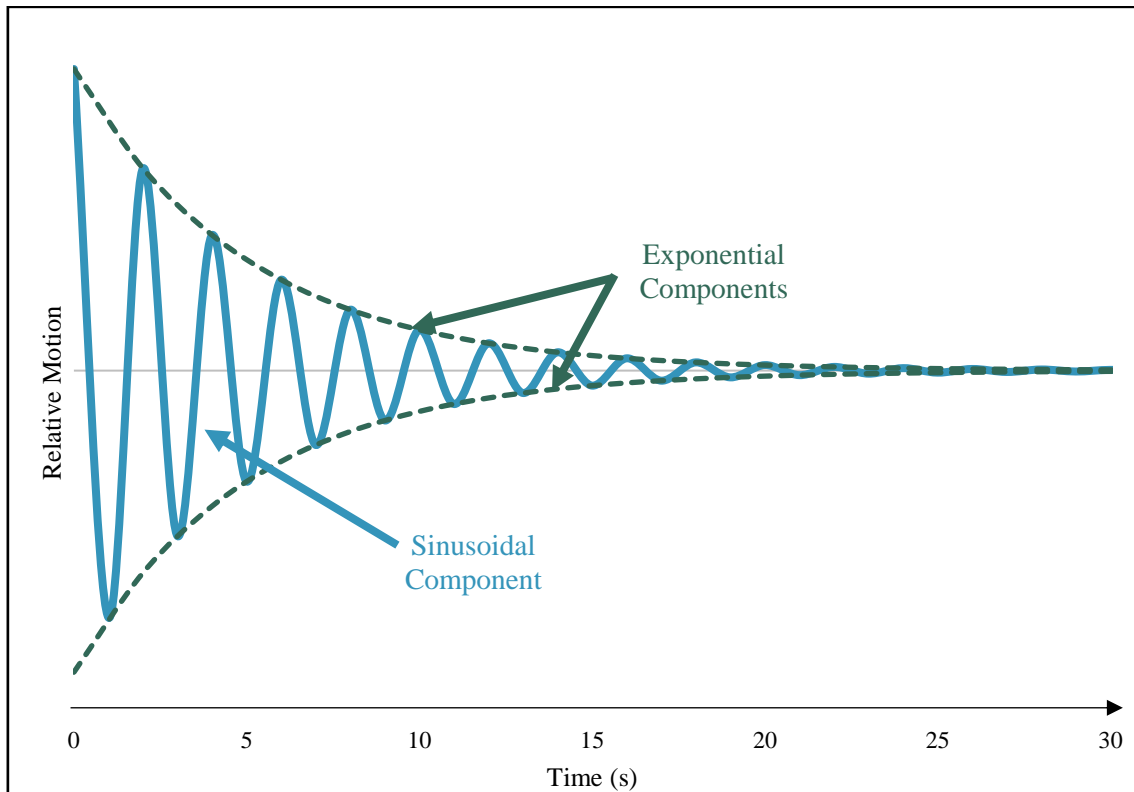


Figure 50. Typical damped pendulum decay graph.

Thus, the equation reduces itself to:

$$\theta(t) = \theta_{MAX} * e^{-\beta * t} \quad (28)$$

Substituting β :

$$\theta(t) = \theta_{MAX} * e^{-\frac{C_D}{2 * I_T} * t} \quad (29)$$

As can be seen, Equation 29 relates the damping coefficient with the time of the test and with the angular displacement. Therefore, incorporating it in a MATLAB® code can be quite useful for understanding the behavior of the system and for plotting the video of the pendulum until it stops completely. The full MATLAB® code used can be consulted in Appendix – I at the end of this document.

Once the code was written it was possible to see how long the system would take to full stop with a certain value of C_D . Thus, to get the right C_D value in the brake it was necessary to get the same time for the experimental model. This way, multiple simulations were done with a stopwatch in hands and the time for full stop of the system was measured. After some tries the video of MATLAB® was matching perfectly the real experimental model, meaning that the right C_D was achieved in the brake.

According to the code, between 9 and 10s was the time that the system needed to stop (Figure 51) with an angular damping coefficient of $0,2 \text{ Nsm}^\circ$ and an initial angular displacement of about 49° , that was the upper maximum angle. This C_{AD} value was the only used since was the best damping coefficient for vertical breakwaters (as explained in section 4.4). It was obtained through the SF from Table 20:

$$C_{ADScaleDown} = \frac{C_{ADRealScale}}{s^{3,5}} = \frac{25000}{14^{4,5}} = 0,2 \text{ Nsm}^\circ \quad (30)$$

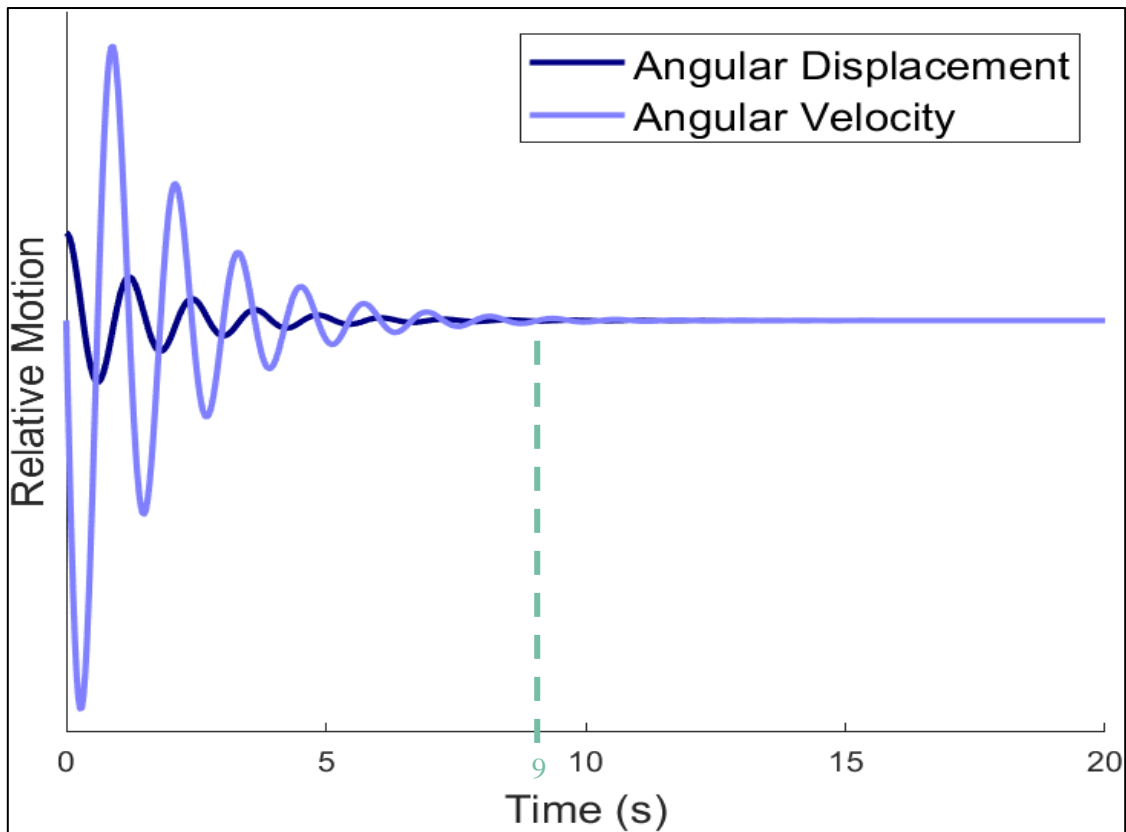


Figure 51. Time that the system would take to completely stop according to the code.

Creating a digital twin of the model in MATLAB® was really helpful in order to characterize the damping value. Other techniques would take significantly more time and probably would have been conducted for more imprecise values. The perfect match between the digital twin and the code emphasizes the potential of digital simulations and the fundamental role they can play in engineering simulations.

5.5. MEASURING AND WORKING EQUIPMENT

Once the device was in the channel, it was time to start testing. However, in order to carry out the measurements that are fundamental to obtaining and then analyzing the results, it was necessary to properly place, configure and calibrate the devices that would be used to carry out the measurements. There were essentially three equipment used: the infrared motion capture system for the measurement of the position of the reflective balls attached to the floater (and hence the floater motions), the probes for measuring the water level and consequently the period and height of the waves, and, finally, the wavemaker, which allows the generation of waves with the required characteristics. Each of these systems needed fine-tuning in order to operate properly, which meant a full day's work in the laboratory.

5.5.1. QUALISYS® MOTION CAPTURE SYSTEM

Qualisys® is a Swedish company that specializes in motion capture systems, including cameras and software, used for various applications such as biomechanics, sports analysis, animation, robotics, and more. Qualisys cameras are primarily known for their optical motion capture technology. They are largely used in marine and coastal studies due to their high precision recording capacity, allowing the movement of the body to be fully characterized. A good way of understanding the functioning of the cameras in this study is given below:

- 1) **Camera Setup:** Qualisys systems typically consist of multiple high-speed cameras placed around a capture area. These cameras are synchronized to work together, capturing the movement of markers placed on the floater. As can be seen in Figure 53, there were 3 cameras capturing the movement around the floater, each of them in a different position in order to improve the accuracy of the global results;
- 2) **Marker Placement:** In order to track the floater motion, small reflective markers were attached to specific points on the object. Those markers were attached in the form of a tower to the floater center (Figure 52a). These markers reflect light back to the cameras, making them visible to the system;
- 3) **Infrared Light:** Qualisys cameras use infrared light for tracking. They emit infrared light, and the reflective markers on objects reflect this light back towards the cameras. That is why the other reflective points, namely the metallic arm, part of the fork and some other screws were also painted black, ensuring that no mistaken reflections would be captured;
- 4) **Camera Observation:** When the object moves, the reflective markers also move. The synchronized cameras observe these markers from different angles. By triangulating the position of each marker based on the angles from multiple cameras, the system can determine the 3D position of each marker in space;
- 5) **Data Processing:** The raw data from all cameras is sent to a computer where the software performs complex calculations to reconstruct the 3D positions of the markers in real-time. This data is then used to recreate the object's movement, allowing to understand how the floater behaved in each simulation;
- 6) **Data Output:** The captured motion data can be visualized in real-time or post-processed using specialized software. The TXT files generated were after handled to Excel® in order to calculate the body velocity;
- 7) **Calibration:** Before the motion capture session, the cameras and the capture area need to be calibrated. This involves capturing known reference points to establish the relationship between camera positions and the real-world coordinates. This calibration ensures accurate tracking. This step was carried out using a specific reflective arm and a stick with little reflective balls on top.

The TXT files generated after each simulation contained the X, Y and Z coordinates (Figure 52b) of each marker for every time step (defined as 154Hz). Considering that each simulation was recorded for 70s, there were at least 10.780 records for each marker on each axis. After 28 simulations, there were more than 3.622.080 position records to be carefully analyzed.

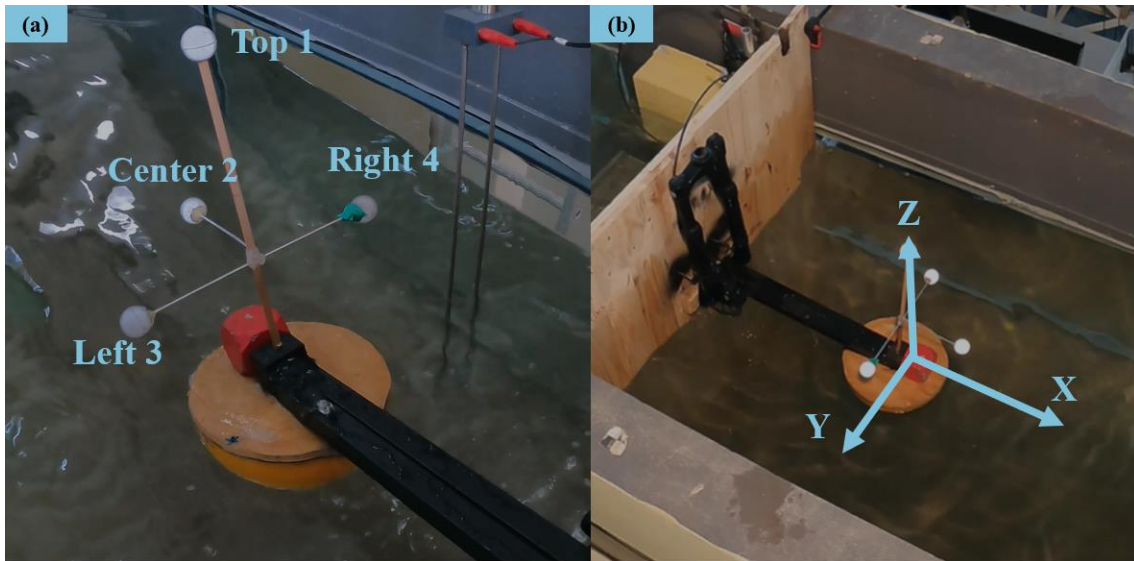


Figure 52. Coordinates system adopted and name of the markers.

Qualisys cameras are known for their high accuracy and flexibility, making them popular in both research and professional applications. In this study, their technology was crucial to measure the body velocity and then to estimate the power output through its motion capture analysis.



Figure 53. Qualisys® cameras setup and positioning.

5.5.2. WAVES PROBES

Waves probes are fundamental for measuring the water free surface elevation and thus to estimate the wave height and the wave period. There were 4 probes installed in the channel in order to take water level measures. Those probes were distancing 0,0m-0,5m-0,8m-1,1m respectively from the first probe, as can be seen in Figure 54.

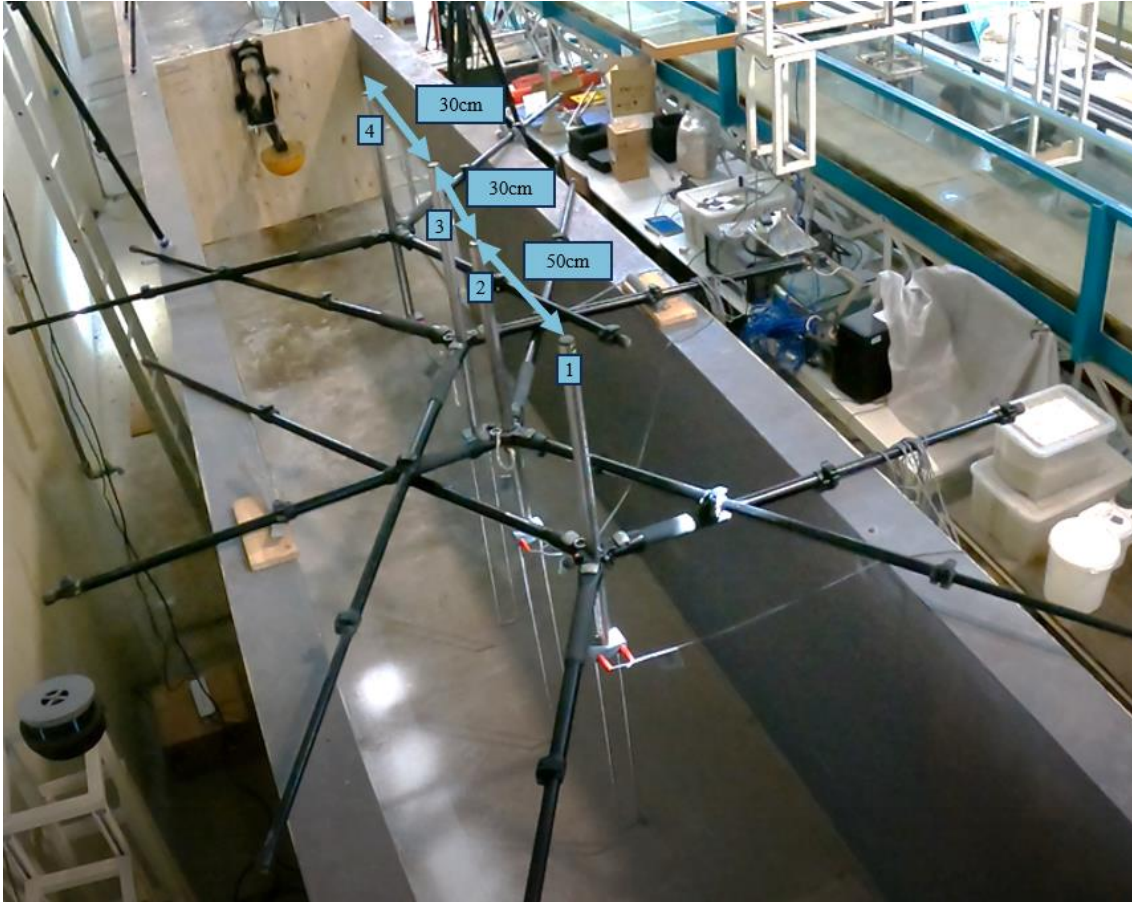


Figure 54. The four probes and their distance in the channel.

In the first use, it was necessary to calibrate the probes for the selected water level. The water level in the channel was selected to be between 55 to 60cm deep, assuring that 8m of real scale were represented. To calibrate the probes, they were initially positioned at their lowest point and then measurements were taken. Subsequently, the probes were placed at the highest position, and measurements were taken again. Finally, the probes were positioned at the middle point, and measurements were taken once more. This process made it possible to plot a graph with different calibration curves, all of which passed through the zero point, so that the height of the water in the tank could be measured directly.

The probes operate by measuring the current passing through the stainless-steel metal arms. This value is directly affected by contact with the water, so by the difference in current along the arm it is possible to know precisely how high the water is at a given moment.

All the probes are connected to an information receiver which decodes the signals sent by the probes and calculates the water height for each of the probes. The software called HRDAQ® processes the information and plots graphs, tables and figures about the simulations that were run. This software was used on a separate computer while running the simulations.

5.5.3. WAVE MAKER

The wave generator used in the study is also from HR Wallingford® and is essentially the same size as the channel, *i.e.*, 1m wide and 1,3m high (Figure 55a). The generator consists of a vertical metal paddle that moves back and forth by means of an electrical system and generates waves with the desired frequencies and heights. There is also special software for using the wave maker called HR Waves®, in which you can make changes to the characteristics of the wave and prepare the simulation.



Figure 55. HR Wallingford® wave maker and concrete blocks used.

5.6. EXPERIMENTAL TESTS

After all measuring devices were correctly calibrated and installed, it was finally possible to start testing with wave generation. The wooden breakwater was built with dimensions such that it occupied the entire width of the channel (Figure 53). Therefore, two sections were created within the channel. The wave propagation section that encompassed everything up to before the breakwater and a section after the breakwater, for equalization, where the effect of the waves was almost no longer felt.

The channel reached the required water height (around 0,6m) in less than 30 minutes with an inflow of about 38L/s. The biggest issue was regulating the flow of new water in order to compensate for water losses due to leakage at the last section of this wave-current flume. After another 2h of testing, it was possible to determine that the flow rate should be maintained at 4,5L/s so that the water level remained constant.

Once the channel had the WEC properly installed, the measuring devices configured and the water height was constant, it was finally time to start testing. To this end, two groups of tests were defined that encompassed the 14 SSTs analyzed in the numerical study. One of the groups admitted that waves were regular, and the other group considered the waves to be irregular (real). It was also necessary to adjust wave heights and wave periods to the scale of the experimental model, following the Froude criteria (Table 20). Table 22 shows the values of H_S and T_P used in the 28 tests.

Table 22. Experimental tests H_S and T_P values

Simulation	SST	Waves	Duration (s)	Real (Numerical)		Experimental (Scale Down)	
				H_S (m)*	T_P (s)*	H_S (m)*	T_P (s)*
E01 E02	SS1.1	Reg.	60	3,00	9,00	0,22	2,44
		Irre.					
E03 E04	SS2.1	Reg.	60	3,00	10,00	0,22	2,71
		Irre.					
E05 E06	SS3.1	Reg.	60	3,00	11,00	0,22	2,98
		Irre.					
E07 E08	SS4.1	Reg.	60	3,00	12,00	0,22	3,25
		Irre.					
E09 E10	SS5.1	Reg.	60	2,00	7,00	0,15	1,90
		Irre.					
E11 E12	SS6.1	Reg.	60	2,00	8,00	0,15	2,17
		Irre.					
E13 E14	SS7.1	Reg.	60	2,00	9,00	0,15	2,44
		Irre.					
E15 E16	SS8.1	Reg.	60	2,00	10,00	0,15	2,71
		Irre.					
E17 E18	SS9.1	Reg.	60	2,00	11,00	0,15	2,98
		Irre.					
E19 E20	SS10.1	Reg.	60	2,00	12,00	0,15	3,25
		Irre.					
E21 E22	SS11.1	Reg.	60	1,00	6,00	0,07	1,62
		Irre.					
E23 E24	SS12.1	Reg.	60	1,00	7,00	0,07	1,90
		Irre.					
E25 E26	SS13.1	Reg.	60	1,00	8,00	0,07	2,17
		Irre.					
E27 E28	SS14.1	Reg.	60	1,00	9,00	0,07	2,44
		Irre.					

* H_S and T_P values are only meaningful for irregular waves due to its random behavior. For the regular waves those values were adjusted for normal amplitude and waves period.

The wave maker would take approximately 1min to prepare each test and another minute to complete the tests. To generate the desired waves, the only required input for irregular waves was the H_S and T_P and for regular waves the frequency and wave height. Furthermore, it was also necessary to wait until the water calmed down completely in the channel before starting the next test. This way, the entire process of each simulation took between 17-22min depending on the time until the water stabilized. Thus, to run 28 simulations, 9h of testing were necessary, which were carried out on two consecutive days in the laboratory.

At the end of each test there were 3 files to be saved. The first one was the Qualisys® files with the floater motions along the test, the second were the water levels measured by the wave probes and the third one was the wave generator files, displaying some technical information about the test, such as paddle velocity, paddle displacement and some other parameters.

5.7. OBTAINED POWER MATRIX

Data processing took place again using an Excel® spreadsheet that had already been previously prepared. The velocities of the WEC floater were calculated by Qualisys® based on the difference in positions of the reflective markers between two time-steps and the elapsed time. For the power, Equation 11 was used based on the previously defined C_D value. The most representative values were considered to be those of the Left 3 and Right 4 markers, as these were the only ones with equal distances in Z and X from the floater.

As can be seen in Figure 52a, the Top 1 marker is at a different Z coordinate from the floater (higher) and the Center 2 marker is at a further forward dimension of the floater. Therefore, the velocities calculated for these points do not exactly match the velocities of the floater. However, as the Left 3 and Right 4 markers have the same X and Z positions, they were used to extract the average power values. Several averages were analyzed in order to reduce possible associated errors. They included raw averages, averages without zeros, averages without outliers, and averages without outliers and without zeros. The most reliable values were found in the averages without zeros and without outliers (defined as 20%).

Figure 56 displays the time-series for the Top 1 marker under the first test (most of time-series followed the same pattern). This figure shows how the choice of the setup based on a bicycle system was correct. The undesirable movement in Y axis is residual throughout the entire test. The bicycle fork together with the hub only allows the floater to move up and down depending on the arrival of incident waves. Apart from that, it was also possible to realize the “warm-up” time of the floater, where the incident waves are still not the desired waves as the wave maker just started moving. This warm-up time happens to take usually between 30 to 40s.

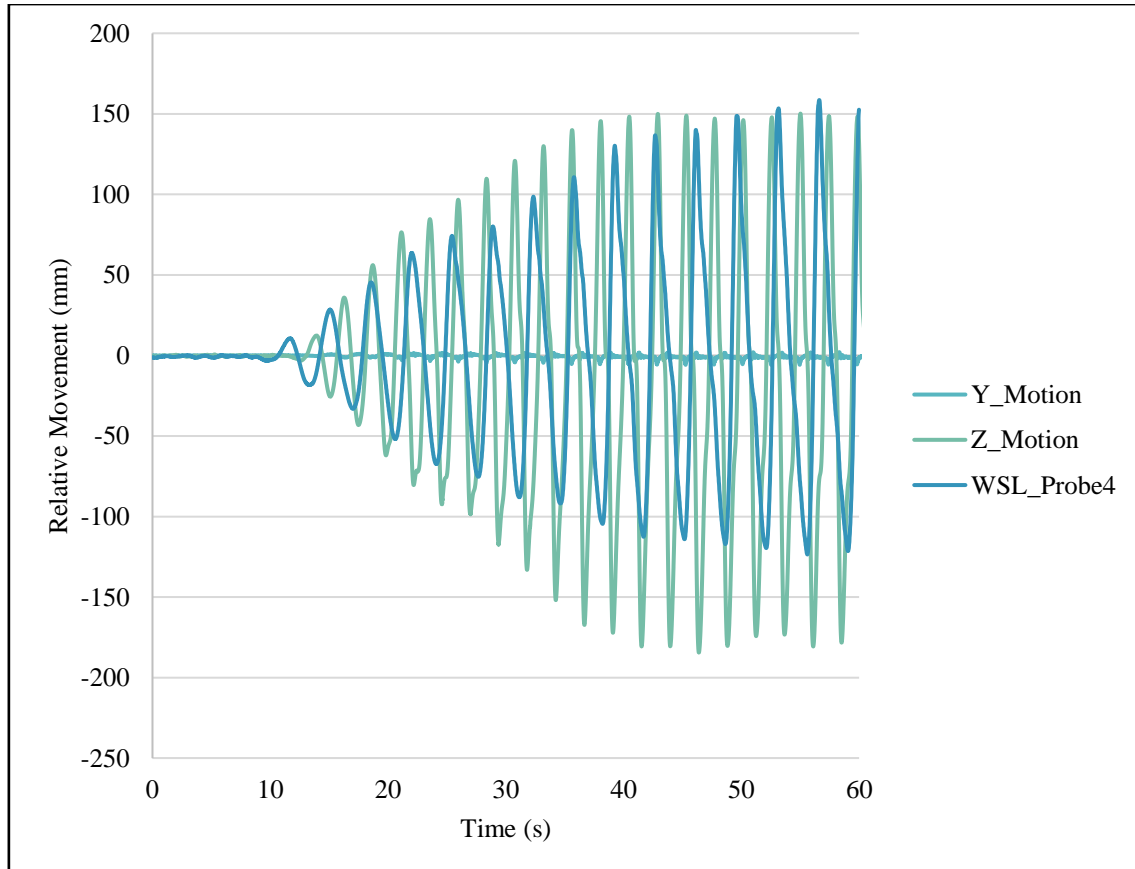


Figure 56. Time-series for Top 1 marker.

Table 23 and Table 24 display the power matrix obtained after running the tests in the channel and after processing the data for both regular and irregular waves tests. Appendix – II contains all the power values before and after the scaling process. As can be seen, regular waves are showing themselves to be way power productors than irregular waves. These differences are significantly linked to the short duration of the tests in the channel (60s). The channel, being a closed structure, with a vertical breakwater where the WEC was located downstream, and a vertical "breakwater" where the waves were generated upstream, creates a true "ping-pong" of waves, with reflection rates higher than 80%. Therefore, it becomes impossible to carry out long tests under these conditions, as from a given moment the waves no longer behave as expected due to the high reflection rates. That's why tests had to be short.

However, short-term tests may not be representative of irregular waves, unless they are meticulously defined. Irregular waves have varied behavior and their analysis must be done with long time-series so that random effects are disregarded and only the average values are analyzed. Combining this fact with the short duration of the tests carried out, it can be concluded that there was not enough time for the irregular SST to develop and thus the power value was compromised. A lengthy analysis would be necessary to truly understand the device's performance under irregular waves. Therefore, due to the low quality of data for irregular waves (errors up to 60%), their values were left aside and the analysis from now on will only compare the regular waves, which proved to be much closer to the desired values (errors lower than 20%).

Table 23. Power matrix obtained from regular waves experimental simulations

Experimental Reg. Power Matrix (kW)		T (s)								
		5	6	7	8	9	10	11	12	13
H (m)	4,0	Storm Protection Mode								
	3,0	-	-	-	-	38,6	24,9	28,7	28,4	-
	2,0	-	-	15,2	16,7	17,7	15,6	13,7	11,8	-
	1,0	-	4,1	4,0	4,1	4,0	-	-	-	-
	0,0	No waves								

Table 24. Power matrix obtained from irregular waves experimental simulations

Experimental Irreg. Power Matrix (kW)		T_P (s)								
		5	6	7	8	9	10	11	12	13
H_S (m)	4,0	Storm Protection Mode								
	3,0	-	-	-	-	14,5	12,7	7,2	14,5	-
	2,0	-	-	9,1	7,7	5,3	4,9	4,5	3,9	-
	1,0	-	3,9	6,3	1,2	1,0	-	-	-	-
	0,0	No waves								

Nevertheless, it is worth mentioning that given the same wave height and period, regular waves have twice as much available power than irregular waves. This happen because the denominator of Equation 1 becomes 32π instead of 64π . Hence, the CWR (Equation 15) for irregular waves might be even larger than the ones calculated to regular waves, once the available power is less.

Enhancing the regular waves power matrix with 125% of ADO (Table 25) and comparing to the EWP matrix gives an estimate error of 16,5%, that in this study was considered as very good, since the power rises in the power of 3,5 when scaling the model. The CWR average was 32%, which is 10% more than the value obtained in the numerical study. Table 26 shows the CWR for all the 14 SST. Again, both enhanced power matrix and CWR values are in good accordance with the values found in the literature.

Table 25. Enhanced power matrix from regular waves experimental tests

Enhanced Reg. Experimental Power Matrix (kW)		T (s)								
		5	6	7	8	9	10	11	12	13
H (m)	4,0	Storm Protection Mode								
	3,0	-	-	-	-	48,0	31,0	35,8	35,4	-
	2,0	-	-	18,9	20,8	22,0	19,5	17,0	14,7	-
	1,0	-	5,1	4,9	5,1	5,0	-	-	-	-
	0,0	No waves								

Table 26. CWR values for the experimental study

CWR		T (s)								
		5	6	7	8	9	10	11	12	13
H (m)	4,0	Storm Protection Mode								
	3,0	-	-	-	-	35%	20%	21%	19%	-
	2,0	-	-	40%	38%	36%	29%	23%	18%	-
	1,0	-	50%	42%	37%	33%	-	-	-	-
	0,0	No waves								

Finally, the annual production amounts to 128,5MWh of clean electricity. Thus, using 230m as the length available for deployment in the north Douro River breakwater, the value would reach 5.787MWh/year, avoiding more than 1.354t of CO₂eq/year.

EWP currently holds a plan of installing multiple devices in the north vertical breakwater of Douro River. However, due to strong visual impacts in a region that many consider as a touristic spot and lack of knowledge of the technology, the project will face difficulties in getting the necessary permits.

5.8. VALIDATION OF NUMERICAL MODEL

Finally, validating a numerical model with an experimental model is crucial to ensure the accuracy and reliability of the study findings. With this study was no different. The experimental model ultimately serves as a means of validation for the numerical model, that is, the experimental model allows to approve or not what was numerically simulated. Sometimes, the complexity of the model is such that the experimental validation may fail the numerical model, meaning that the numerical model must be revised in order to incorporate more variables and more details so that the experimental model can validate the numerical model with some precision. This section presents two parameters that allow for analyzing the coupling between the models. Those are relative errors and RAO values.

5.8.1. RELATIVE ERROR

In the context of this study, the validation of the experimental model takes place by comparing the power matrix for the experimental and for the numerical model. If the two are similar, it means that the physical representation of the study matched what had been simulated on the computer, thus validating the numerical model. To do this, the relative error (Equation 31) is used, which allows quantifying the distance between the results obtained and what was supposed to be obtained.

Table 27 displays the relative errors associated with each SST analyzed. As can be seen there were large variations between different SSTs, however, the average value showed itself to be a reasonable value. Averaging 21%, the relative error made it possible to conclude that the experimental model was a good representation of the numerical model simulated in ANSYS®. Therefore, both models are matching and are a good representation between computational and physical studies. Lower values for relative errors could be achieved if some issues were better addressed, as discussed in the next section. Further research should be able to address those issues in order to get even more precise values.

Table 27. Error matrix for model validation

Relative Error Matrix		T (s)								
		5	6	7	8	9	10	11	12	13
H_S (m)	4,0	Storm Protection Mode								
	3,0	-	-	-	-	1%	30%	11%	2%	-
	2,0	-	-	33%	18%	4%	31%	55%	2%	-
	1,0	-	2%	53%	53%	1%	-	-	-	-
	0,0	No waves								

$$Error(\%) = \frac{|P_{Numerical} - P_{Experimental}|}{P_{Numerical}} * 100 \quad (31)$$

5.8.2. RESPONSE AMPLITUDE OPERATOR

In the field of ship and maritime structures design, such as WECs, a response amplitude operator (RAO) is an engineering statistic, or set of such statistics, that are used to determine the likely behavior of a floating structure when operating at sea. Known by the acronym of RAO, response amplitude operators are usually obtained from models of proposed floaters designs tested in a model basin, or from running specialized CFD computer programs, often both. RAOs are usually calculated for all motions and for all wave headings.

Comparing the RAO behavior for both numerical and experimental models can also be an interesting and smart way of validating the results obtained. In the purpose of this study, the parameter is defined as the ratio between the heave motion and the wave amplitude (Equation. 32), thus, it is a dimensionless parameter.

$$RAO = \frac{Heave\ Motion}{Wave\ Amplitude} \quad (32)$$

Using the wave probes water surface elevation data and the CSV files obtained with the numerical modelling, it was possible to compare both results. Figure 57 displays the comparison between the numerical values (shown in curves) and the experimental values (shown in points).

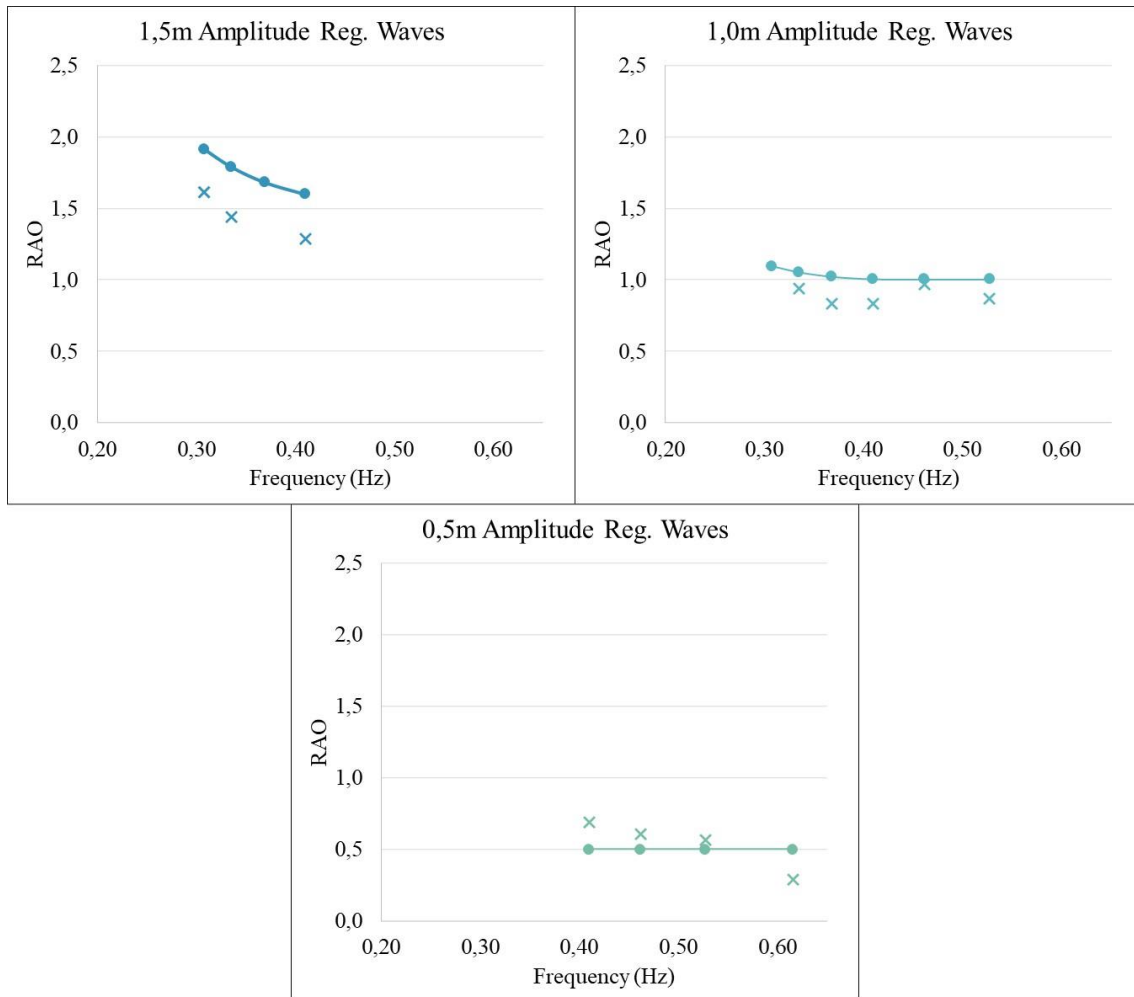


Figure 57. RAO values compared for different regular waves amplitudes.

As can be seen, the RAO value tends to reduce together with the decrease in regular wave amplitude. The larger RAO values were obtained for higher wave heights values. This fact emphasizes the non-linearity of the system. A complete linear system would have the exact same response for different waves heights. Hence, the RAO value for a linear system would only vary with the wave frequency.

Even though linear systems are desired because of their simple behavior, they are very uncommon. This is because most of the systems are not perfect, meaning that there will be always some friction, roughness and many other characteristics that together make the whole system move away from linearity. Therefore, a good analysis should take these effects into account while evaluating the fundamental parameters of the system.

5.8.3. FINAL CONSIDERATIONS

Therefore, the potential of the WEC tested and studied throughout this dissertation was proven synchronously both numerically and experimentally and could move forward to further tests in order to fully characterize it. Its implementation on the northern breakwaters of the Port of Leixões and of the Douro River will contribute significantly to the decarbonization objectives as well as to the port's energy self-sufficiency, as already discussed in section 4.8.

5.9. EXPERIMENTAL MODEL LIMITATIONS AND RECOMMENDATIONS

5.9.1. LIMITATIONS

While the experimental model presented in this dissertation has provided valuable insights into the behavior of the hinged WEC when fixed to vertical breakwaters, it is essential to acknowledge several limitations that may impact the interpretation and generalization of the results. These limitations are as follows:

- 1) **Simplified Environmental Conditions:** The wave channel used in the experiments does not fully replicate the complex and dynamic conditions of an open-water environment. Real-world conditions, such as variable wave spectra, irregular wave trains, and changing tide levels, were simplified for experimental purposes. Also, wave characteristics and their interactions with the breakwaters were simplified, and the experiments did not consider the effects of extreme weather conditions or storm surges;
- 2) **Scale Model:** The experimental model is a scaled-down representation of the actual WEC and breakwater system. Scaling laws were applied to maintain similarity, but the effects of scale on fluid dynamics and structural behavior may not be fully accounted for. The scaling process introduces limitations in terms of Reynolds number, Froude number, and other dimensionless parameters, which can affect the accuracy of the results;
- 3) **Limited Test Duration due to Excessive Reflection:** The test could not have a longer duration due to the excessive effects of waves reflections in the channel. However, short duration test may not be as representative as long duration tests, mainly under irregular waves.
- 4) **Boundary Effects:** The experiments focused primarily on the behavior of the WEC near the breakwater. Boundary effects, such as wave reflections and interactions with neighboring WECs, were not considered but could be significant in a real-world array of devices;
- 5) **Limited Parameter Range:** The range of input parameters, such as wave height, wave period, and breakwater inclination angle, was limited in the experiments. This limitation may restrict the understanding of the system's behavior under a wider range of conditions.

In conclusion, future research should aim to address these limitations by incorporating more realistic environmental conditions and enhancing scale modeling techniques. These steps will contribute to a more comprehensive understanding of the system's behavior and its potential for practical applications in wave energy conversion.

5.9.2. RECOMMENDATIONS

No experimental and numerical work can be completely free from errors, unforeseen events, technical failures and a series of other events that can delay the progress of the work and reduce the quality of the results. Unfortunately, this study was no different. Mainly during the experimental part, there were a series of challenges that were not planned and countless other details that ended up taking much more time than they seemed. However, this is how engineering is done, finding smart and functional solutions to the challenges that come our way.

Regarding the experimental model, it is recommended that more days be reserved for the study so that all its components can be calmly analyzed. Every step will come up with a multitude of challenges and sometimes it requires a significant amount of time to solve them. Furthermore, larger tanks that do not suffer from very high wave reflection rates are recommended as they would allow longer and significantly more representative simulations. Apart from that, the use of wood for the construction of the breakwater is also no longer recommended, as the wood swells in contact with the water and ends up expanding, leading to the model becoming larger than what would have been previously planned. Also, the care taken with the calibration of the Qualisys camera system could have also been improved. Many trials lost contact with at least one of the markers after a certain point and stopped recording information for that marker. Isolating the surroundings of the object under study with non-reflective materials is highly recommended as cameras are very sensitive to changes. Finally, the leaks along the channel made the process of finding the correct water level much longer than it should have been, in addition to the fact that the electricity spent by the water pump to keep the water level constant at 4,5L/s is much greater.

6

CONCLUSIONS

6.1. CONCLUSIONS

After developing a complete numerical and experimental study on the application of a device capable of converting wave energy of the point absorber type on the northern breakwaters of Porto de Leixões and the Douro River, contributing to decarbonization goals through the generation of clean electricity and the energy self-sufficiency of the ports, some interesting conclusions were raised and deserve to be discussed in this section.

Firstly, before any discussion of the technical point of view of the device, it is worth highlighting negative points that must change in the mentality of port management so that the goals of self-sufficiency are achieved. Unfortunately, generating clean electricity is not enough if it cannot be used for port activities. As shown, more than half of the gross energy of the Port of Leixões is not electricity, but fossil fuels. In this way, for the port to one day become energy self-sufficient, it is necessary, along with the generation of local and clean energy, also the electrification of processes so that this energy can be consumed. Therefore, the first major conclusion of this work is one of sustainability and involves a change in the way the processes are thought, in order to achieve complete electrification, giving rise to the injection of clean electricity.

Then, secondly, it was possible to realize the great power of point absorber WECs installed in robust coastal structures for generating clean and renewable electricity. In both breakwater configurations, the device demonstrated individual annual productions exceeding 14.000MWh, avoiding more than 3.500t of CO₂eq to be released into the atmosphere. This value, when multiplied by the large number of floaters that can be installed in sequence next to each other can reach even higher values of electricity produced. For the Port of Leixões case study, it was enough to supply all the electricity demand of the port. Therefore, in some cases, and depending on the resource and the area available, it may even exceed the port's consumption and contribute to the national energy distribution network.

Furthermore, the device under study proved to be efficient in converting wave energy, reaching efficiencies above 30%. Validation of the numerical model through the scheme using bicycle components proved to be a very effective way of carrying out numerical simulations, leading to relative errors of around 20%, which demonstrates a good relationship between the numerical and experimental model.

Finally, it is concluded that wave energy has a high potential to contribute significantly in the future to meeting the electricity needs of the world's population, which is constantly growing and increasingly consuming more and more energy. However, there are still major steps to be taken

so that the technologies begin to appear commercially in the world's energy markets. Finding ways to reduce costs and increase the efficiency of devices is a crucial step in making them viable, in addition to effective ways of dealing with the harsh marine environment. However, with enough research and development, the generation of clean energy from waves is getting closer and closer.

6.2. FURTHER RESEARCH

Additional studies must be carried out in order to understand the dynamics between the floaters and the random behavior of the incident waves. This component is fundamental for the proper functioning of hinged WECs and should be further explored for better results. Furthermore, research in the field of optimization of the damping coefficient value could significantly impact the expansion of the WECs market. After all, increasing device efficiencies directly reduces its levelized cost of energy (LCOE), making it more competitive with other forms of electricity generation.

Moreover, real breakwater energy dissipation effects such as roughness, water infiltration and turbulence should be addressed. Those effects were not considered under this study and might have a significant impact on the overall efficiency of the system. Apart from that, further research should test not only with vertical breakwaters but also with sloped breakwaters, to fully understand and characterize the WEC behavior when attached to these structures.

Other interesting studies that will certainly have major impacts on the commercialization of WECs have to do with the challenges of the marine environment. During the preparation of this thesis, it was noticed that many of the devices that reached the testing phase were later discontinued, such as Pelamis®, PICO's OWC, which was destroyed in 2018 [31], and the WaveRoller®, which had to be removed of water before what was supposed, and many other devices that were not able to survive the harsh conditions of the marine environment. Therefore, further studies on how to deal with the corrosive environment, with high loads of forces and exposed stress, is a crucial step in the development of consolidated and robust technologies.

Much is already known about wave energy, but unfortunately there has not yet been a device that is attractive and competitive enough for attention to start turning to wave energy. For this to happen, a lot of research and development (R&D) is needed in the field. Only in this way will the best devices be capable of contributing to the electrical mix of countries and, of course, to the decarbonization of societies and the slowdown of global warming.

BIBLIOGRAPHY

- [1] B. Pillot, M. Muselli, P. Poggi, and J. B. Dias, “On the Impact of the Global Energy Policy Framework on the Development and Sustainability of Renewable Power Systems in Sub-Saharan Africa: the Case of Solar PV,” Apr. 2017, [Online]. Available: <http://arxiv.org/abs/1704.01480>
- [2] “Electricity Consumption by Country 2023.” Accessed: Mar. 14, 2023. [Online]. Available: <https://worldpopulationreview.com/country-rankings/electricity-consumption-by-country>
- [3] M. Sofia Tavares Valente Correia, “Concept, design and energy simulation of a Net Zero Energy Home for the Mediterranean climate,” Faculdade de Ciências da Universidade de Lisboa, Lisboa, 2020.
- [4] SEAI, “OCEAN ENERGY Roadmap,” 2010.
- [5] A. Pecher and J. P. Kofoed, *Handbook Ocean Wave Energy*. New Orleans, USA: Springer Open, 2016.
- [6] M. A. Mustapa, O. B. Yaakob, Y. M. Ahmed, C. K. Rheem, K. K. Koh, and F. A. Adnan, “Wave Energy Device and Breakwater Integration: A Review,” *Renewable and Sustainable Energy Reviews*, vol. 77. Elsevier Ltd, pp. 43–58, 2017. doi: 10.1016/j.rser.2017.03.110.
- [7] K. Gunn and C. Stock-Williams, “Quantifying the Global Wave Power Resource,” *Renew Energy*, vol. 44, pp. 296–304, Aug. 2012, doi: 10.1016/j.renene.2012.01.101.
- [8] E. Edwards, “Optimization of the Geometry of Axisymmetric Point-Absorber Wave Energy Converters,” Massachusetts Institute of Technology, Cambridge, 2020.
- [9] “Paving the Way for a Decarbonized Shipping Industry that Leaves No One Behind - Climate Champions.” Accessed: Mar. 18, 2023. [Online]. Available: <https://climatechampions.unfccc.int/paving-the-way-for-a-decarbonized-shipping-industry-that-leaves-no-one-behind/>
- [10] “Home | Portos Project.” Accessed: Jun. 28, 2023. [Online]. Available: <https://portosproject.eu/>
- [11] H. Bailey, “The effect of a nonlinear Power Take Off on a Wave Energy Converter,” 2009.
- [12] “Stability of Rubble Mound Breakwaters and Shore Revetments - Coastal Wiki.” Accessed: Mar. 11, 2023. [Online]. Available: http://www.coastalwiki.org/wiki/Stability_of_rubble_mound_breakwaters_and_shore_revetments
- [13] T. Bruce, J. van der Meer, T. Pullen, and W. Allsop, “Wave Overtopping at Vertical and Steep Structures,” in *Handbook of Coastal and Ocean Engineering*, World Scientific Publishing Co., 2009, pp. 411–441. doi: 10.1142/9789812819307_0016.
- [14] P. Janardhan, “Parametric Studies on Stability of Reshaped Berm Breakwater with Concrete Cubes as Armor Unit,” National Institute of Technology Karnataka, Mangalore, 2013. [Online]. Available: <https://www.researchgate.net/publication/273694926>

- [15] “Estruturas de proteção costeira (parte 02) – Quebra-mar.” Accessed: Sep. 04, 2023. [Online]. Available: http://edsonprof.blogspot.com/2018/02/estruturas-de-protecao-costeira-parte_10.html
- [16] “mWave™ | Bombora.” Accessed: Sep. 04, 2023. [Online]. Available: <https://bomborawave.com/mwave/>
- [17] “WAVEROLLER HAS BEEN RE-VALIDATED WITH THE ‘SOLAR IMPULSE EFFICIENT SOLUTION’ LABEL - AW-Energy.” Accessed: Sep. 04, 2023. [Online]. Available: <https://aw-energy.com/waveroller-has-been-re-validated-with-the-solar-impulse-efficient-solution-label/>
- [18] T. V. Heath, “A Review of Oscillating Water Columns,” in *Philosophical Transactions of the Royal Society A: Mathematical, Physical and Engineering Sciences*, Royal Society, Jan. 2012, pp. 235–245. doi: 10.1098/rsta.2011.0164.
- [19] J. H. Todalshaug, “On the Maximum and Actual Capture Width Ratio of Wave Energy Converters,” 2011. [Online]. Available: <https://www.researchgate.net/publication/269703869>
- [20] V. E. Kralli, N. Theodossiou, and T. Karambas, “Optimal Design of Overtopping Breakwater for Energy Conversion (OBREC) Systems Using the Harmony Search Algorithm,” *Front Energy Res*, vol. 7, Aug. 2019, doi: 10.3389/fenrg.2019.00080.
- [21] J. Xie and L. Zuo, “Dynamics and Control of Ocean Wave Energy Converters,” *Int J Dyn Control*, vol. 1, no. 3, pp. 262–276, Sep. 2013, doi: 10.1007/s40435-013-0025-x.
- [22] B. Drew, A. R. Plummer, and M. N. Sahinkaya, “A review of wave energy converter technology,” *Proceedings of the Institution of Mechanical Engineers, Part A: Journal of Power and Energy*, vol. 223, no. 8, pp. 887–902, Dec. 01, 2009. doi: 10.1243/09576509JPE782.
- [23] “Mutriku Wave Energy Plant, Basque Country, Spain.” Accessed: Mar. 11, 2023. [Online]. Available: <https://www.power-technology.com/projects/mutriku-wave/>
- [24] A. F. O. Falcão and J. C. C. Henriques, “Oscillating-Water-Column Wave Energy Converters and Air Turbines: A Review,” *Renewable Energy*, vol. 85. Elsevier Ltd, pp. 1391–1424, Jan. 01, 2016. doi: 10.1016/j.renene.2015.07.086.
- [25] “Eco Wave Power Commences Real Conditions Test Runs of its Newest EWP-EDF One Wave Energy Project at Jaffa Port, Israel - Eco Wave Power.” Accessed: Mar. 11, 2023. [Online]. Available: <https://www.ecowavepower.com/eco-wave-power-commences-real-conditions-test-runs-of-its-newest-ewp-edf-one-wave-energy-project-at-jaffa-port-israel/>
- [26] “Gibraltar - Eco Wave Power.” Accessed: Mar. 13, 2023. [Online]. Available: <https://www.ecowavepower.com/gibraltar/>
- [27] “Gibraltar Wave Power Project Surfs Up Possibilities Across Europe - Power Technology.” Accessed: Mar. 13, 2023. [Online]. Available: <https://www.power-technology.com/features/featuregibraltar-wave-power-project-surfs-up-possibilities-across-europe-4996030/>

- [28] “Eco Wave Power to Relocate Wave Energy Plant from Gibraltar to Los Angeles - Offshore Energy.” Accessed: Mar. 14, 2023. [Online]. Available: <https://www.offshore-energy.biz/eco-wave-power-to-relocate-wave-energy-plant-from-gibraltar-to-l-a/>
- [29] P. Contestabile, E. Di Lauro, and D. Vicinanza, “Prototype Overtopping Breakwater for Wave Energy Conversion at Port of Naples,” 2016.
- [30] “Pico OWC.” Accessed: Mar. 14, 2023. [Online]. Available: <http://www.pico-owc.net/en/cms499b.html?page=541&wnsid=456f3662aa1d8d9ce324a61635844400>
- [31] A. F. O. Falcão, A. J. N. A. Sarmiento, L. M. C. Gato, and A. Brito-Melo, “The Pico OWC Wave Power Plant: Its Lifetime from Conception to Closure 1986–2018,” *Applied Ocean Research*, vol. 98, p. 102104, May 2020, doi: 10.1016/J.APOR.2020.102104.
- [32] S. Heo and W. Koo, “Dynamic response analysis of a wavestar-type wave energy converter using augmented formulation in korean nearshore areas,” *Processes*, vol. 9, no. 10, Oct. 2021, doi: 10.3390/pr9101721.
- [33] “History – Wave Star.” Accessed: May 08, 2023. [Online]. Available: <https://wavestarenergy.com/news/>
- [34] L. Marquis, M. Kramer, and P. Frigaard, “First Power Production figures from the Wave Star Roshage Wave Energy Converter.”
- [35] Mônica Reis Pires Rodarte Oliveira, “Um estudo de caso da Usina de ondas de Pecém - CE,” UFOP, Ouro Preto - MG, 2016.
- [36] “Você sabe como funciona a energia das ondas? – AUTOSSUSTENTÁVEL.” Accessed: May 08, 2023. [Online]. Available: <https://autossustentavel.com/2020/04/ondomotriz-energia-ondas.html>
- [37] P. Mota and J. P. Pinto, “Wave Energy Potential Along the Western Portuguese Coast,” *Renew Energy*, vol. 71, pp. 8–17, 2014, doi: 10.1016/j.renene.2014.02.039.
- [38] P. R. Santos, “Slides - Tidal and Wave Energy - Lecture 1.” 2022. [Online]. Available: <https://www.youtube.com/watch?v=gW-3XkycedQ>
- [39] “Electricity Consumption Worldwide by Region | Statista.” Accessed: Mar. 16, 2023. [Online]. Available: <https://www.statista.com/statistics/688164/worldwide-consumption-of-electricity-by-region/>
- [40] R. C. Guimarães, P. H. Oleinik, E. de P. Kirinus, B. V. Lopes, T. B. Trombetta, and W. C. Marques, “An Overview of the Brazilian Continental Shelf Wave Energy Potential,” *Reg Stud Mar Sci*, vol. 25, Jan. 2019, doi: 10.1016/j.rsma.2018.100446.
- [41] C. Pegorelli, M. Dottori, and J. F. Fortes, “Evaluating the Gravity Wave Energy Potential off the Brazilian Coast,” *Braz J Oceanogr*, vol. 66, no. 2, pp. 220–233, Apr. 2018, doi: 10.1590/s1679-87592018011706602.
- [42] G. J. Dalton, R. Alcorn, and T. Lewis, “Case Study Feasibility Analysis of the Pelamis Wave Energy Converter in Ireland, Portugal and North America.” [Online]. Available: <http://finance.yahoo.com/q/bc?s=EURUSD=X&t=5y&l=on&z=m&q=l&c=>

- [43] I. B. Araújo, M. S. Bos, L. C. Bastos, and M. M. Cardoso, “Analysing the 100year Sea Level Record of Leixões, Portugal,” *J Hydrol (Amst)*, vol. 481, pp. 76–84, Feb. 2013, doi: 10.1016/j.jhydrol.2012.12.019.
- [44] Nemus, “Estudo de Impacte Ambiental do Prolongamento do Quebra-Mar Exterior do Porto de Leixões - Volume I - Relatório Síntese,” 2018.
- [45] “A História - APDL.” Accessed: Apr. 08, 2023. [Online]. Available: https://www.apdl.pt/pt_PT/historia
- [46] LNEC - Laboratório Nacional de Engenharia Civil, “Estudos Em Modelo Físico E Numérico Do Prolongamento Do Quebra-Mar Exterior E Das Acessibilidades Marítimas Do Porto De Leixões: Estudo II - Avaliação dos Impactes do Prolongamento do Quebra-Mar Exterior do Porto de Leixões nas Condições de Agitação da Praia de Matosinhos,” 2017.
- [47] APDL - Administração dos Portos Douro - Leixões - Viana, “Relatório de Sustentabilidade 2020: É Hora de Dar um Passo pelo Planeta,” Porto, 2020.
- [48] APS - Administração dos Portos de Sines e do Algarve S.A., “Relatório de Sustentabilidade 2020 - Porto de Sines e do Algarve,” 2020.
- [49] Y. Wang, S. Huang, G. Xue, and Y. Liu, “Influence of Hydraulic PTO Parameters on Power Capture and Motion Response of a Floating Wind-Wave Hybrid System,” *J Mar Sci Eng*, vol. 10, no. 11, Nov. 2022, doi: 10.3390/jmse10111660.
- [50] EcoWavePower, “Technical Brochure - 100kW - 1MW Wave Energy Array,” 2020.
- [51] G. Giannini *et al.*, “Wave energy converter power take-off system scaling and physical modelling,” *J Mar Sci Eng*, vol. 8, no. 9, Sep. 2020, doi: 10.3390/JMSE8090632.
- [52] C. Li *et al.*, “A Constant-Pressure Hydraulic PTO System for a Wave Energy Converter Based on a Hydraulic Transformer and Multi-Chamber Cylinder,” *Energies (Basel)*, vol. 15, no. 1, Jan. 2022, doi: 10.3390/en15010241.
- [53] “Wave Energy - Cna Meccanica - YouTube.” Accessed: May 04, 2023. [Online]. Available: https://www.youtube.com/watch?v=S_rSXKA30cA&t=1s&ab_channel=DarioDicembrino
- [54] O. M. Mazzaretto, M. Menéndez, and H. Lobeto, “A global evaluation of the JONSWAP spectra suitability on coastal areas,” *Ocean Engineering*, vol. 266, p. 112756, Dec. 2022, doi: 10.1016/J.OCEANENG.2022.112756.
- [55] D. Wilson *et al.*, “A comparison of WEC control strategies.” [Online]. Available: <http://www.ntis.gov/help/ordermethods.asp?loc=7-4-0#online>
- [56] Y. Çengel, M. Boles, and M. Kanoglu, *Thermodynamics: An Engineering Approach*, 9th ed. McGrawHill.
- [57] “SHRHA.” Accessed: Sep. 07, 2023. [Online]. Available: https://paginas.fe.up.pt/~shrha/laboratorios/desc_func.html

APPENDIX I – MATLAB® CODE FOR DAMPING CHARACTERIZATION

```

% Input values

L = (44.3/100); % Radius of Pendulum arc in m (arm length)
mf = 0.475; % Mass of floater in kg
mb= 1.232; % Mass of arm in kg
Cd = 0.2; % Angular damping coefficient in Nsm/°
g = 9.81; % Acceleration due to gravity m/s^2

% Conditions
in_ang_disp = 0.851720675 ; % Initial angular displacement
in_ang_v = 0; % Initial angular velocity in radians/s (still start)

theta_0 = [in_ang_disp;in_ang_v];

t_span = 20; % Total time of video in seconds
fps = 30; % Frames per second
t_pts = linspace(0,t_span,fps*t_span); % Time points for t_span seconds

% ODE Solver
[t, results] = ode45(@(t,theta)
simp_pend_ode_func(L,theta,Cd,g,mf,mb),t_pts,theta_0);

ang_disps = results(:,1); % Angular displacement array
ang_vs = results(:,2); % Angular velocity array

% Fixed point of the pendulum
x0 = 0; % x origin coordinate
y0 = 0; % y origin coordinate

ct = 1; % Counter for counting the total number of frames

% Pendulum ball dimensions
r = 0.1; % Radius in m

% Angular displacement & Angular velocity v/s time plot

figure()
hold on
title("Angular displacement & Angular Velocity v/s time of a simple damped
pendulum")
plot(t,ang_disps)
text(3.052,0.3727,'leftarrow Angular Displacement')
plot(t,ang_vs)
text(2.088,2.83,'leftarrow Angular Velocity ')
ylabel('Plots')
xlabel('time (s)')

% The animation loop

figure()
for i = 1:length(t_pts)
    pos = ang_disps(i); % Angular displacement of pendulum at a point of time

    y = -L*cos(pos); % x coordinate of pendulum at a point of time
    x = -L*sin(pos); % y coordinate of pendulum at a point of time

```

```

% Animation plots

plot([x0 x],[y0
y], 'linewidth',3, 'Marker', 'O', 'Markersize',15, 'MarkerFaceColor', 'r', 'MarkerEdgeColor', 'r') % The pendulum plot
axis([-1.5 1.5 -1.5 1.5]) % Axis of the plot

rectangle('Position',[-1.5 0 3 0.5], 'Facecolor',[0.2 0 0], 'Edgecolor',[0
0 0])

pause(t(2)) % Determines the time b/w the frames Also, t(2) = 1/fps
M(ct) = getframe(gcf);
ct = ct+1; % Counter gets incremented after the frame is collected
end

% The movie

movie(M);
videofile = VideoWriter('simple_pendulum.avi', 'Uncompressed AVI'); % Naming
and formatting the video
open(videofile) % Open the video editor
writeVideo(videofile,M) % Convert the image to frame
close(videofile) % Close the video writer

% Ode Function

function [dtheta_dt] = simp_pend_ode_func(L,theta,Cd,g,mf,mb)
theta1 = theta(1); % Theta 1 = 1st column of theta
theta2 = theta(2); % Theta 2 = 2nd column of theta
dtheta1_dt = theta2; % dtheta1/dt = theta2
% dtheta2_dt = -(b/m)*theta2 - (g/L)*sin(theta1);
dtheta2_dt = -(Cd/((L^2)*(1/3*mb+mf)))*theta2-
((mf/L+mb/(2*L))*g*theta1)/(1/3*mb+mf);
dtheta_dt = [dtheta1_dt; dtheta2_dt]; % t, angular displacements and
angular velocities
end

```

APPENDIX II – POWER VALUES OBTAINED FOR EXPERIMENTAL MODEL

Table 28. Power values for numerical and experimental models under regular waves

Regular Waves				
Simulations	Power Numerical (kW)	Power Experimental Scale Down (W)	Power Experimental Scale Up (kW)	Error
S01_1_Reg	38,90	4,11	38,55	1%
S02_1_Reg	35,56	2,66	24,88	30%
S03_1_Reg	32,38	3,07	28,73	11%
S04_1_Reg	28,93	3,03	28,42	2%
S05_1_Reg	15,21	1,09	10,20	33%
S06_1_Reg	16,67	1,45	13,62	18%
S07_1_Reg	17,66	1,81	17,01	4%
S08_1_Reg	15,64	1,16	10,86	31%
S09_1_Reg	13,68	0,65	6,11	55%
S10_1_Reg	11,80	1,24	11,62	2%
S11_1_Reg	4,11	0,43	4,01	2%
S12_1_Reg	3,96	0,20	1,86	53%
S13_1_Reg	4,08	0,21	1,93	53%
S14_1_Reg	4,04	0,44	4,08	1%
			Average	21%

Table 29. Power values for numerical and experimental models under irregular waves

Irregular Waves				
Simulations	Power Numerical (kW)	Power Experimental Scale Down (W)	Power Experimental Scale Up (kW)	Error
S01_1_Irreg	38,90	1,55	14,50	63%
S02_1_Irreg	35,56	1,35	12,67	64%
S03_1_Irreg	32,38	0,77	7,24	78%
S04_1_Irreg	28,93	1,54	14,47	50%
S05_1_Irreg	15,21	0,97	9,07	40%
S06_1_Irreg	16,67	0,82	7,69	54%
S07_1_Irreg	17,66	0,57	5,35	70%
S08_1_Irreg	15,64	0,52	4,88	69%
S09_1_Irreg	13,68	0,48	4,51	67%
S10_1_Irreg	11,80	0,41	3,89	67%
S11_1_Irreg	4,11	0,41	3,89	5%
S12_1_Irreg	3,96	0,67	6,28	58%
S13_1_Irreg	4,08	0,12	1,15	72%
S14_1_Irreg	4,04	0,10	0,95	76%
			Average	60%

$$P_{ScaleUp} = P_{ScaleDown} * 13,64^{3,5}$$

$$Error = \frac{|P_{Numerical} - P_{Experimental}|}{P_{Numerical}}$$

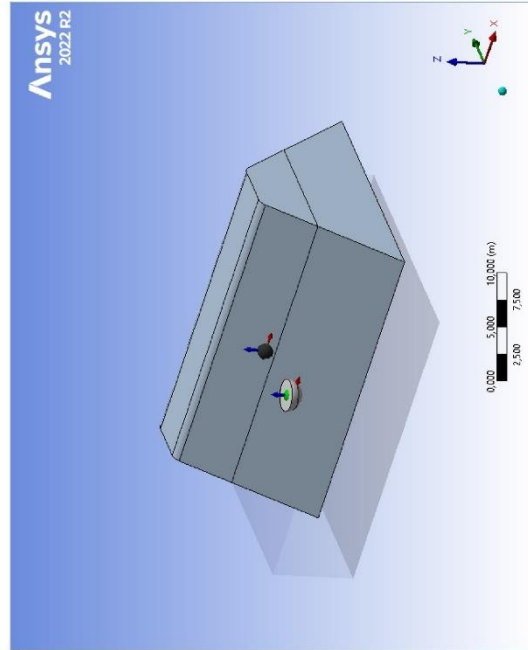
APPENDIX III – ANSYS® REPORT FOR THE NUMERICAL MODEL

The image on top always displays the report for the sloped breakwater, while the image on the bottom always displays the report for the vertical breakwater.



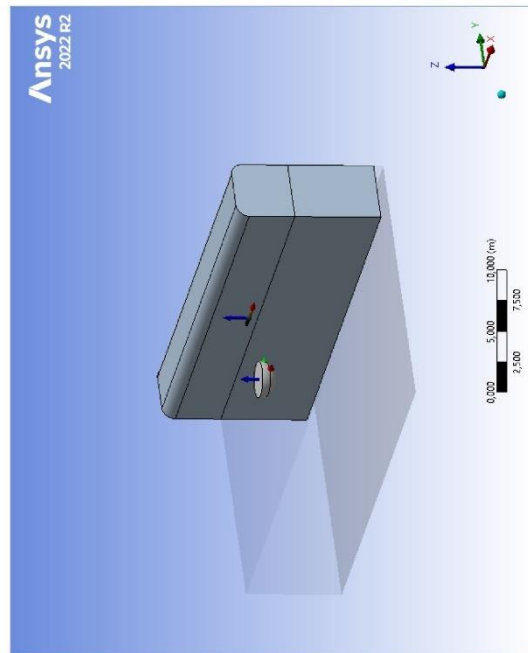
Project

Name	Project
Author	Giovanni Martins
Project Title	Innovative Hinged System
Hydrodynamic Solver Unit System	Metric: kg, m, N
Export CSV Simulation Position	Current View: 17/04/2023 15:39:00
Export CSV Simulation Position	References: ""
Date of Creation	17/04/2023 15:39:00
Last Modified	03/08/2023 13:09:43
Data Folder Root	C:\Users\up201800705\Desktop\Half Sphere 2.B_files\up0AQWAGW
Product Version	2022 R2



Project

Name	Project
Author	Giovanni Martins
Project Title	Innovative Hinged System
Hydrodynamic Solver Unit System	Metric: kg, m, N
Export CSV Simulation Position	Current View: 17/04/2023 15:39:00
Export CSV Simulation Position	References: ""
Date of Creation	17/04/2023 15:39:00
Last Modified	03/08/2023 13:09:20
Data Folder Root	C:\Users\up201800705\Desktop\Half Sphere 2.B_files\up0AQWAGW
Product Version	2022 R2



Contents

- **Units**
- **Model (B3, C3)**
 - **Geometry**
 - **Floater**
 - Surface Body
 - Floater Axes
 - Surface Body
 - Point Mass
 - Connection Floater
 - **Fixed Points**
 - Fixed Floater
 - Fixed Breakwater
 - **Breakwater**
 - Surface Body
 - Surface Body
 - Breakwater Axes
 - Point Mass
 - Connection Breakwater
 - **Connections**
 - **Connection Data**
 - Joint Floater
 - Joint Axes On Fixed Point
 - Joint Axes On Structure
 - Joint Breakwater
 - Joint Axes On Fixed Point
 - Joint Axes On Structure
 - **Mesh**
 - Mesh Strip
 - **Hydrodynamic Diffraction (B4)**
 - Analysis Settings
 - Structure Selection
 - Wave Directions
 - Wave Frequencies
 - Solution (B5)
 - Pressures and Motions
 - Parameters vs Frequency
 - Radiation Damping
 - Parameters vs Frequency
 - Added Mass
 - **Hydrodynamic Response (C4)**
 - Analysis Settings
 - Irregular Wave
 - Solution (C5)
 - Animation
 - Parameters vs Time
 - Structure Position, Actual Response
 - Structure Position, Actual Response
 - Structure Velocity, Actual Response
 - Structure Position, RAO-Based Response

Units

TABLE 1

Length	Meter
Mass	Kilogram
Angle	Degree
Force	Newton
Frequency	Hertz
Time	Second

Model (B3, C3)

Geometry

Contents

- **Units**
- **Model (B3, C3)**
 - **Geometry**
 - **Floater**
 - Surface Body
 - Floater Axes
 - Surface Body
 - Point Mass
 - Connection Floater
 - **Fixed Points**
 - Fixed Floater
 - Fixed Breakwater
 - **Breakwater**
 - Surface Body
 - Surface Body
 - Breakwater Axes
 - Point Mass
 - Connection Breakwater
 - **Connections**
 - **Connection Data**
 - Joint Floater
 - Joint Axes On Fixed Point
 - Joint Axes On Structure
 - Joint Breakwater
 - Joint Axes On Fixed Point
 - Joint Axes On Structure
 - **Mesh**
 - Mesh Strip
 - **Hydrodynamic Diffraction (B4)**
 - Analysis Settings
 - Structure Selection
 - Wave Directions
 - Wave Frequencies
 - Solution (B5)
 - Pressures and Motions
 - Parameters vs Frequency
 - Radiation Damping
 - Parameters vs Frequency
 - Added Mass
 - **Hydrodynamic Response (C4)**
 - Analysis Settings
 - Irregular Wave
 - Solution (C5)
 - Animation
 - Parameters vs Time
 - Structure Position, Actual Response
 - Structure Position, Actual Response
 - Structure Velocity, Actual Response
 - Structure Position, RAO-Based Response

Units

TABLE 1

Length	Meter
Mass	Kilogram
Angle	Degree
Force	Newton
Frequency	Hertz
Time	Second

Model (B3, C3)

Geometry

TABLE 2
Model (B3, C3) > Geometry

Name	Geometry
State	Fully Defined
Details of Geometry	
Attached Assembly Path	C:\Users\up201800705\Desktop\HalfSphere 2.4_files\up0\Geom\DM\Geom.agdb
Environment Constants	
Water Depth	8 m
Water Density	1029 kg/m ³
Wave Period	9.89645 s
Water Size X	30 m
Water Size Y	22 m
Stability/Time Response-Specific Options	
Tube Drag Coefficients	Defined in Line Body Details
Seabed Inline Friction Coefficient	0.0
Seabed Lateral Friction Coefficient	0.0
Composite Cable Seabed Definition	
Seabed Type	No Composite Cable Seabed
Import Preferences	
Import Solid Bodies	No
Import Surface Bodies	Yes
Import Line Bodies	Yes

Floator

TABLE 2
Model (B3, C3) > Geometry

Name	Geometry
State	Fully Defined
Details of Geometry	
Attached Assembly Path	C:\Users\up201800705\Desktop\HalfSphere 2.4_files\up0\Geom\DM\Geom.agdb
Environment Constants	
Water Depth	8 m
Water Density	1029 kg/m ³
Wave Period	9.89645 s
Water Size X	30 m
Water Size Y	22 m
Stability/Time Response-Specific Options	
Tube Drag Coefficients	Defined in Line Body Details
Seabed Inline Friction Coefficient	0.0
Seabed Lateral Friction Coefficient	0.0
Composite Cable Seabed Definition	
Seabed Type	No Composite Cable Seabed
Import Preferences	
Import Solid Bodies	No
Import Surface Bodies	Yes
Import Line Bodies	Yes

Floator

TABLE 3
Model (B3, C3) > Geometry > Part

Name	Floator
State	Fully Defined
Details of Floator	
Part Visibility	Visible
Activity	Not Suppressed
Part Color	1486604B
Mass Properties	
Center of Gravity X	2542.7 kg
Center of Gravity Y	0.0 m
Center of Gravity Z	0.11 m
Moment of Inertia Ixx	2237.31 kg·m ²
Moment of Inertia Iyy	0.0 kg·m ²
Moment of Inertia Izz	2237.31 kg·m ²
Moment of Inertia Ixy	0.0 kg·m ²
Moment of Inertia Iyz	0.0 kg·m ²
Moment of Inertia Ixz	3387.03 kg·m ²
Advanced Options	
Generate Internal Lid	No
Current Calculation Position	At Fixed Depth
Current Calculation Depth	0.0 m
Submerged Structure Detection	Program Controlled
Override Calculated GMX	No
Override Calculated GMY	No
Override Calculated GMZ	No
Force Multiplying Factors	
Drag Multiplying Factor	1
Mass Multiplying Factor	1
Slam Multiplying Factor	0.0
Shear Force/Bending Moment Options	
Calculate Shear Force/Bending Moment	Not Permitted for Multiple Structures

Floator

TABLE 3
Model (B3, C3) > Geometry > Part

Name	Floator
State	Fully Defined
Details of Floator	
Part Visibility	Visible
Activity	Not Suppressed
Part Color	1486604B
Mass Properties	
Center of Gravity X	2542.7 kg
Center of Gravity Y	0.0 m
Center of Gravity Z	0.11 m
Moment of Inertia Ixx	2237.31 kg·m ²
Moment of Inertia Iyy	0.0 kg·m ²
Moment of Inertia Izz	2237.31 kg·m ²
Moment of Inertia Ixy	0.0 kg·m ²
Moment of Inertia Iyz	0.0 kg·m ²
Moment of Inertia Ixz	3387.03 kg·m ²
Advanced Options	
Generate Internal Lid	No
Current Calculation Position	At Fixed Depth
Current Calculation Depth	0.0 m
Submerged Structure Detection	Program Controlled
Override Calculated GMX	No
Override Calculated GMY	No
Override Calculated GMZ	No
Force Multiplying Factors	
Drag Multiplying Factor	1
Mass Multiplying Factor	1
Slam Multiplying Factor	0.0
Shear Force/Bending Moment Options	
Calculate Shear Force/Bending Moment	Not Permitted for Multiple Structures

Floator

TABLE 4
Model (B3, C3) > Geometry > Floator > Body

Name	Surface Body
State	Fully Defined
Details of Surface Body	
Body Visibility	Visible
Activity	Not Suppressed
Body Color Definition	Inherited from Part
Structure Type	Physical Geometry
Surface Type	Program Controlled

Floator

TABLE 4
Model (B3, C3) > Geometry > Floator > Body

Name	Surface Body
State	Fully Defined
Details of Surface Body	
Body Visibility	Visible
Activity	Not Suppressed
Body Color Definition	Inherited from Part
Structure Type	Physical Geometry
Surface Type	Program Controlled

Floator

TABLE 5 Model (B3, C3) > Geometry > Floater > Axes

Name	Floater/Axes	State	Fully Defined
Details of Floater Axes			
Visibility		Visible	
Axes Alignment			
Alignment Method	Global Axes		
Rotation About Global X		0°	
Rotation About Global Y		0°	
Rotation About Global Z		0°	
Rotation About Local X		0.0°	
Rotation About Local Y		0.0°	
Rotation About Local Z		0.0°	
Unit Vector X		[1, 0.0, 0.0]	
Unit Vector Y		[0.0, 1, 0.0]	
Unit Vector Z		[0.0, 0.0, 1]	

TABLE 6 Model (B3, C3) > Geometry > Floater > Body

Name	Surface Body	State	Fully Defined
Details of Surface Body			
Body Visibility		Visible	
Activity		Not Suppressed	
Body Color Definition	Inherited from Part		
Structure Type	Physical Geometry		
Surface Type	Program Controlled		

TABLE 7 Model (B3, C3) > Geometry > Floater > Structural Mass

Name	Point Mass	State	Fully Defined
Details of Point Mass			
Visibility		Visible	
Activity		Not Suppressed	
Point Mass Properties			
Mass Definition	Manual Definition		
Mass		X	0.0 m
		Y	-3.33 m
		Z	0.11 m
Inertia Properties			
Define Inertia Values by	Direct Input of Inertia		
Kxx	0.938027391281068 m		
Kyy	0.938027391281068 m		
Kzz	1.15073981348215 m		
Ixy	0.0 kg·m²		
Iyz	2237.31 kg·m²		
Ixz	0.0 kg·m²		
Iyyz	2237.31 kg·m²		
Izzx	0.0 kg·m²		
Izzz	3387.03 kg·m²		

TABLE 8 Model (B3, C3) > Geometry > Floater > Connection Point

Name	Connection Floater	State	Fully Defined
Details of Connection Floater			
Visibility		Visible	
Point Definition			
Type	Attached to Structure		
Structure	Floater		
Position Coordinates			
X		0.0 m	
Y		0.0 m	
Z		0.75 m	
Hydrodynamic Response Nodal Motions Output			
Include in Results		Yes	

TABLE 5 Model (B3, C3) > Geometry > Floater > Axes

Name	Floater/Axes	State	Fully Defined
Details of Floater Axes			
Visibility		Visible	
Axes Alignment			
Alignment Method	Global Axes		
Rotation About Global X		0°	
Rotation About Global Y		0°	
Rotation About Global Z		0°	
Rotation About Local X		0.0°	
Rotation About Local Y		0.0°	
Rotation About Local Z		0.0°	
Unit Vector X		[1, 0.0, 0.0]	
Unit Vector Y		[0.0, 1, 0.0]	
Unit Vector Z		[0.0, 0.0, 1]	

TABLE 6 Model (B3, C3) > Geometry > Floater > Body

Name	Surface Body	State	Fully Defined
Details of Surface Body			
Body Visibility		Visible	
Activity		Not Suppressed	
Body Color Definition	Inherited from Part		
Structure Type	Physical Geometry		
Surface Type	Program Controlled		

TABLE 7 Model (B3, C3) > Geometry > Floater > Structural Mass

Name	Point Mass	State	Fully Defined
Details of Point Mass			
Visibility		Visible	
Activity		Not Suppressed	
Point Mass Properties			
Mass Definition	Manual Definition		
Mass		X	0.0 m
		Y	-3.33 m
		Z	0.11 m
Inertia Properties			
Define Inertia Values by	Direct Input of Inertia		
Kxx	0.938027391281068 m		
Kyy	0.938027391281068 m		
Kzz	1.15073981348215 m		
Ixy	0.0 kg·m²		
Iyz	2237.31 kg·m²		
Ixz	0.0 kg·m²		
Iyyz	2237.31 kg·m²		
Izzx	0.0 kg·m²		
Izzz	3387.03 kg·m²		

TABLE 8 Model (B3, C3) > Geometry > Floater > Connection Point

Name	Connection Floater	State	Fully Defined
Details of Connection Floater			
Visibility		Visible	
Point Definition			
Type	Attached to Structure		
Structure	Floater		
Position Coordinates			
X		0.0 m	
Y		0.0 m	
Z		0.75 m	
Hydrodynamic Response Nodal Motions Output			
Include in Results		Yes	

Fixed Points

Fixed Points

TABLE 9

TABLE 9

Model (B3, C3) > Geometry > Fixed Points

Name	Fixed Breakwater
State	Fully Defined
Visibility	Visible
Details of Fixed Points	
Visibility	Visible

TABLE 10 Model (B3, C3) > Geometry > Fixed Points > Connection Point

Name	Fixed Breakwater
State	Fully Defined
Visibility	Visible
Details of Fixed Breakwater	
Point Definition	Visible
Type	Fixed
Definition of Position X, Y and Z Coordinates	
Position Coordinates	
X	0.0 m
Y	-3.33 m
Z	0.75 m

TABLE 11 Model (B3, C3) > Geometry > Fixed Points > Connection Point

Name	Fixed Breakwater
State	Fully Defined
Visibility	Visible
Details of Fixed Breakwater	
Point Definition	Visible
Type	Fixed
Definition of Position X, Y and Z Coordinates	
Position Coordinates	
X	0.0 m
Y	-3.33 m
Z	0.0 m

Breakwater

Model (B3, C3) > Geometry > Fixed Points

Name	Fixed Breakwater
State	Fully Defined
Visibility	Visible
Details of Fixed Points	
Visibility	Visible

TABLE 10 Model (B3, C3) > Geometry > Fixed Points > Connection Point

Name	Fixed Breakwater
State	Fully Defined
Visibility	Visible
Details of Fixed Breakwater	
Point Definition	Visible
Type	Fixed
Definition of Position X, Y and Z Coordinates	
Position Coordinates	
X	0.0 m
Y	-3.33 m
Z	0.75 m

TABLE 11 Model (B3, C3) > Geometry > Fixed Points > Connection Point

Name	Fixed Breakwater
State	Fully Defined
Visibility	Visible
Details of Fixed Breakwater	
Point Definition	Visible
Type	Fixed
Definition of Position X, Y and Z Coordinates	
Position Coordinates	
X	0.0 m
Y	-3.33 m
Z	0.0 m

Breakwater

Model (B3, C3) > Geometry > Part

Name	Breakwater
State	Fully Defined
Details of Breakwater	
Part Visibility	Visible
Part Activity	Not Suppressed
Part Color	15454648
Mass Properties	
Total Mass	1106333.1463902 kg
Center of Gravity X	0.0 m
Center of Gravity Y	8.5 m
Center of Gravity Z	-7 m
Moment of Inertia Ixx	1106333.1463902 kg m ²
Moment of Inertia Iyy	0.0 kg m ²
Moment of Inertia Izz	0.0 kg m ²
Moment of Inertia Ixy	1106333.1463902 kg m ²
Moment of Inertia Iyz	0.0 kg m ²
Moment of Inertia Ixz	1106333.1463902 kg m ²
Advanced Options	
Generate Internal Lid	No
Current Calculation Position	At Fixed Depth
Submerged Structure Detection	Program Controlled
Override Calculated GMX	No
Override Calculated GMY	No
Fixity Options	
Structure Fixity	Structure is Fixed in Place
Force Multiplying Factors	
Drag Multiplying Factor	1
Mass Multiplying Factor	1
Stem Multiplying Factor	0.0
Shear Force/Bending Moment Options	
Calculate Shear Force/Bending Moment	Not Permitted for Multiple Structures

Breakwater

Model (B3, C3) > Geometry > Part

Name	Breakwater
State	Fully Defined
Details of Breakwater	
Part Visibility	Visible
Part Activity	Not Suppressed
Part Color	15454648
Mass Properties	
Total Mass	1106333.14636 kg
Center of Gravity X	0.0 m
Center of Gravity Y	8.5 m
Center of Gravity Z	-7 m
Moment of Inertia Ixx	1106333.1463602 kg m ²
Moment of Inertia Iyy	0.0 kg m ²
Moment of Inertia Izz	0.0 kg m ²
Moment of Inertia Ixy	1106333.1463602 kg m ²
Moment of Inertia Iyz	0.0 kg m ²
Moment of Inertia Ixz	1106333.1463602 kg m ²
Advanced Options	
Generate Internal Lid	No
Current Calculation Position	At Fixed Depth
Submerged Structure Detection	Program Controlled
Override Calculated GMX	No
Override Calculated GMY	No
Fixity Options	
Structure Fixity	Structure is Fixed in Place
Force Multiplying Factors	
Drag Multiplying Factor	1
Mass Multiplying Factor	1
Stem Multiplying Factor	0.0
Shear Force/Bending Moment Options	
Calculate Shear Force/Bending Moment	Not Permitted for Multiple Structures

Breakwater

Model (B3, C3) > Geometry > Breakwater > Body

TABLE 13

Name	Surface Body
State	Fully Defined
Details of Surface Body	
Body Visibility	Visible
Activity	Not Suppressed
Body Color Definition	Inherited from Part
Structure Type	Physical Geometry
Surface Type	Program Controlled

Model (B3, C3) > Geometry > Breakwater > Body

TABLE 13

Name	Surface Body
State	Fully Defined
Details of Surface Body	
Body Visibility	Visible
Activity	Not Suppressed
Body Color Definition	Inherited from Part
Structure Type	Physical Geometry
Surface Type	Program Controlled

Model (B3, C3) > Geometry > Breakwater > Body

TABLE 14

Name	Surface Body
State	Fully Defined
Details of Surface Body	
Body Visibility	Visible
Activity	Not Suppressed
Body Color Definition	Inherited from Part
Structure Type	Physical Geometry
Surface Type	Program Controlled

Model (B3, C3) > Geometry > Breakwater > Body

TABLE 14

Name	Surface Body
State	Fully Defined
Details of Surface Body	
Body Visibility	Visible
Activity	Not Suppressed
Body Color Definition	Inherited from Part
Structure Type	Physical Geometry
Surface Type	Program Controlled

Model (B3, C3) > Geometry > Breakwater > Axes

TABLE 15

Name	Breakwater Axes
State	Fully Defined
Details of Breakwater Axes	
Visibility	Visible
Axes Alignment	
Alignment Method	Global Axes
Rotation About Global Z	0.0°
Rotation About Local X	0.0°
Rotation About Local Y	0.0°
Unit Vector X	[1, 0.0, 0.0]
Unit Vector Y	[0.0, 1, 0.0]
Unit Vector Z	[0.0, 0.0, 1]

Model (B3, C3) > Geometry > Breakwater > Axes

TABLE 15

Name	Breakwater Axes
State	Fully Defined
Details of Breakwater Axes	
Visibility	Visible
Axes Alignment	
Alignment Method	Global Axes
Rotation About Global Z	0.0°
Rotation About Local X	0.0°
Rotation About Local Y	0.0°
Unit Vector X	[1, 0.0, 0.0]
Unit Vector Y	[0.0, 1, 0.0]
Unit Vector Z	[0.0, 0.0, 1]

Model (B3, C3) > Geometry > Breakwater > Structural Mass

TABLE 16

Name	Point Mass
State	Fully Defined
Details of Point Mass	
Visibility	Visible
Activity	Not Suppressed
Point Mass Properties	
Mass Definition	Manual Definition
X	0.0 m
Y	0.0 m
Z	-7 m
Mass	1106333.14635902 kg
Inertia Properties	
Define Inertia Values By	Radius of Gyration
Kxx	1 m
Kyy	1 m
Kzz	1106333.14635902 kg.m ²
Ixy	0.0 kg.m ²
Iyz	0.0 kg.m ²
Ixz	0.0 kg.m ²
Iyy	1106333.14635902 kg.m ²
Iyz	0.0 kg.m ²
Izz	1106333.14635902 kg.m ²

Model (B3, C3) > Geometry > Breakwater > Structural Mass

TABLE 16

Name	Point Mass
State	Fully Defined
Details of Point Mass	
Visibility	Visible
Activity	Not Suppressed
Point Mass Properties	
Mass Definition	Program Controlled
X	0.0 m
Y	0.0 m
Z	-7 m
Mass	1106333.14635902 kg
Inertia Properties	
Define Inertia Values By	Radius of Gyration
Kxx	1 m
Kyy	1 m
Kzz	1106333.14635902 kg.m ²
Ixy	0.0 kg.m ²
Iyz	0.0 kg.m ²
Ixz	0.0 kg.m ²
Iyy	1106333.14635902 kg.m ²
Iyz	0.0 kg.m ²
Izz	1106333.14635902 kg.m ²

Model (B3, C3) > Geometry > Breakwater > Connection Point

TABLE 17

Name	Connection Breakwater
State	Fully Defined
Details of Connection Breakwater	
Visibility	Visible
Point Definition	
Type	Attached to Structure
Structure	Breakwater

Model (B3, C3) > Geometry > Breakwater > Connection Point

TABLE 17

Name	Connection Breakwater
State	Fully Defined
Details of Connection Breakwater	
Visibility	Visible
Point Definition	
Type	Attached to Structure
Structure	Breakwater

Definition of Position	X, Y and Z Coordinates
Position Coordinates	
X	0.0 m
Y	-3.0 m
Z	0.0 m
Hydrodynamic Response Nodal Motions Output	
Include in Results	Yes

Connections

TABLE 18
Model (B3, C3) > Connections

Name	Joint
State	Fully Defined
Details of Connections	

TABLE 19
Model (B3, C3) > Connections

Activity	Connection	Area Ind. 1	Type	Connectivity	First Attachment	Second Attachment
Joint Floater	Joint	1	Hinged	Fixed Point to Structure	Fixed Floater (Fixed)	Connection Floater (Floater)
Joint Breakwater	Joint	2	Rigid	Fixed Point to Structure	Fixed Breakwater (Fixed)	Connection Breakwater (Breakwater)

TABLE 20
Model (B3, C3) > Connections > Connection Data

Name	Joint
State	Fully Defined
Details of Connection Data	

TABLE 21
Model (B3, C3) > Connections > Joint

Name	Joint Floater
State	Fully Defined
Details of Joint Floater	
Visibility	Visible
Activity	Not Suppressed
Type	Hinged
Connected to	Fixed Point to Structure
Connection Point	Fixed Floater (Fixed)
Connection Point	Connection Floater (Floater)
Joint Properties	
Stiffness About Local Joint X	0.0 N m ²
Damping About Local Joint X	25000 N m/(V/s)
Transverse Force Friction Coefficient (K1)	0.0 m
Overturning Moment Friction Coefficient (K2)	0.0
Axis Constant Friction Coefficient (K3)	0.0 m
Constant Friction Moment (k4)	0.0 N m

TABLE 22
Model (B3, C3) > Connections > Joint Floater > Axes

Name	Joint Axes On Fixed Point
State	Fully Defined
Details of Joint Axes On Fixed Point	
Visibility	Visible
Axes Alignment	
Alignment Method	Global Axes
Rotation About Global Z	0.0°
Rotation About Local Y	0.0°
Rotation About Local X	0.0°
Unit Vector X	[1, 0.0, 0.0]
Unit Vector Y	[0, 1, 0.0]
Unit Vector Z	[0, 0, 1]

TABLE 23
Model (B3, C3) > Connections > Joint Floater > Axes

Name	Joint Axes On Structure
State	Fully Defined
Details of Joint Axes On Structure	
Visibility	Visible

Definition of Position	X, Y and Z Coordinates
Position Coordinates	
X	0.0 m
Y	-3.0 m
Z	0.0 m
Hydrodynamic Response Nodal Motions Output	
Include in Results	Yes

Connections

TABLE 18
Model (B3, C3) > Connections

Name	Joint
State	Fully Defined
Details of Connections	

TABLE 19
Model (B3, C3) > Connections

Activity	Connection	Area Ind. 1	Type	Connectivity	First Attachment	Second Attachment
Joint Floater	Joint	1	Hinged	Fixed Point to Structure	Fixed Floater (Fixed)	Connection Floater (Floater)
Joint Breakwater	Joint	2	Rigid	Fixed Point to Structure	Fixed Breakwater (Fixed)	Connection Breakwater (Breakwater)

TABLE 20
Model (B3, C3) > Connections > Connection Data

Name	Joint
State	Fully Defined
Details of Connection Data	

TABLE 21
Model (B3, C3) > Connections > Joint

Name	Joint Floater
State	Fully Defined
Details of Joint Floater	
Visibility	Visible
Activity	Not Suppressed
Type	Hinged
Connected to	Fixed Point to Structure
Connection Point	Fixed Floater (Fixed)
Connection Point	Connection Floater (Floater)
Joint Properties	
Stiffness About Local Joint X	0.0 N m ²
Damping About Local Joint X	40000 N m/(V/s)
Transverse Force Friction Coefficient (K1)	0.0 m
Overturning Moment Friction Coefficient (K2)	0.0
Axis Constant Friction Coefficient (K3)	0.0 m
Constant Friction Moment (k4)	0.0 N m

TABLE 22
Model (B3, C3) > Connections > Joint Floater > Axes

Name	Joint Axes On Fixed Point
State	Fully Defined
Details of Joint Axes On Fixed Point	
Visibility	Visible
Axes Alignment	
Alignment Method	Global Axes
Rotation About Global Z	0.0°
Rotation About Local Y	0.0°
Rotation About Local X	0.0°
Unit Vector X	[1, 0.0, 0.0]
Unit Vector Y	[0, 1, 0.0]
Unit Vector Z	[0, 0, 1]

TABLE 23
Model (B3, C3) > Connections > Joint Floater > Axes

Name	Joint Axes On Structure
State	Fully Defined
Details of Joint Axes On Structure	
Visibility	Visible

Axes Alignment	
Alignment Method	Global Axes
Rotation About Global Z	0.0°
Rotation About Global Y	0.0°
Rotation About Local X	0.0°
Unit Vector X	[1, 0.0, 0.0]
Unit Vector Y	[0.0, 1, 0.0]
Unit Vector Z	[0.0, 0.0, 1]

TABLE 24
Model (B3, C3) > Connections > Joint Breakwater > Axes

Name		Joint Breakwater	
Name	Joint Breakwater	State	Fully Defined
Visibility	Visible	Activity	Not Suppressed
Type	Rigid	Connectivity	Fixed Point to Structure
Fixed Point to Structure	Fixed Point to Structure	Fixed Point to Structure	Fixed Point to Structure
Connection Point	Connection Breakwater (Breakwater)	Connection Point	Connection Breakwater (Breakwater)

TABLE 25
Model (B3, C3) > Connections > Joint Breakwater > Axes

Name		Joint Breakwater > Axes	
Name	Joint Breakwater > Axes	State	Fully Defined
Visibility	Visible	Activity	Not Suppressed
Type	Rigid	Connectivity	Fixed Point to Structure
Fixed Point to Structure	Fixed Point to Structure	Fixed Point to Structure	Fixed Point to Structure
Connection Point	Connection Breakwater (Breakwater)	Connection Point	Connection Breakwater (Breakwater)

TABLE 26
Model (B3, C3) > Connections > Joint Breakwater > Axes

Name		Joint Breakwater > Axes	
Name	Joint Breakwater > Axes	State	Fully Defined
Visibility	Visible	Activity	Not Suppressed
Type	Rigid	Connectivity	Fixed Point to Structure
Fixed Point to Structure	Fixed Point to Structure	Fixed Point to Structure	Fixed Point to Structure
Connection Point	Connection Breakwater (Breakwater)	Connection Point	Connection Breakwater (Breakwater)

Mesh

TABLE 27
Model (B3, C3) > Mesh

Name		Mesh	
Name	Mesh	State	Meshed
Element Size	3.3 m	Maximum Allowed Frequency	0.49342 Hz
Waterline Node Generation	No	Create Automatic Waterline Nodes	No
Meshing Engine	AnshMeshing	String and Dewatering	No
Display Information For	All Structures	Total Nodes	1487
Total Elements	1508		

Axes Alignment	
Alignment Method	Global Axes
Rotation About Global Z	0.0°
Rotation About Global Y	0.0°
Rotation About Local X	0.0°
Unit Vector X	[1, 0.0, 0.0]
Unit Vector Y	[0.0, 1, 0.0]
Unit Vector Z	[0.0, 0.0, 1]

TABLE 24
Model (B3, C3) > Connections > Joint Breakwater > Axes

Name		Joint Breakwater	
Name	Joint Breakwater	State	Fully Defined
Visibility	Visible	Activity	Not Suppressed
Type	Rigid	Connectivity	Fixed Point to Structure
Fixed Point to Structure	Fixed Point to Structure	Fixed Point to Structure	Fixed Point to Structure
Connection Point	Connection Breakwater (Breakwater)	Connection Point	Connection Breakwater (Breakwater)

TABLE 25
Model (B3, C3) > Connections > Joint Breakwater > Axes

Name		Joint Breakwater > Axes	
Name	Joint Breakwater > Axes	State	Fully Defined
Visibility	Visible	Activity	Not Suppressed
Type	Rigid	Connectivity	Fixed Point to Structure
Fixed Point to Structure	Fixed Point to Structure	Fixed Point to Structure	Fixed Point to Structure
Connection Point	Connection Breakwater (Breakwater)	Connection Point	Connection Breakwater (Breakwater)

TABLE 26
Model (B3, C3) > Connections > Joint Breakwater > Axes

Name		Joint Breakwater > Axes	
Name	Joint Breakwater > Axes	State	Fully Defined
Visibility	Visible	Activity	Not Suppressed
Type	Rigid	Connectivity	Fixed Point to Structure
Fixed Point to Structure	Fixed Point to Structure	Fixed Point to Structure	Fixed Point to Structure
Connection Point	Connection Breakwater (Breakwater)	Connection Point	Connection Breakwater (Breakwater)

Mesh

TABLE 27
Model (B3, C3) > Mesh

Name		Mesh	
Name	Mesh	State	Meshed
Element Size	3.3 m	Maximum Allowed Frequency	0.4719 Hz
Waterline Node Generation	No	Create Automatic Waterline Nodes	No
Meshing Engine	AnshMeshing	String and Dewatering	No
Display Information For	All Structures	Total Nodes	964
Total Elements	973		

External Surface Diffracting Nodes	1051
External Surface Diffracting Elements	1018
External Surface Non-Diffracting Nodes	326
External Surface Non-Diffracting Elements	489

TABLE 28

Model (B3, C3) > Mesh > Mesh Sizing	
Name	Mesh Sizing
State	Fully Defined
Details of Mesh Sizing	
Activity	Not Suppressed
Select Geometry	2 Bodies
Local Element Size	1.2 m
Local Defeature Size	Default (0.0165 m)

TABLE 29

Model (B3, C3) > Mesh > Mesh Sizing	
Name	Mesh Sizing
State	Fully Defined
Details of Mesh Sizing	
Activity	Not Suppressed
Select Geometry	2 Bodies
Local Element Size	0.42 m
Local Defeature Size	Default (0.0165 m)

Hydrodynamic Diffraction (B4)

TABLE 30

Model (B3, C3) > Analysis	
Name	Hydrodynamic Diffraction (B4)
State	Solved
Details of Hydrodynamic Diffraction	
Analysis Type	Hydrodynamic Diffraction/Radiation

Model (B3, C3) > Hydrodynamic Diffraction (B4) > Analysis Settings

Model (B3, C3) > Hydrodynamic Diffraction (B4) > Analysis Settings	
Name	Analysis Settings
State	Fully Defined
Details of Analysis Settings	
External Operation before Solving	None
External Operation after Solving	None
Parallel Processing	Program Controlled
Generate Wave Grid Pressures	Yes
Wave Grid Resolution	Fine (161 x 101)
Wave Grid Spacing	Z
Common Analysis Options	
Ignore Modelling Rule Violations	Yes
Calculate Extreme Low/High Frequencies	Yes
Include Multi-Directional Wave Interaction	Yes
Near Field Solution	Program Controlled
Linearized Morison Drag	No
QIF Options	
Calculate QIF	Yes
Output File Options	
Source Strengths	No
Potentials	No
Centroid Pressures	No
Element Properties	No
ASCI Hydrodynamic Database	No
Example of Hydrodynamic Database	No
Generate AHD Pressure Output	No

TABLE 32

Model (B3, C3) > Hydrodynamic Diffraction (B4) > Structure Selection	
Name	Structure Selection
State	Fully Defined
Details of Structure Selection	
Structures to Exclude	None
Group of Structures	All
Interacting Structure Group	All

External Surface Diffracting Nodes	539
External Surface Diffracting Elements	504
External Surface Non-Diffracting Nodes	326
External Surface Non-Diffracting Elements	489

TABLE 28

Model (B3, C3) > Mesh > Mesh Sizing	
Name	Mesh Sizing
State	Fully Defined
Details of Mesh Sizing	
Activity	Not Suppressed
Select Geometry	2 Bodies
Local Element Size	1.2 m
Local Defeature Size	Default (0.0165 m)

TABLE 29

Model (B3, C3) > Mesh > Mesh Sizing	
Name	Mesh Sizing
State	Fully Defined
Details of Mesh Sizing	
Activity	Not Suppressed
Select Geometry	2 Bodies
Local Element Size	0.42 m
Local Defeature Size	Default (0.0165 m)

Hydrodynamic Diffraction (B4)

TABLE 30

Model (B3, C3) > Analysis	
Name	Hydrodynamic Diffraction (B4)
State	Solved
Details of Hydrodynamic Diffraction	
Analysis Type	Hydrodynamic Diffraction/Radiation

Model (B3, C3) > Hydrodynamic Diffraction (B4) > Analysis Settings

Model (B3, C3) > Hydrodynamic Diffraction (B4) > Analysis Settings	
Name	Analysis Settings
State	Fully Defined
Details of Analysis Settings	
External Operation before Solving	None
External Operation after Solving	None
Parallel Processing	Program Controlled
Generate Wave Grid Pressures	Yes
Wave Grid Resolution	Fine (161 x 101)
Wave Grid Spacing	Z
Common Analysis Options	
Ignore Modelling Rule Violations	Yes
Calculate Extreme Low/High Frequencies	Yes
Include Multi-Directional Wave Interaction	Yes
Near Field Solution	Program Controlled
Linearized Morison Drag	No
QIF Options	
Calculate QIF	Yes
Output File Options	
Source Strengths	No
Potentials	No
Centroid Pressures	No
Element Properties	No
ASCI Hydrodynamic Database	No
Example of Hydrodynamic Database	No
Generate AHD Pressure Output	No

TABLE 32

Model (B3, C3) > Hydrodynamic Diffraction (B4) > Structure Selection	
Name	Structure Selection
State	Fully Defined
Details of Structure Selection	
Structures to Exclude	None
Group of Structures	All
Interacting Structure Group	All

Interacting Structure Group 2	None
Motion Locks	No
Apply Motion Lock to Group	No
Structure 1	Flotation
Structure 2	Breakwater

TABLE 33
Model (B3, C3) > Hydrodynamic Diffraction (B4) > Wave Direction

Direction Number	Wave Direction (°)
1	-180
2	-135
3	-90
4	-45
5	0.0
6	45
7	90
8	135
9	180

TABLE 33
Model (B3, C3) > Hydrodynamic Diffraction (B4) > Wave Direction

Direction Number	Wave Direction (°)
1	-180
2	-135
3	-90
4	-45
5	0.0
6	45
7	90
8	135
9	180

TABLE 34
Model (B3, C3) > Hydrodynamic Diffraction (B4) > Wave Directions

Direction Number	Wave Direction (°)
1	-180
2	-135
3	-90
4	-45
5	0.0
6	45
7	90
8	135
9	180

TABLE 35
Model (B3, C3) > Hydrodynamic Diffraction (B4) > Wave Frequency

State	Fully Defined
Incident Wave Frequency/Period Definition	Period
Lowest Frequency	0.01592 Hz
Highest Frequency	0.40942 Hz
Number of Intermediate Values	18
Interval Period	3.17539 s
Additional Frequencies A	None
Additional Frequencies B	None
Additional Frequencies C	None
Additional Frequencies D	None

Solution (B5)

TABLE 36
Model (B3, C3) > Hydrodynamic Diffraction (B4) > Solution (B5) > Pressures and Motions Results

Interacting Structure Group 2	None
Motion Locks	No
Apply Motion Lock to Group	No
Structure 1	Flotation
Structure 2	Breakwater

TABLE 33
Model (B3, C3) > Hydrodynamic Diffraction (B4) > Wave Direction

Direction Number	Wave Direction (°)
1	-180
2	-135
3	-90
4	-45
5	0.0
6	45
7	90
8	135
9	180

TABLE 33
Model (B3, C3) > Hydrodynamic Diffraction (B4) > Wave Direction

Direction Number	Wave Direction (°)
1	-180
2	-135
3	-90
4	-45
5	0.0
6	45
7	90
8	135
9	180

TABLE 34
Model (B3, C3) > Hydrodynamic Diffraction (B4) > Wave Directions

Direction Number	Wave Direction (°)
1	-180
2	-135
3	-90
4	-45
5	0.0
6	45
7	90
8	135
9	180

TABLE 35
Model (B3, C3) > Hydrodynamic Diffraction (B4) > Wave Frequency

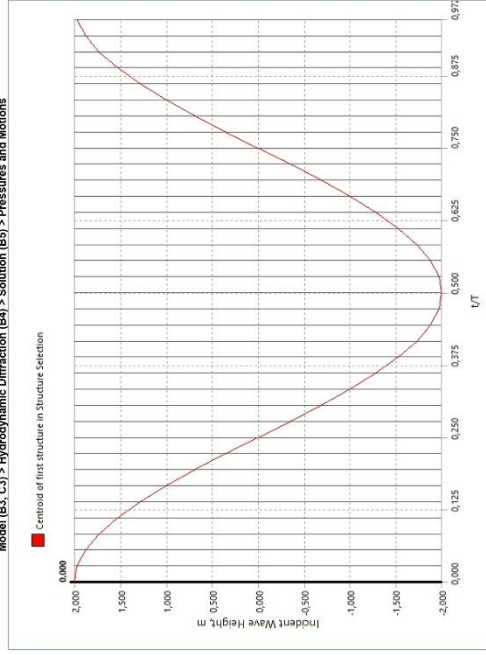
State	Fully Defined
Incident Wave Frequency/Period Definition	Period
Lowest Frequency	0.01592 Hz
Highest Frequency	0.4219 Hz
Number of Intermediate Values	18
Interval Period	3.18219 s
Additional Frequencies A	None
Additional Frequencies B	None
Additional Frequencies C	None
Additional Frequencies D	None

Solution (B5)

TABLE 36
Model (B3, C3) > Hydrodynamic Diffraction (B4) > Solution (B5) > Pressures and Motions Results

Name	Pressures and Motions
State	Solved
Details of Pressures and Motions	
Structure Selection	All
Result Selection	
Frequency	0.11365 Hz
Direction	0.0°
Incident Wave Amplitude	2 m
Result Type	Phase Angle
Wave Position (Phase)	Sequence
Number of Steps	36
Contour Selection	
Contour Type	Structure Interpolated Pressure
Water Elements Shown As	Opaque
Pressure Measurement	Head of Water
Component Selection	
Include Incident Wave	Yes
Include Diffracted Wave	Yes
Include Radiation Wave	Yes
Include Hydrostatic Varying	Yes
Results	
Minimum Value	-3.264429230202552 m
Maximum Value	3.264429230202552 m

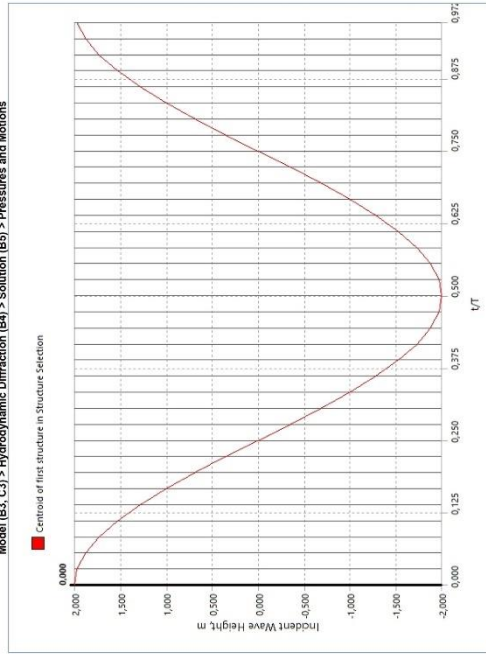
Model (B5, C3) > Hydrodynamic Diffraction (B4) > Solution (B5) > Pressures and Motions



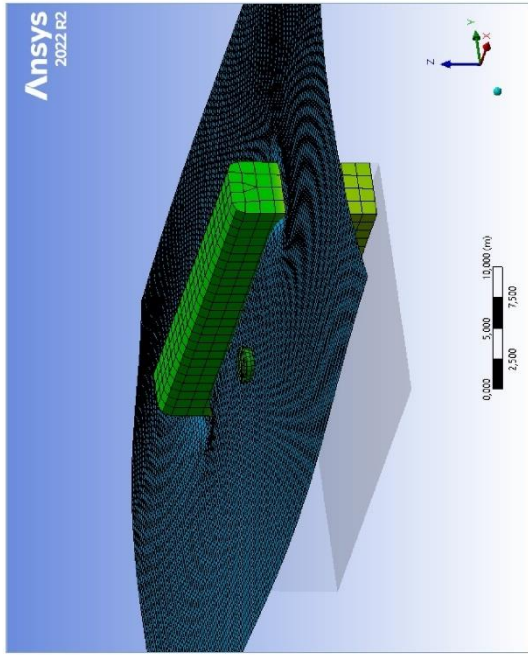
Model (B5, C3) > Hydrodynamic Diffraction (B4) > Solution (B5) > Pressures and Motions

Name	Pressures and Motions
State	Solved
Details of Pressures and Motions	
Structure Selection	All
Result Selection	
Frequency	0.11449 Hz
Direction	-90°
Incident Wave Amplitude	2 m
Result Type	Phase Angle
Wave Position (Phase)	Sequence
Number of Steps	36
Contour Selection	
Contour Type	Structure Interpolated Pressure
Water Elements Shown As	Opaque
Pressure Measurement	Head of Water
Component Selection	
Include Incident Wave	Yes
Include Diffracted Wave	Yes
Include Radiation Wave	Yes
Include Hydrostatic Varying	Yes
Results	
Minimum Value	-4.47725328681272 m
Maximum Value	4.47725328681272 m

Model (B5, C3) > Hydrodynamic Diffraction (B4) > Solution (B5) > Pressures and Motions



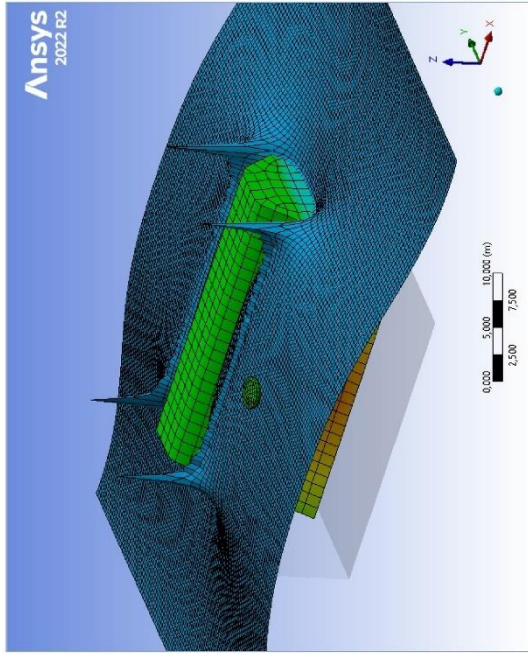
Model (B5, C3) > Hydrodynamic Diffraction (B4) > Solution (B5) > Pressures and Motions



Model (B3, C3) > Hydrodynamic Diffraction (B4) > Solution (B5) > Hydrodynamic Graph Results

Name		Parameters vs Frequency
State	Selected	
Details of Parameters vs Frequency		
Presentation Method	Line	
Axes Selection	Parameters vs Frequency	
Frequency or Period Scale	Frequency	
Export CSV File	Select CSV File...	
Line A		
Abcissas Position of Minimum	0.01692 Hz	
Abcissas Position of Maximum	0.4719 Hz	
Minimum Value	100.29435 N/(m/s)	
Maximum Value	6300.45117 N/(m/s)	

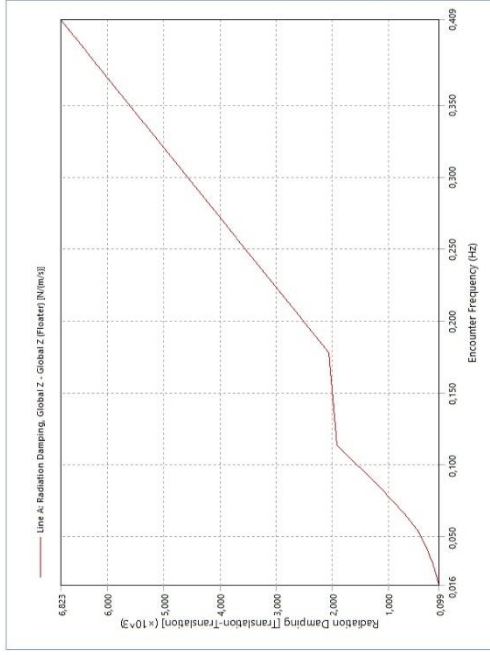
Model (B3, C3) > Hydrodynamic Diffraction (B4) > Solution (B5) > Parameters vs Frequency



Model (B3, C3) > Hydrodynamic Diffraction (B4) > Solution (B5) > Hydrodynamic Graph Results

Name		Parameters vs Frequency
State	Selected	
Details of Parameters vs Frequency		
Presentation Method	Line	
Axes Selection	Parameters vs Frequency	
Frequency or Period Scale	Frequency	
Export CSV File	Select CSV File...	
Line A		
Abcissas Position of Minimum	0.01692 Hz	
Abcissas Position of Maximum	0.46942 Hz	
Minimum Value	99.056175 N/(m/s)	
Maximum Value	6823.21338 N/(m/s)	

Model (B3, C3) > Hydrodynamic Diffraction (B4) > Solution (B5) > Parameters vs Frequency



Model (B3, C3) > Hydrodynamic Diffraction (B4) > Solution (B5) > Parameters vs Frequency > Hydrodynamic Graph Results

TABLE 38
Input

Name	Radiation Damping	Solved
State		Solved
Details of Radiation Damping		
Line Inputs		
Structure	Floatier	
Type	Radiation Damping	
Sub Type	Global Z	
Component	Global Z	
Line Values		
Abscissa (X) Position of Minimum	0.016592 Hz	
Abscissa (X) Position of Maximum	0.449 Hz	
Minimum Value	99.05073 N/(m/s)	
Maximum Value	6882.21338 N/(m/s)	

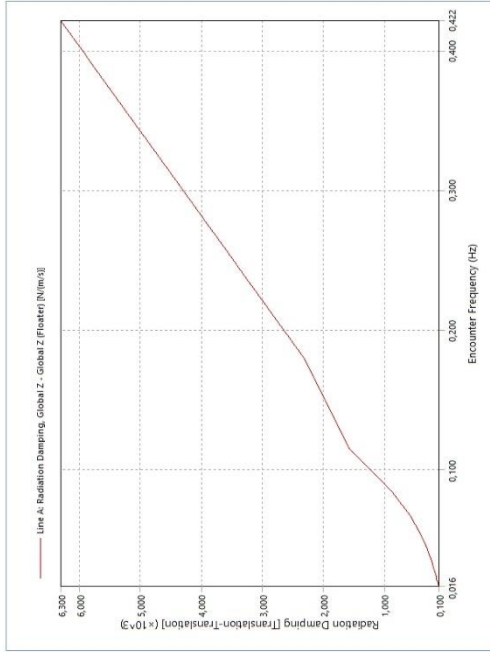
Model (B3, C3) > Hydrodynamic Diffraction (B4) > Solution (B5) > Hydrodynamic Graph Results

TABLE 39
Parameters vs Frequency

Name	Parameters vs Frequency	Solved
State		Solved
Details of Parameters vs Frequency		
Line		
Presentation Method	Line	
Axes Selection	Parameters vs Frequency	
Frequency or Period Scale	Frequency	
Export CSV File	Select CSV File...	
Line A		
Abscissa Position of Minimum	0.016592 Hz	
Abscissa Position of Maximum	0.449 Hz	
Minimum Value	265.103664 kg	
Maximum Value	6875.30229 kg	

FIGURE 4

Model (B3, C3) > Hydrodynamic Diffraction (B4) > Solution (B5) > Parameters vs Frequency



Model (B3, C3) > Hydrodynamic Diffraction (B4) > Solution (B5) > Parameters vs Frequency > Hydrodynamic Graph Results

TABLE 38
Input

Name	Radiation Damping	Solved
State		Solved
Details of Radiation Damping		
Line Inputs		
Structure	Floatier	
Type	Radiation Damping	
Sub Type	Global Z	
Component	Global Z	
Line Values		
Abscissa (X) Position of Minimum	0.016592 Hz	
Abscissa (X) Position of Maximum	0.452 Hz	
Minimum Value	100.29455 N/(m/s)	
Maximum Value	6300.45117 N/(m/s)	

Model (B3, C3) > Hydrodynamic Diffraction (B4) > Solution (B5) > Hydrodynamic Graph Results

TABLE 39
Parameters vs Frequency

Name	Parameters vs Frequency	Solved
State		Solved
Details of Parameters vs Frequency		
Line		
Presentation Method	Line	
Axes Selection	Parameters vs Frequency	
Frequency or Period Scale	Frequency	
Export CSV File	Select CSV File...	
Line A		
Abscissa Position of Minimum	0.016592 Hz	
Abscissa Position of Maximum	0.452 Hz	
Minimum Value	3248.11453 kg	
Maximum Value	6571.77383 kg	

FIGURE 4

Model (B3, C3) > Hydrodynamic Diffraction (B4) > Solution (B5) > Parameters vs Frequency

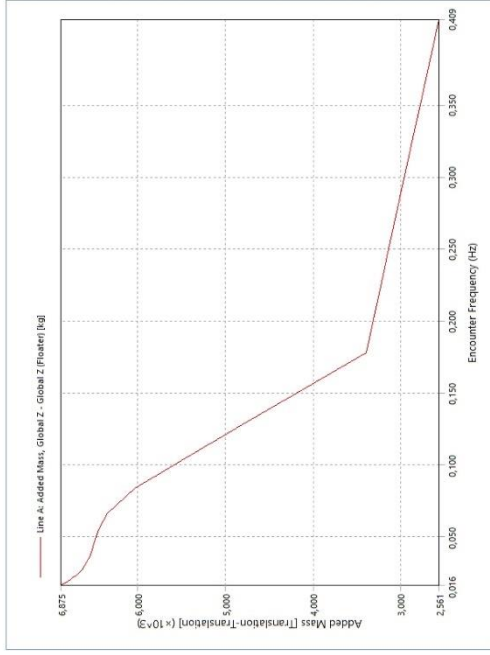


TABLE 40
Model (B3, C3) > Hydrodynamic Diffraction (B4) > Solution (B5) > Parameters vs Frequency > Hydrodynamic Graph Results

Name	Added Mass	Solved
Details of Added Mass		
Line Inputs		
Structure	Floatier	
Type	Added Mass	
Sub Type	Global Z	
Component	Global Z	
Line Values		
Abscissa (X) Position of Minimum	0.40847 Hz	
Abscissa (X) Position of Maximum	0.016 Hz	
Minimum Value	2581.03564 kg	
Maximum Value	6875.30029 kg	

Hydrodynamic Response (C4)

TABLE 41
Model (B3, C3) > Analysis

Name	Hydrodynamic Response (C4)
State	Solved
Details of Hydrodynamic Response	
Analysis Type	Hydrodynamic Time Response

TABLE 42
Model (B3, C3) > Hydrodynamic Response (C4) > Analysis Settings

Name	Analysis Settings
State	Fully Defined
Details of Analysis Settings	
Computation Type	Time Response Analysis
External Operation before Solving	None
External Operation after Solving	None

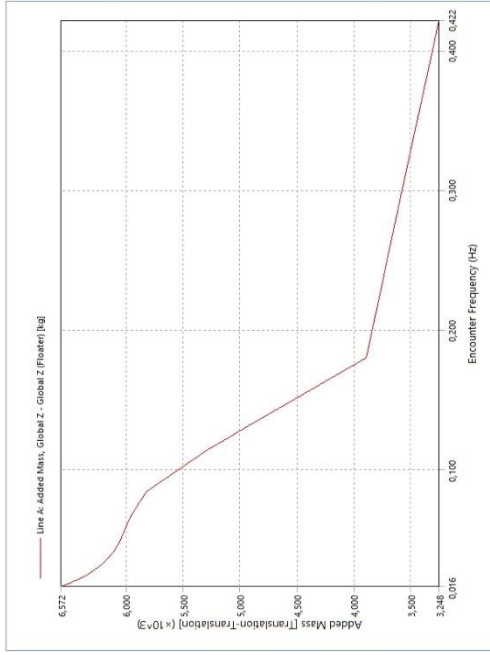


TABLE 40
Model (B3, C3) > Hydrodynamic Diffraction (B4) > Solution (B5) > Parameters vs Frequency > Hydrodynamic Graph Results

Name	Added Mass	Solved
Details of Added Mass		
Line Inputs		
Structure	Floatier	
Type	Added Mass	
Sub Type	Global Z	
Component	Global Z	
Line Values		
Abscissa (X) Position of Minimum	0.4216 Hz	
Abscissa (X) Position of Maximum	0.016 Hz	
Minimum Value	3248.11553 kg	
Maximum Value	6871.77393 kg	

Hydrodynamic Response (C4)

TABLE 41
Model (B3, C3) > Analysis

Name	Hydrodynamic Response (C4)
State	Solved
Details of Hydrodynamic Response	
Analysis Type	Hydrodynamic Time Response

TABLE 42
Model (B3, C3) > Hydrodynamic Response (C4) > Analysis Settings

Name	Analysis Settings
State	Fully Defined
Details of Analysis Settings	
Computation Type	Time Response Analysis
External Operation before Solving	None
External Operation after Solving	None

Parallel Processing	Program Controlled
Use Cable Dynamics	Yes
Time Response Specific Options	
Irregular Wave Response	Irregular Wave Response
Start Time	0.0 s
Time Step	0.05 s
Output Step	0.1 s
Duration	100 s
Number of Steps	2001
Finish Time	100 s
Starting Position	Based on Allocated Positions
X-Position for Wave Surface Elevation Output	0.0 m
Y-Position for Wave Surface Elevation Output	0.0 m
Time Response Pressure Output	
Output for Structure	None
Common Analysis Options	
Convolution	Yes
Call Routine "user_force"	No
Connect to Server for External "user_force" Calculation	No
Use Linear Stiffness Matrix to Calculate Hydrostatic	No
Account for Current Phase Shift	Yes
Include Maneuvering Force	No
Use Wheeler Stretching	With Linear Wave Theory
Output File Options	
Axis System for Joint Reactions	Fixed Reference Axes
Data List	Yes
Element Properties	No
Dynamic Cable/Fiber Drag	No
Co-simulation FEM Package	
Output FEM Package	No

Parallel Processing	Program Controlled
Use Cable Dynamics	Yes
Time Response Specific Options	
Irregular Wave Response	Irregular Wave Response
Start Time	0.0 s
Time Step	0.05 s
Output Step	0.1 s
Duration	100 s
Number of Steps	2001
Finish Time	100 s
Starting Position	Based on Allocated Positions
X-Position for Wave Surface Elevation Output	0.0 m
Y-Position for Wave Surface Elevation Output	0.0 m
Time Response Pressure Output	
Output for Structure	None
Common Analysis Options	
Convolution	Yes
Call Routine "user_force"	No
Connect to Server for External "user_force" Calculation	No
Use Linear Stiffness Matrix to Calculate Hydrostatic	No
Account for Current Phase Shift	Yes
Include Maneuvering Force	No
Use Wheeler Stretching	With Linear Wave Theory
Output File Options	
Axis System for Joint Reactions	Fixed Reference Axes
Data List	Yes
Element Properties	No
Dynamic Cable/Fiber Drag	No
Co-simulation FEM Package	
Output FEM Package	No

TABLE 43 Model (B3, C3) > Hydrodynamic Response (C4) > Irregular Wave

Irregular Wave	Irregular Wave
Fully Defined	Fully Defined
Details of Irregular Wave	
Visibility	Visible
Activity	Not Suppressed
Wave Range Defined By	Period
Ramping Method	Program Controlled
Wave Spectrum Details	
Wave Type	JONSWAP (Hs)
Direction of Spreading	90°
Wave Spreading	None (Long-Crested Waves)
Spectrum Presentation Method	1D Graph
Seed Definition	Program Controlled
Number of Spectral Lines Definition	Program Controlled
Start and Finish Period Definition	Program Controlled
Start Period	17.08331 s
Finish Period	2.4977 s
Significant Wave Height	3.3
Gamma	3.3
Peak Period	10 s
Export CSV File	Select CSV File...
Cross Swell Details	
Wave Type	None

FIGURE 5 Model (B3, C3) > Hydrodynamic Response (C4) > Irregular Wave

TABLE 43 Model (B3, C3) > Hydrodynamic Response (C4) > Irregular Wave

Irregular Wave	Irregular Wave
Fully Defined	Fully Defined
Details of Irregular Wave	
Visibility	Visible
Activity	Not Suppressed
Wave Range Defined By	Period
Ramping Method	Program Controlled
Wave Spectrum Details	
Wave Type	JONSWAP (Hs)
Direction of Spreading	90°
Wave Spreading	None (Long-Crested Waves)
Spectrum Presentation Method	1D Graph
Seed Definition	Program Controlled
Number of Spectral Lines Definition	Program Controlled
Start and Finish Period Definition	Program Controlled
Start Period	17.08331 s
Finish Period	2.4977 s
Significant Wave Height	3.3
Gamma	3.3
Peak Period	10 s
Export CSV File	Select CSV File...
Cross Swell Details	
Wave Type	None

FIGURE 5 Model (B3, C3) > Hydrodynamic Response (C4) > Irregular Wave

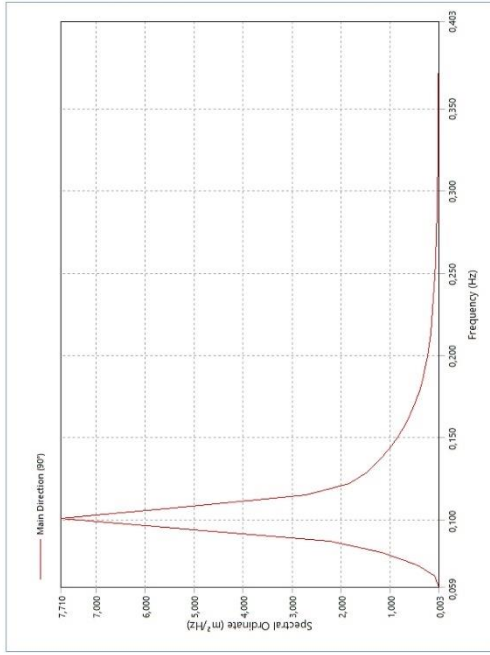


TABLE 44
Model (B3, C3) > Hydrodynamic Response (C4) > Irregular Wave

Direction (°)	Period (s)	Spectral Ordinate (m ² /s)	90
Sub-Weight	→	→	1
2.48077		1.24555e-3	
2.52481		1.31261e-3	
2.57044		1.38454e-3	
2.61766		1.46166e-3	
2.66682		1.54487e-3	
2.71778		1.63431e-3	
2.77072		1.73075e-3	
2.82576		1.83485e-3	
2.88304		1.94741e-3	
2.94269		2.06929e-3	
3.00485		2.20146e-3	
3.06952		2.34509e-3	
3.13741		2.50088e-3	
3.20818		2.67103e-3	
3.28221		2.85662e-3	
3.35974		3.05852e-3	
3.44101		3.28736e-3	
3.52632		3.52559e-3	
3.61597		3.78357e-3	
3.70963		4.06263e-3	
3.80665		4.36345e-3	
3.91452		4.77466e-3	
4.0253		5.17584e-3	
4.14253		5.61649e-3	
4.2668		6.10896e-3	
4.39875		6.6576e-3	
4.53912		7.26985e-3	
4.68815		7.95006e-3	
4.84658		8.7189e-3	

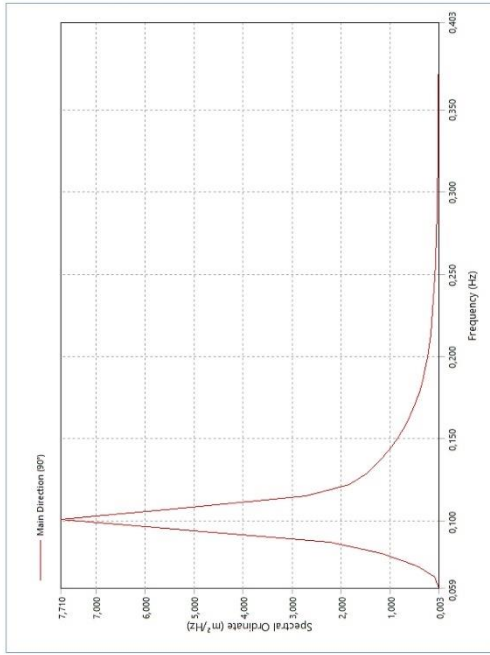
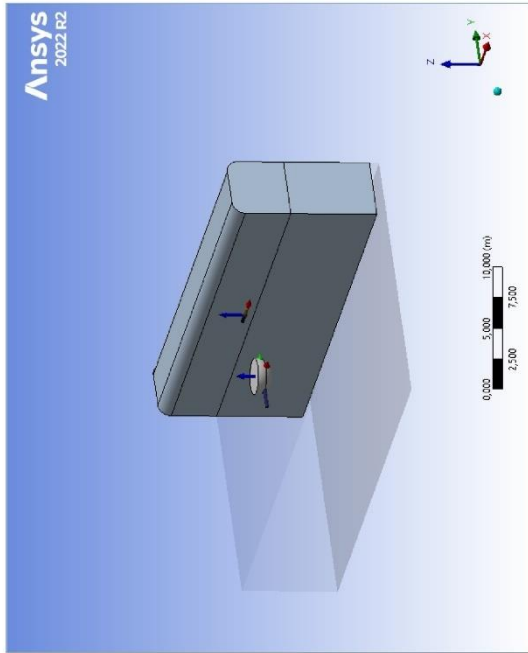


TABLE 44
Model (B3, C3) > Hydrodynamic Response (C4) > Irregular Wave

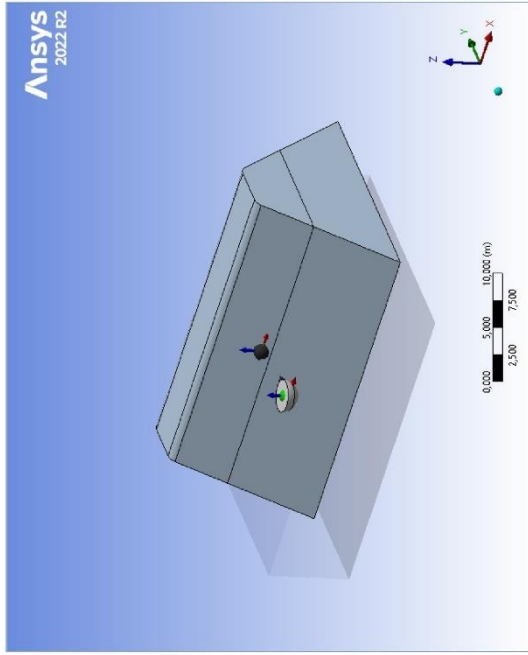
Direction (°)	Period (s)	Spectral Ordinate (m ² /s)	90
Sub-Weight	→	→	1
2.48077		1.24555e-3	
2.52481		1.31261e-3	
2.57044		1.38454e-3	
2.61766		1.46166e-3	
2.66682		1.54487e-3	
2.71778		1.63431e-3	
2.77072		1.73075e-3	
2.82576		1.83485e-3	
2.88304		1.94741e-3	
2.94269		2.06929e-3	
3.00485		2.20146e-3	
3.06952		2.34509e-3	
3.13741		2.50088e-3	
3.20818		2.67103e-3	
3.28221		2.85662e-3	
3.35974		3.05852e-3	
3.44101		3.28736e-3	
3.52632		3.52559e-3	
3.61597		3.78357e-3	
3.70963		4.06263e-3	
3.80665		4.36345e-3	
3.91452		4.77466e-3	
4.0253		5.17584e-3	
4.14253		5.61649e-3	
4.2668		6.10896e-3	
4.39875		6.6576e-3	
4.53912		7.26985e-3	
4.68815		7.95006e-3	
4.84658		8.7189e-3	

5.01989	9.57677e-3
5.20332	0.01064
5.39675	0.01181
5.59018	0.01301
5.78361	0.01425
5.97704	0.01551
6.17047	0.01681
6.36390	0.01814
6.55733	0.01951
6.75076	0.02091
6.94419	0.02234
7.13762	0.02381
7.33105	0.02531
7.52448	0.02684
7.71791	0.02841
7.91134	0.03001
8.10477	0.03164
8.29820	0.03331
8.49163	0.03504
8.68506	0.03681
8.87849	0.03861
9.07192	0.04044
9.26535	0.04231
9.45878	0.04421
9.65221	0.04614
9.84564	0.04811
10.03907	0.05014
10.23250	0.05221
10.42593	0.05434
10.61936	0.05651
10.81279	0.05874
11.00622	0.06101
11.19965	0.06334
11.39308	0.06571
11.58651	0.06814
11.77994	0.07061
11.97337	0.07314
12.16680	0.07571
12.36023	0.07834
12.55366	0.08101
12.74709	0.08374
12.94052	0.08651
13.13395	0.08934
13.32738	0.09221
13.52081	0.09514
13.71424	0.09811
13.90767	0.10114
14.10110	0.10421
14.29453	0.10734
14.48796	0.11051
14.68139	0.11374
14.87482	0.11701
15.06825	0.12034
15.26168	0.12371
15.45511	0.12714
15.64854	0.13061
15.84197	0.13414
16.03540	0.13771
16.22883	0.14134
16.42226	0.14501
16.61569	0.14874
16.80912	0.15251
17.00255	0.15634
17.19598	0.16021
17.38941	0.16414
17.58284	0.16811
17.77627	0.17214
17.96970	0.17621
18.16313	0.18034
18.35656	0.18451
18.55000	0.18874
18.74343	0.19301
18.93686	0.19734
19.13029	0.20171
19.32372	0.20614
19.51715	0.21061
19.71058	0.21514
19.90401	0.21971
20.09744	0.22434
20.29087	0.22901
20.48430	0.23374
20.67773	0.23851
20.87116	0.24334
21.06459	0.24821
21.25802	0.25314
21.45145	0.25811
21.64488	0.26314
21.83831	0.26821
22.03174	0.27334
22.22517	0.27851
22.41860	0.28374
22.61203	0.28901
22.80546	0.29434
23.00000	0.29971
23.19343	0.30514
23.38686	0.31061
23.58029	0.31614
23.77372	0.32171
23.96715	0.32734
24.16058	0.33301
24.35401	0.33874
24.54744	0.34451
24.74087	0.35034
24.93430	0.35621
25.12773	0.36214
25.32116	0.36811
25.51459	0.37414
25.70802	0.38021
25.90145	0.38634
26.09488	0.39251
26.28831	0.39874
26.48174	0.40501
26.67517	0.41134
26.86860	0.41771
27.06203	0.42414
27.25546	0.43061
27.44889	0.43714
27.64232	0.44371
27.83575	0.45034
28.02918	0.45701
28.22261	0.46374
28.41604	0.47051
28.60947	0.47734
28.80290	0.48421
29.00000	0.49114
29.19343	0.49811
29.38686	0.50514
29.58029	0.51221
29.77372	0.51934
29.96715	0.52651
30.16058	0.53374
30.35401	0.54101
30.54744	0.54834
30.74087	0.55571
30.93430	0.56314
31.12773	0.57061
31.32116	0.57814
31.51459	0.58571
31.70802	0.59334
31.90145	0.60101
32.09488	0.60874
32.28831	0.61651
32.48174	0.62434
32.67517	0.63221
32.86860	0.64014
33.06203	0.64811
33.25546	0.65614
33.44889	0.66421
33.64232	0.67234
33.83575	0.68051
34.02918	0.68874
34.22261	0.69701
34.41604	0.70534
34.60947	0.71371
34.80290	0.72214
35.00000	0.73061
35.19343	0.73914
35.38686	0.74771
35.58029	0.75634
35.77372	0.76501
35.96715	0.77374
36.16058	0.78251
36.35401	0.79134
36.54744	0.80021
36.74087	0.80914
36.93430	0.81811
37.12773	0.82714
37.32116	0.83621
37.51459	0.84534
37.70802	0.85451
37.90145	0.86374
38.09488	0.87301
38.28831	0.88234
38.48174	0.89171
38.67517	0.90114
38.86860	0.91061
39.06203	0.92014
39.25546	0.92971
39.44889	0.93934
39.64232	0.94901
39.83575	0.95874
40.02918	0.96851
40.22261	0.97834
40.41604	0.98814
40.60947	0.99801
40.80290	1.00784
41.00000	1.01771
41.19343	1.02764
41.38686	1.03751
41.58029	1.04744
41.77372	1.05734
41.96715	1.06721
42.16058	1.07714
42.35401	1.08701
42.54744	1.09694
42.74087	1.10681
42.93430	1.11674
43.12773	1.12661
43.32116	1.13654
43.51459	1.14641
43.70802	1.15634
43.90145	1.16621
44.09488	1.17614
44.28831	1.18601
44.48174	1.19584
44.67517	1.20571
44.86860	1.21554
45.06203	1.22541
45.25546	1.23524
45.44889	1.24511
45.64232	1.25494
45.83575	1.26481
46.02918	1.27464
46.22261	1.28451
46.41604	1.29434
46.60947	1.30421
46.80290	1.31404
47.00000	1.32391
47.19343	1.33374
47.38686	1.34354
47.58029	1.35341
47.77372	1.36324
47.96715	1.37301
48.16058	1.38284
48.35401	1.39261
48.54744	1.40244
48.74087	1.41221
48.93430	1.42204
49.12773	1.43181
49.32116	1.44154
49.51459	1.45131
49.70802	1.46104
49.90145	1.47081
50.09488	1.48054
50.28831	1.49031
50.48174	1.50004
50.67517	1.50981
50.86860	1.51954
51.06203	1.52931
51.25546	1.53904
51.44889	1.54881
51.64232	1.55854
51.83575	1.56831
52.02918	1.57804
52.22261	1.58781
52.41604	1.59754
52.60947	1.60731
52.80290	1.61704
53.00000	1.62681
53.19343	1.63654
53.38686	1.64631
53.58029	1.65604
53.77372	1.66581
53.96715	1.67554
54.16058	1.68531
54.35401	1.69504
54.54744	1.70481
54.74087	1.71454
54.93430	1.72431
55.12773	1.73404
55.32116	1.74381
55.51459	1.75354
55.70802	1.76331
55.90145	1.77304
56.09488	1.78281
56.28831	1.79254
56.48174	1.80231
56.67517	1.81204
56.86860	1.82181
57.06203	1.83154
57.25546	1.84131
57.44889	1.85104
57.64232	1.86081
57.83575	1.87054
58.02918	1.88031
58.22261	1.89004
58.41604	1.90000
58.60947	1.90981
58.80290	1.91954
59.00000	1.92931
59.19343	1.93904
59.38686	1.94881
59.58029	1.95854
59.77372	1.96831
59.96715	1.97804
60.16058	1.98781
60.35401	1.99754
60.54744	2.00731
60.74087	2.01704
60.93430	2.02681
61.12773	2.03654
61.32116	2.04631
61.51459	2.05604
61.70802	2.06581
61.90145	2.07554
62.09488	2.08531
62.28831	2.09504
62.48174	2.10481
62.67517	2.11454
62.86860	2.12431
63.06203	2.13404
63.25546	2.14381
63.44889	2.15354
63.64232	2.16331
63.83575	2.17304
64.02918	2.18281
64.22261	2.19254
64.41604	2.20231
64.60947	2.21204
64.80290	2.22181
65.00000	2.23154
65.19343	2.24131
65.38686	2.25104
65.58029	2.26081
65.77372	2.27054
65.96715	2.28031
66.16058	2.29004
66.35401	2.30000
66.54744	2.30981
66.74087	2.31954
66.93430	2.32931
67.12773	2.33904
67.32116	2.34881
67.51459	2.35854
67.70802	2.36831
67.90145	2.37804
68.09488	2.38781
68.28831	2.39754
68.48174	2.40731
68.67517	2.41704
68.86860	2.42681
69.06203	2.43654
69.25546	2.44631
69.44889	2.45604
69.64232	2.46581
69.83575	2.47554
70.02918	2.48531
70.22261	2.49504
70.41604	2.50481
70.60947	2.51454
70.80290	2.52431
71.00000	2.53404
71.19343	2.54381
71.38686	2.55354
71.58029	2.56331
71.77372	2.57304
71.96715	2.58281
72.16058	2.59254
72.35401	2.60231
72.54744	2.61204
72.74087	2.62181
72.93430	2.63154
73.12773	2.64131
73.32116	2.65104
73.51459	2.66081
73.70802	2.67054
73.90145	2.68031
74.09488	2.69004
74.28831	2.70000
74.48174	2.70981
74.67517	2.71954
74.86860	2.72931
75.06203	2.73904
75.25546	2.74881
75.44889	2.75854
75.64232	2.76831
75.83575	2.77804
76.02918	2.78781
76.22261	2.79754
76.41604	2.80731
76.60947	2.81704
76.80290	2.82681
77.00000	2.83654
77.19343	2.84631
77.38686	2.85604
77.58029	2.86581
77.77372	2.87554
77.96715	2.88531
78.16058	2.89504
78.35401	2.90481
78.54744	2.91454
78.74087	2.92431
78.93430	2.93404
79.12773	2.94381
79.32116	2.95354
79.51459	2.96331
79.70802	2.97304
79.90145	2.98281
80.09488	2.99254
80.28831	3.00231
80.48174	3.01204
80.67517	3.02181
80.86860	3.03154
81.06203	3.04131
81.25546	3.05104
81.44889	3.06081
81.64232	3.07054
81.83575	3.08031
82.02918	3.09004
82.22261	3.10000
82.41604	3.10981
82.60947	3.11954
82.80290	3.12931
83.00000	3.13904
83.19343	3.14881
83.38686	3.15854
83.58029	3.16831



Model (B3, C3) > Hydrodynamic Response (C4) > Solution (C5) > Hydrodynamic Graph Results

Node		Parameters vs Time	
State	Parameter	Value	Time
Details of Parameters vs Time			
Presentation Method	Line		
Axes Selection	Parameters vs Time		
Show Tabulated Results Data	Yes		
Export CSV File	Select CSV File...		
Line A			
Abscissa Position of Minimum	69.6 s		
Abscissa Position of Maximum	59.1 s		
Minimum Value	-14.3382°		
Maximum Value	18.461°		
Line B			
Abscissa Position of Minimum	59.1 s		
Abscissa Position of Maximum	69.6 s		
Minimum Value	-17.5702 m		
Maximum Value	1.61181 m		
Line C			
Abscissa Position of Minimum	57.4 s		
Abscissa Position of Maximum	53.2 s		
Minimum Value	-1.14489 m		
Maximum Value	0.95358 m		
Line D			
Abscissa Position of Minimum	57.2 s		
Abscissa Position of Maximum	69.7 s		
Minimum Value	-1.53927 m/s		
Maximum Value	2.14022 m/s		
Line E			
Abscissa Position of Minimum	94.7 s		
Abscissa Position of Maximum	57.8 s		



Model (B3, C3) > Hydrodynamic Response (C4) > Solution (C5) > Hydrodynamic Graph Results

Node		Parameters vs Time	
State	Parameter	Value	Time
Details of Parameters vs Time			
Presentation Method	Line		
Axes Selection	Parameters vs Time		
Show Tabulated Results Data	Yes		
Export CSV File	Select CSV File...		
Line A			
Abscissa Position of Minimum	54.8 s		
Abscissa Position of Maximum	59.2 s		
Minimum Value	-13.1972°		
Maximum Value	14.46676°		
Line B			
Abscissa Position of Minimum	59.2 s		
Abscissa Position of Maximum	54.8 s		
Minimum Value	-1.53649 m		
Maximum Value	1.65197 m		
Line C			
Abscissa Position of Minimum	56.8 s		
Abscissa Position of Maximum	52.7 s		
Minimum Value	-1.17457 m		
Maximum Value	0.94361 m		
Line D			
Abscissa Position of Minimum	57.5 s		
Abscissa Position of Maximum	69.7 s		
Minimum Value	-1.62074 m/s		
Maximum Value	1.7916 m/s		
Line E			
Abscissa Position of Minimum	83.6 s		
Abscissa Position of Maximum	57.6 s		

Minimum Value	0.0227 m
Maximum Value	3.15467 m

FIGURE 8
Model (B3, C3) > Hydrodynamic Response (C4) > Solution (C5) > Parameters vs Time

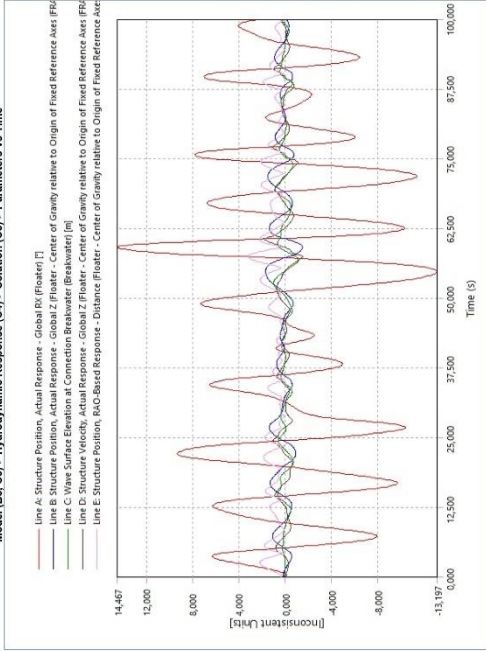


TABLE 47
Model (B3, C3) > Hydrodynamic Response (C4) > Solution (C5) > Parameters vs Time > Hydrodynamic Graph Results Input

Name	State	Solved
Details of Structure Position, Actual Response		
Result Source	Hydrodynamic Response > Solution (C5)	
Structure	Floater	
SubType	Structure Position	
Component	Actual Response	
Global FX		
Line Values		
Abcissa (X) Position of Minimum	54.8 s	
Abcissa (X) Position of Maximum	59.2 s	
Minimum Value	-13.1972	
Maximum Value	14.46676	

TABLE 48
Model (B3, C3) > Hydrodynamic Response (C4) > Solution (C5) > Parameters vs Time > Hydrodynamic Graph Results Input

Name	State	Solved
Details of Structure Position, Actual Response		
Result Source	Hydrodynamic Response > Solution (C5)	
Structure	Floater	
SubType	Structure Position	
Component	Actual Response	
Global Z		
Reference Point	Center of Gravity [Floater]	
Motion Relative To	Origin of Fixed Reference Axes (FRA)	

Minimum Value	0.01501 m
Maximum Value	2.42207 m

FIGURE 8
Model (B3, C3) > Hydrodynamic Response (C4) > Solution (C5) > Parameters vs Time

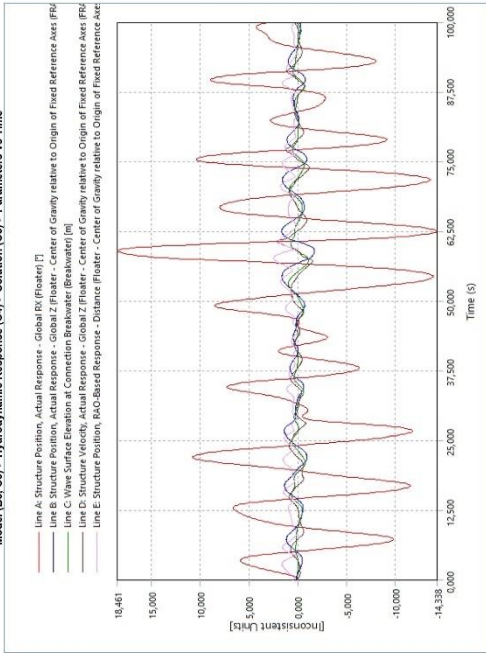


TABLE 47
Model (B3, C3) > Hydrodynamic Response (C4) > Solution (C5) > Parameters vs Time > Hydrodynamic Graph Results Input

Name	State	Solved
Details of Structure Position, Actual Response		
Result Source	Hydrodynamic Response > Solution (C5)	
Structure	Floater	
SubType	Structure Position	
Component	Actual Response	
Global FX		
Line Values		
Abcissa (X) Position of Minimum	62.6 s	
Abcissa (X) Position of Maximum	59.1 s	
Minimum Value	-14.3382	
Maximum Value	18.4611	

TABLE 48
Model (B3, C3) > Hydrodynamic Response (C4) > Solution (C5) > Parameters vs Time > Hydrodynamic Graph Results Input

Name	State	Solved
Details of Structure Position, Actual Response		
Result Source	Hydrodynamic Response > Solution (C5)	
Structure	Floater	
SubType	Structure Position	
Component	Actual Response	
Global Z		
Reference Point	Center of Gravity [Floater]	
Motion Relative To	Origin of Fixed Reference Axes (FRA)	

Line Values	
Abscissa (X) Position of Minimum	50.2 s
Abscissa (X) Position of Maximum	57.8 s
Minimum Value	-1.53949 m
Maximum Value	1.65197 m

TABLE 49
Model (B3, C3) > Hydrodynamic Response (C4) > Solution (C5) > Parameters vs Time > Hydrodynamic Graph Results Input

Name	State	Solved
Wave Surface Elevation		
Details of Wave Surface Elevation		
Line Inputs		
Result Source	Hydrodynamic Response > Solution (C5)	
Type	Wave Surface Elevation	
Reference Point	Connection Breakwater (Breakwater)	
Line Values		
Abscissa (X) Position of Minimum	56.9 s	
Abscissa (X) Position of Maximum	57.8 s	
Minimum Value	-1.3745 m	
Maximum Value	0.94381 m	

TABLE 50
Model (B3, C3) > Hydrodynamic Response (C4) > Solution (C5) > Parameters vs Time > Hydrodynamic Graph Results Input

Name	State	Solved
Structure Velocity, Actual Response		
Details of Structure Velocity, Actual Response		
Line Inputs		
Result Source	Hydrodynamic Response > Solution (C5)	
Type	Structure Velocity	
Sub Type	Actual Response	
Component	Global Z	
Reference Point	Center of Gravity (Floater)	
Motion Relative To	Origin of Fixed Reference Axes (FRA)	
Line Values		
Abscissa (X) Position of Minimum	57.5 s	
Abscissa (X) Position of Maximum	60.7 s	
Minimum Value	-1.60247 m/s	
Maximum Value	1.79116 m/s	

TABLE 51
Model (B3, C3) > Hydrodynamic Response (C4) > Solution (C5) > Parameters vs Time > Hydrodynamic Graph Results Input

Name	State	Solved
Structure Position, RAO-Based Response		
Details of Structure Position, RAO-Based Response		
Line Inputs		
Result Source	Hydrodynamic Response > Solution (C5)	
Type	Structure Position	
Sub Type	RAO-Based Response	
Component	Distance	
Reference Point	Center of Gravity (Floater)	
Motion Relative To	Origin of Fixed Reference Axes (FRA)	
Line Values		
Abscissa (X) Position of Minimum	63.6 s	
Abscissa (X) Position of Maximum	57.5 s	
Minimum Value	0.0227 m	
Maximum Value	3.15407 m	

Line Values	
Abscissa (X) Position of Minimum	59.1 s
Abscissa (X) Position of Maximum	57.8 s
Minimum Value	-1.25702 m
Maximum Value	1.61581 m

TABLE 49
Model (B3, C3) > Hydrodynamic Response (C4) > Solution (C5) > Parameters vs Time > Hydrodynamic Graph Results Input

Name	State	Solved
Wave Surface Elevation		
Details of Wave Surface Elevation		
Line Inputs		
Result Source	Hydrodynamic Response > Solution (C5)	
Type	Wave Surface Elevation	
Reference Point	Connection Breakwater (Breakwater)	
Line Values		
Abscissa (X) Position of Minimum	57.4 s	
Abscissa (X) Position of Maximum	57.8 s	
Minimum Value	-1.19468 m	
Maximum Value	0.95588 m	

TABLE 50
Model (B3, C3) > Hydrodynamic Response (C4) > Solution (C5) > Parameters vs Time > Hydrodynamic Graph Results Input

Name	State	Solved
Structure Velocity, Actual Response		
Details of Structure Velocity, Actual Response		
Line Inputs		
Result Source	Hydrodynamic Response > Solution (C5)	
Type	Structure Velocity	
Sub Type	Actual Response	
Component	Global Z	
Reference Point	Center of Gravity (Floater)	
Motion Relative To	Origin of Fixed Reference Axes (FRA)	
Line Values		
Abscissa (X) Position of Minimum	57.2 s	
Abscissa (X) Position of Maximum	60.8 s	
Minimum Value	-1.53972 m/s	
Maximum Value	2.14022 m/s	

TABLE 51
Model (B3, C3) > Hydrodynamic Response (C4) > Solution (C5) > Parameters vs Time > Hydrodynamic Graph Results Input

Name	State	Solved
Structure Position, RAO-Based Response		
Details of Structure Position, RAO-Based Response		
Line Inputs		
Result Source	Hydrodynamic Response > Solution (C5)	
Type	Structure Position	
Sub Type	RAO-Based Response	
Component	Distance	
Reference Point	Center of Gravity (Floater)	
Motion Relative To	Origin of Fixed Reference Axes (FRA)	
Line Values		
Abscissa (X) Position of Minimum	94.7 s	
Abscissa (X) Position of Maximum	57.8 s	
Minimum Value	0.01501 m	
Maximum Value	2.42207 m	